Department of Electrical and Computer Engineering

Application of Unified Power Flow Controller to Improve the Performance of Wind Energy Conversion System

Yasser Mohammed R Alharbi

March 2016

Declaration

To the best of my knowledge and belief this thesis contains no material previously published by any other person except where due acknowledgment has been made. This thesis contains no material which has been accepted for the award of any other degree or diploma in any university.

Yasser M Alharbi

30/03/2015

ABSTRACT

With the enormous global growth in electrical power demand and the associated decrease in conventional power resources, electricity generation from renewable energy sources have been furiously sought worldwide, as they represent infinite and clean natural resources. Wind energy is one of the most efficient renewable energy sources. However, due to the fluctuating behaviour of wind energy and the need of electronic devices to link wind turbine generator with existing electricity grids, problems such as frequency oscillations, voltage instability and harmonic distortion may arise. Flexible alternative current transmission system (FACTS) devices, such as unified power flow controller (UPFC), can provide technical solutions to improve the overall performance of wind energy conversion systems (WECS). This research introduces the UPFC as an effective FACTS device to improve the overall performance of WECS through the development of an appropriate control algorithm. Application of the proposed UPFC control algorithm is also investigated in this research to overcome some problems associated with the internal faults associated with WECS- voltage source converter (VSC), such as miss-fire, fire-through and dc-link faults.

ACKNOWLEDGMENTS

LIST OF PUBLICATIONS

[1] **Y. M. Alharbi**, A. M. Shiddiq Yunus, and A. Abu-Siada, "Application of STATCOM to improve the high-voltage-ride-through capability of wind turbine generator," in Innovative Smart Grid Technologies Asia (ISGT), 2011 IEEE PES, 2011, pp. 1-5.

[2] **Y. M. Alharbi**, A. M. S. Yunus, and A. Abu-Siada, "Application of UPFC to improve the LVRT capability of wind turbine generator," in Universities Power Engineering Conference (AUPEC), 2012 22nd Australasian, 2012, pp. 1-4

[3] M. S. Yunus, A. Abu-Siada, M. A. Masoum and **Y. M. Alharbi**, " Overview of Storage Energy Systems for Renewable Energy System Application," in Makassar International Conference on Electrical Engineering and Informatics (MICEEI12), 2012,

[4] S. Yunus, **Y. M. Alharbi**, A. A. Siada, and M. A. Masoum, "Investigation of near flicker source impact on the dynamic performance of FCWECS," in Power Engineering Conference (AUPEC), 2013 Australasian Universities, 2013, pp. 1-4.

[5] **Y. M. Alharbi**, A. Abu Siada, and A. F. Abdou, "Application of UPFC on stabilizing torsional oscillations and improving transient stability," in Power Engineering Conference (AUPEC), 2013 Australasian Universities, 2013, pp. 1-4

[6] **Yasser M. Alharbi**, A. M. ShiddiqYunus, and A. Abu-Siada, "Application of UPFC to Improve the FRT Capability of Wind Turbine Generator," International Journal of Electrical Energy, Vol. 1, No. 4, pp. 188-193, December 2013. doi: 10.12720/ijoee.1.4.188-193.

[7] F. Abdou, H. R. Pota, A. Abu-Siada, and **Y. M. Alharbi**, "Application of STATCOM-HTS to improve DFIG performance and FRT during IGBT short circuit," in Power Engineering Conference (AUPEC), 2014 Australasian Universities, 2014, pp. 1-5.

[8] **Y. M. Alharbi** and A. Abu-Siada, "Application of UPFC to improve the Low-Voltage-Ride-Through capability of DFIG," in Industrial Electronics (ISIE), 2015 IEEE 24th International Symposium on, 2015.

[9] **Y. M. Alharbi** and A. Abu-Siada, " Impacts of Converter Station Faults on the performance of WECS," in Power Engineering Conference (AUPEC), 2015 Australasian Universities, 2014.

[10] M. Y. Khamaira, A. Abu-Siada, and **Y. M. Alharbi**, "A New Converter Topology for Wind   Energy Conversion System," Accepted at the IEEE PES Asia-Pacific Power and Energy Engineering Conference Brisbane, Australia, 2015.

TABLE OF CONTENTS

LIST OF FIGURES

LIST OF TABLES

LIST OF ABBREVIATIONS

AC	Alternating Current
DFIG	Doubly Fed Induction Generator
DC	Direct Current
IG	Induction Generator
FACTS	Flexible AC Transmission System
FRT	Fault Ride Through
GSC	Grid-side Converter
GTO	Gate Turn-off Thyristor
GWEC	Global Wind Energy Council
HVDC	High Voltage Direct Current
HVRT	High Voltage Ride Through
HCC	Hysteresis Current Controller
IGBT	Insulated-Gate Bipolar Transistor
IPFC	Interline Power Flow Controller
LVRT	Low-voltage Ride-through
MW	Mega Watts
PCC	Point of Common Coupling
PI	Proportional Integral
PLL	Phase-locked Loop
PV	Photovoltaic
PWM	Pulse Width Modulation
RSC	Rotor-side Converter
SCIG	Squirrel Cage Induction Generator
SSR	Sub-synchronous Resonance
SSSC	Static Synchronous Series Compensator

STATCOM	Static Synchronous Compensator
SVC	Static Var Compensator
SMES	superconducting magnetic energy storage
TCSC	Thyristor-controlled Series Compensator
TSO	Transmission System Operators
UPFC	Unified Power Flow Controller
VSC	Voltage Source Converter
WECS	Wind Energy Conversion System
WTG	Wind Turbine Generator

1

INTRODUCTION

1.1   Background (Problem)

With the global concerns about environmental issues due to excessive emission of CO_2 and other pollutant gases from fossil fuel-based generators, renewable energy sources have been seriously considered worldwide, as they represent both infinite and clean natural resources [1, 2]. Wind energy is one of the most efficient and promising renewable energy resources in the world, which is continuously growing with the increase of electrical power demand and the associated decrease in conventional resources of electricity resources [3]. The growth rate in wind power generation

worldwide was estimated in 2001 to be 21%, and the global wind power capacity is expected to reach 423 GW and 666 GW by the end of 2015 and 2020, respectively [4]. Integration of wind energy sources (as a non-pollutant energy source) with electricity grid networks is necessary. On the other hand, the penetration of wind farms into the power system network can adversely influence the power system; specifically, due to the fluctuation nature of the wind speed, wind turbine generator tends to result in voltage fluctuations at the point of common coupling (PCC), which affects the voltage stability [5]. Moreover, another problem that may arise from the connection of wind farms into interconnected network is the system frequency oscillations due to insufficient system damping and/or violations of the transmission capability margin [6]. And, if variable-speed wind turbines are employed, problems relating to harmonics will occur [7]. One of the available solutions in regards to prevent the problems related to the integration of wind turbines with the exciting ac grid is using proper FACTS devices.

Flexible alternative current transmission system (FACTS) technology plays an important role in improving utilization of existing power systems. They have been extensively used for effective power flow control and dynamic voltage support of systems [8]. As a FACTS device, unified power flow controller (UPFC) allows system to be more flexible by using high-speed response active and reactive power compensations to improve the power flow of the transmission system. Thus, installing a UPFC at critical points of the transmission system will increase both the power

Chapter 1

dispatch (up to the power rating of existing generators and transformers) and the thermal limits of line conductors, by increasing the stability margin [9]. Shunt and series converters of the UPFC can control both active and reactive powers smoothly, rapidly and independently in four quadrant operational moods [10]. The aim of this thesis is to design an appropriate control algorithm for Unified Power Flow Controller (UPFC) to solve the above-mentioned problems.

1.2   Objectives

This thesis aims at introducing several new applications of unified power flow controller (UPFC) to enhance the power quality and stability of electricity grids subjected to penetration of large wind energy conversion systems (WECS). Specifically, the key objectives of this project are to:

- Develop a new control algorithm for UPFC connected to a large WECS to:
- Improve voltage stability,
- Suppress frequency oscillations, and
- Improve power quality.

- Overcome the effects of grid side disturbance on wind turbine generator (WTG), thereby maintaining its compliance with the recent grid codes.

- Extend the application of the proposed controller to prevent the faults that may result from WECS converter stations in the form of misfire, fire-through and dc-link faults.

Chapter 1

1.3 Significance

This thesis introduces a new control (and hence application) for UPFC systems to modulate both active and reactive powers at the point of common coupling of wind turbines with existing electricity grid. Presently, only superconducting magnetic energy storage (SMES) unit is the only FACTS device that can modulate both active and reactive powers. However, using SMES units is a very expensive solution in addition to the fact that they impose significant impact on the surrounding environment due to the generated magnetic field. Fortunately, UPFCs can be used as a successful alternative to SMES units without these side effects, while providing the same technical benefits, at an affordable cost, as will be detailed in this thesis.

1.4 Thesis outline

This thesis is organised in seven chapters as below:

Chapter 1presents a general background, key objectives and significance of the thesis topic: Application of UPFC to improve the overall performance of WECS

Chapter 2 reviews some of the existing renewable energy sources, with focus on wind energy conversion systems, which is the main topic of this thesis. The mathematical modelling and basic control systems of doubly fed induction generator (DFIG) is presented in Chapter 2. In addition, fault-ride through capability of the wind turbine generator and some grid codes are discussed in the chapter.

Chapter 1

Chapter 3 introduces the basic concepts of various flexible AC transmission system (FACTS) devices, along with their applications in power systems. A comparison between the FACTS devices based on their applications and costs is also presented in this chapter. Extensive literature review on unified power flow controller including topology, control system and various applications is presented. The chapter also discusses the proposed control system for the UPFC to improve the performance of wind energy conversion system (WECS).

Chapter 4 introduces the simulation results for the applications of UPFCs to improve the performance of the investigated WECS during intermittent faults (such as voltage sag, voltage swell and three phase short circuit at the grid side).

Chapter 5 investigates the application of UPFC in mitigating the impact of the faults of DFIG converter switches. The investigated faults include switching misfire, fire-through and dc link faults.

Chapter 6 concludes the work presented in this thesis and outlines some thoughts towards future work on the topic covered in the thesis.

Chapter 1

2

WIND ENERGY CONVERSION SYSTEM

2.1   Introduction

The increase in human population in the last few decades has been associated with concerns as to the corresponding rise in demand for life-supporting resources, such as water food and electrical power [11]. As for electrical power, the unparalleled industrial and technology advances are other factors that call for increasing demand in electrical consumption [12]. Globally, the power generation sector is facing significant challenges to meet the increasing demand for power. To date, conventional energy sources including oil, gas and coal are the world's main sources of energy. Unfortunately, these fossil fuel resources are associated with emissions that can severely harm the environment, with the symptoms being as air pollution,

climate change, oil spills and acid rain [13]. Interest in harnessing the benefits of renewable energy has been increasing steadily due to its advantages, which include sustainability, environmental friendly nature and affordable cost. Solar, geothermal and wind resources are among the most promising renewable energy alternatives [14, 15].

As a natural energy source, the radiation delivered by the sun is a promising renewable energy source of electrical power [16]. Nowadays, solar energy is one of the favourable energy alternatives. Photovoltaic (PV) technology is used for converting solar energy to electrical energy [17]. Globally, PV installation has contributed to about 177 GW of electrical power in 2014, and it is expected to deliver 1% of the total global electricity demand by the end of 2015 [18].

The geothermal power has the advantage of using fewer infrastructure elements for electrical power generation when compared with other energy sources such as coal or nuclear power [19]. In 2015, the world's installed capacity of geothermal power reached 12.635 MW, and this is expected to reach about 21.441 MW by 2020 [20].

Since the early stages of using natural energy resources, wind power has been considered as a main renewable energy source. And nowadays, there is a rapid increase in the utilization of wind energy [21], which has led to significant

Chapter 2

advancement in wind energy technology, including wind turbine design and sizing, and integration of wind turbines with existing electricity grids.

2.2 Wind Energy System

Wind energy has become one of the most popular renewable energy sources worldwide. In 2014, there was an additional of 51,473 MW of new wind power capacity that was brought into service [4]. Figure 2.1 illustrates the top 10 installed wind power capacity worldwide during the period from January to December 2014. The diagram shows that China has the highest installed wind power capacity with 23,196 MW generation, followed by Germany at 5,279 MW and USA at 4,279 MW [4].
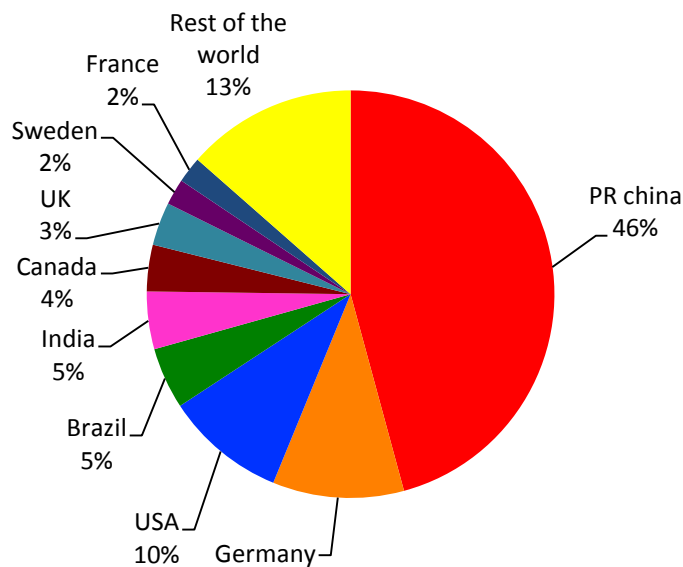
Figure 2.1 Distribution of the top 10 installed wind capacity in 2014

Chapter 2

Figure 2.2 shows the magnitude of the globally installed wind- capacity between 1996 and 2014. It can be seen from Figure 2.2 that the capacity increased from 197,943 MW 369,597 MW over this period.
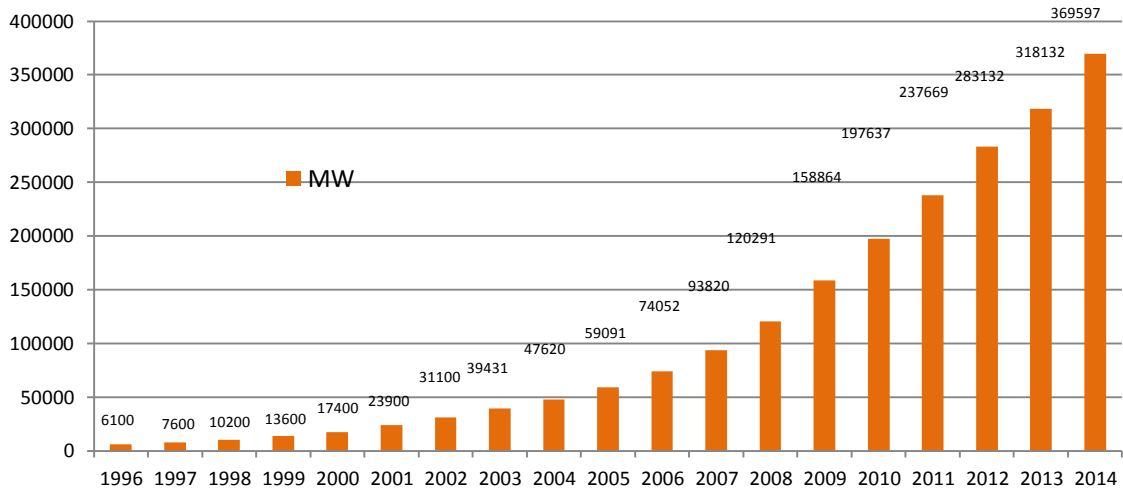
Figure 2.2 Global production of wind power between 1996 and 2014

The installed wind power capacity in Australia reached 3,806 MW by the end of 2014, and the installed wind power capacity in 2014 was 13% less than that installed in 2013 [4]. Despite the decrease in the newly installed capacity in 2014, the wind energy market is leading Australia towards its goal of using renewable energy to supply 20% of the power requirements by 2020 [4].

Chapter 2

2.3   Wind Turbine

Wind turbines capacity ranges from a few kilowatts for standalone units for houses to several megawatts in a wind farm. Small wind turbines are usually rated below 300kW and have the capability to be combined with other energy sources as generation system at farms and houses to support the need for electrical power. However, the integration of small wind turbine with existing grids is difficult and costly [22]. The wind turbine size and rating have been increasing gradually since 1980 as shown in Figure 2.3, thanks to the fact that increasing the size of the wind turbine rotor increases the amount of energy harvested by the wind turbine. In the early stage of wind turbine manufacturing, wind turbine power rating started with 50 kW and a size of 15 m rotor radius but nowadays wind turbines are designed to produce up to 7.5 MW with up to 126 m rotor diameter. A higher rating of 10 MW and associated 160 m rotor diameter is available nowadays as well [22].

Chapter 2

160m
10MW

71m
1.65MW

2010

2000

40m
500kW

27m
250kW

17m
100kW

1995

1990

1985
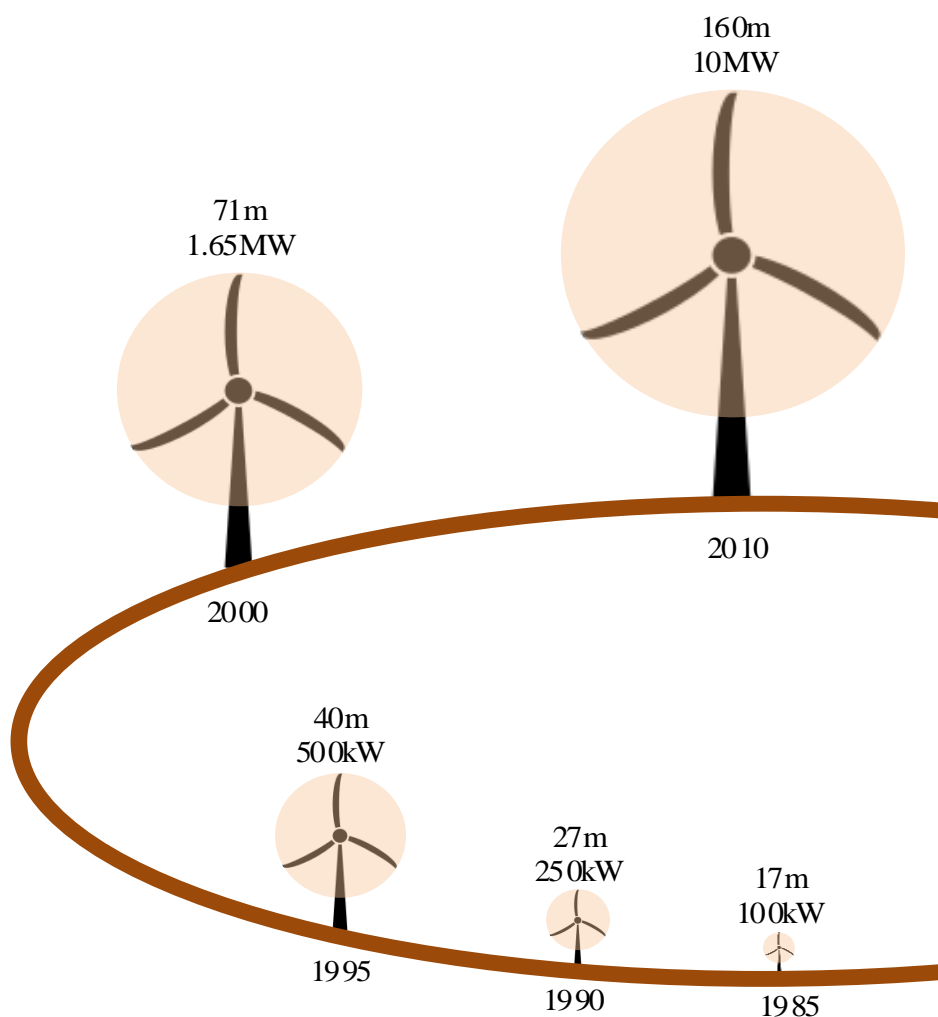
Figure 2.3 Evolution of wind turbine size.

2.4   Wind Energy Conversion Systems

Both fixed speed and variable speed generator can be used in wind energy conversion systems (WECS). In the early stages of the design of (WECS), wind turbines used to function at fixed speeds. Nowadays, with the new concept of generators and power electronics, variable speed wind turbines dominate the wind turbine market. Fig. 2.4

Chapter 2

illustrates different configurations of wind energy conversion systems. A review of the two types of fixed and variable speed systems follows.
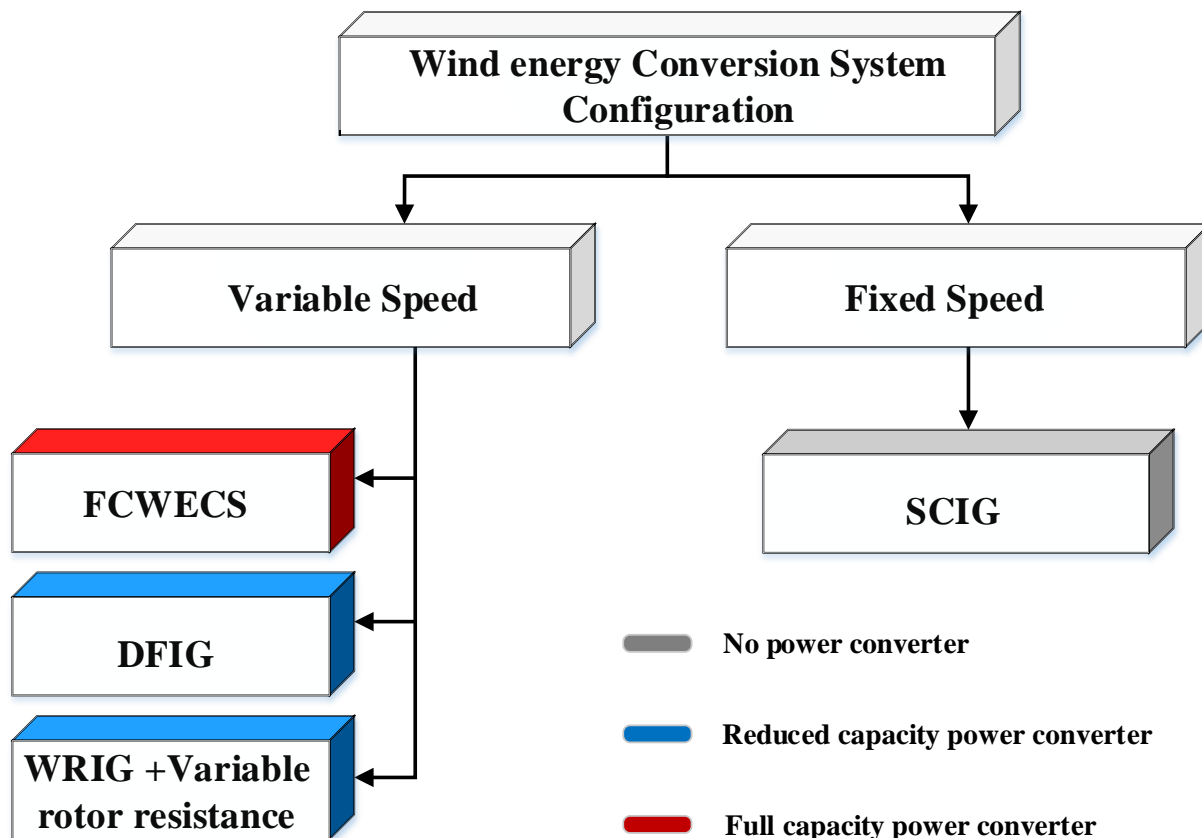
Figure 2.4 Different Configurations of wind energy conversion systems.

2.4.1 Fixed speed wind turbine

A fixed speed wind turbine (Figure 2.5) comprises a generator that is directly coupled to the power network and connected to the wind turbine through a low-speed shaft, a gearbox and a high-speed shaft [23]. It has the advantages of being simple,

inexpensive plus the fact that it does not need a power electronic interface. However, fixed speed wind turbines suffer from the limitation of controlling the power quality; moreover, the uncontrollable reactive power compensation and its shaft experience high mechanical stress [23].
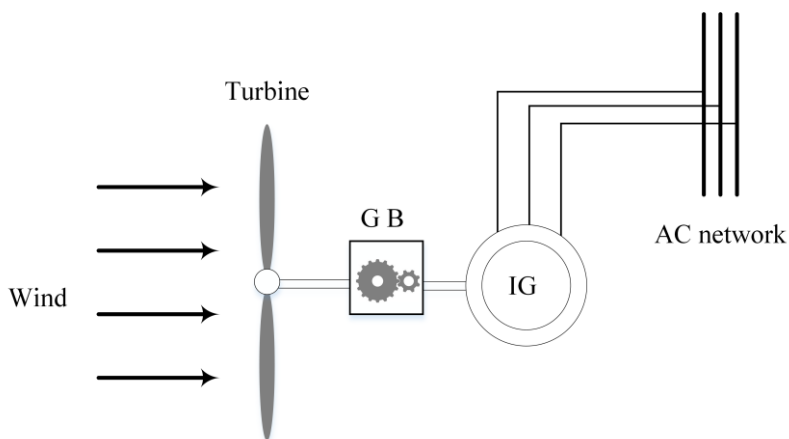
Figure 2.5 Fixed speed WECS configuration

The oldest wind energy conversion system topology employed a fixed speed generator (e.g. synchronous generator) that is coupled directly to the ac network, including mechanical dampers in the drive train. Modern fixed speed wind energy conversion systems use induction generators [24]. Figure 2.6 shows a conceptual scheme of the fixed speed wind energy conversion system.

Chapter 2
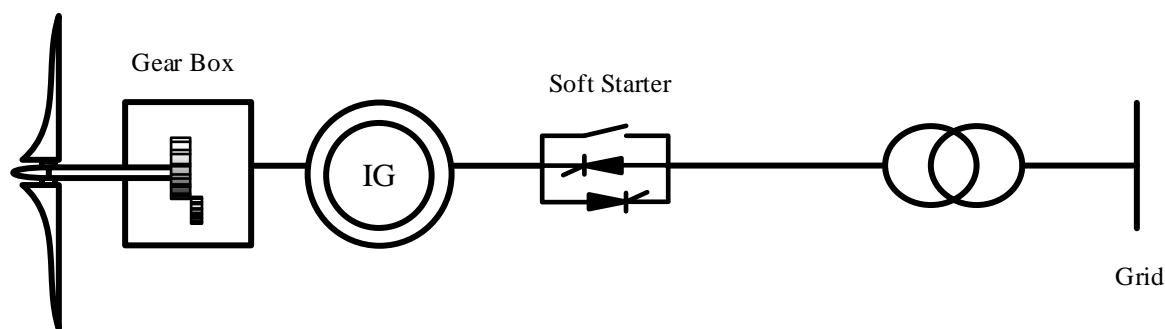
Figure 2.6 Typical configuration of the first generation of WECS

2.4.2 Variable speed wind turbine

Technology advancement has driven the wind turbine operation from being of fixed speed mode to variable speed. A variable speed wind turbine consists of a generator driven by a power converter, which facilitates the variable speed operation mode and aids in improving the WECS dynamic performance [23]. Owing to its variable speed mode, more power can be captured, enhanced power quality can be achieved and reduce mechanical stress on the drive train can be accomplished by wind power generators [23-25]. Comparison between the fixed speed wind turbine and variable speed wind turbine is summarized in Table 2.1

Table 2.1 Comparison of fixed and variable speed-based WECS.

	Variable Speed Wind Turbine	Fixed Speed Wind Turbine
Advantages	Maximized captured power Simple pitch control Reduced mechanical stress Provides dynamic compensation for torque and power pulsation Improved power quality Reduced acoustic noise	Low cost Simple structure Low maintenance
Disadvantages	High cost Complex control system	High mechanical stress High power fluctuations to the grid Relatively low energy-conversion

Chapter 2

2.4.2.1   Partly variable speed wind turbine

Partly variable speed wind turbines (Figure 2.7) or the so-called type B wind turbines operated in a limited variable speed mode. In this concept, the generator is directly coupled to the ac network and the generator rotor is connected to a variable resistance to control the generator speed. Depending on the variable resistance size, the slip can be increased by up to 10% that allows operation at a partly variable speed in the super synchronous range (i.e. up to 10% above the rated speed). The Danish manufacturer, Vestas, used this design feature in limited variable speed wind turbines since mid1990s [23, 24].
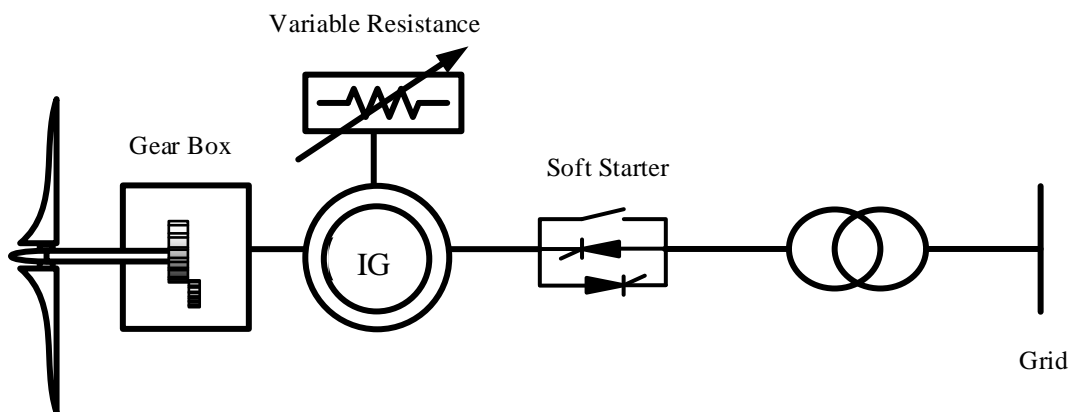
Figure 2.7 Typical configuration of partly variable speed WECS

Chapter 2

2.4.2.2   Full converter variable speed wind turbine

A full converter variable speed wind turbine that is based on a multi-pole synchronous generator is demonstrated in Figure 2.8. In this type, the generator is coupled to the ac network through a full-scale converter station that facilitates the variable speed operation of the wind turbine. The converter station is a combination of grid side converter and generator side converter connected back to back via a DC link. The generator's electrical frequency changes with the change in the wind speed, whereas the power network frequency remains unaffected [23].
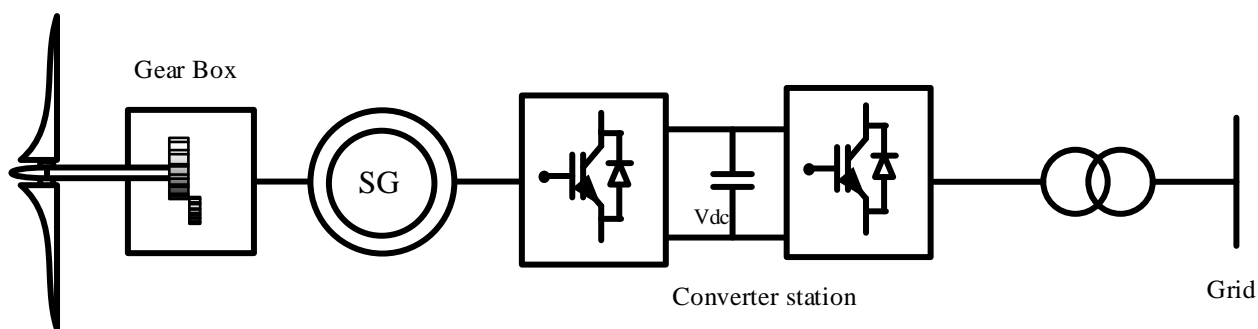
Figure 2.8 Typical configuration of full converter variable speed WECS

2.4.2.3   Doubly fed induction generator wind turbine

Typical configuration of a doubly fed induction generator (DFIG) wind turbine is shown in Figure 2.9. Among the variable speed wind turbine generators, DFIG is the

Chapter 2   17

most popular technology currently dominating the market of wind turbines, because of its superior advantages over other wind turbine technologies [26]. In this concept, the stator circuit is coupled directly with the power network through a coupling transformer while a back-to-back partial-scale voltage source converter (VSC) connects to the rotor circuit to the grid via a coupling transformer. The VSC allows the decoupled control of the generator's active and reactive power [24].
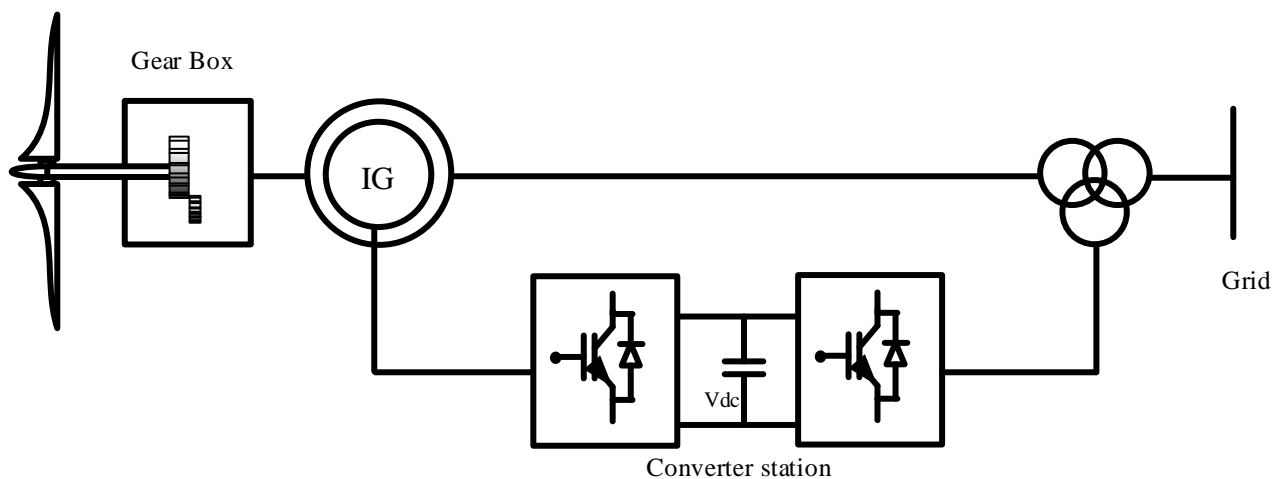
Figure 2.9 Typical configuration of Doubly Fed Induction Generators WECS

In this configuration, the power can be supplied to the grid through both the stator and the rotor, while the rotor can also absorb power in some operational modes that are determined by the generator speed. The produced power is supplied to the existing grid from the rotor via the VSC during the super-synchronous operational

Chapter 2

mode, where the rotor will absorb power from the network through the converter station during the sub synchronous operational mode as can be seen in figure 2.10.

ωᵣ > ωₛ

P

ωᵣ < ωₛ

P

Super-Synchronous
Operation

Sub-Synchronous
Operation
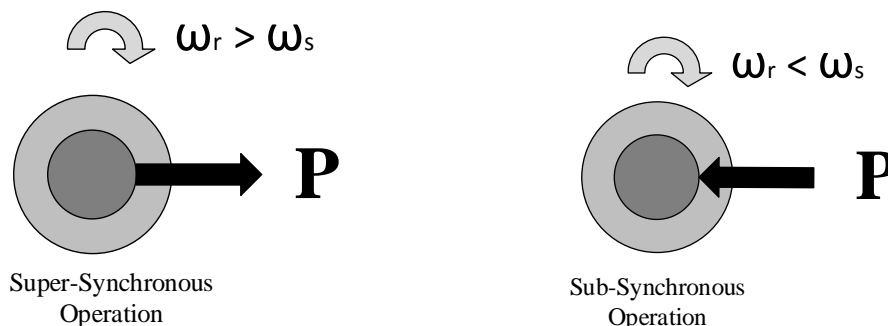
Figure 2.10 Super synchronous and sub synchronous operational modes.

2.4.2.3.1   DFIG model and control system

The induction generator model has been expressed in the d-q reference frame by decomposing the space-vector (shown in figure 2.11) into their equivalent d-q axis forms [27].

$\overrightarrow{\iota_s}$ R_s $j\omega_s\lambda_S$ L_{ls} L_{lr} $j\omega_{sl}\lambda_r$ R_r $\overrightarrow{\iota_r}$

$\overrightarrow{\iota_m}$

$\overrightarrow{v_s}$ $P\overrightarrow{\lambda_s}$ L_m $P\overrightarrow{\lambda_r}$ $\overrightarrow{v_r}$
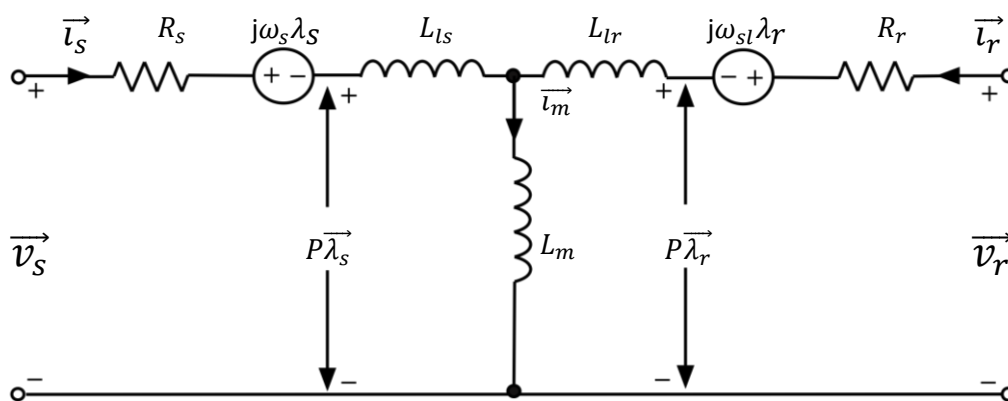
(a) IG model in the synchronous frame

Chapter 2
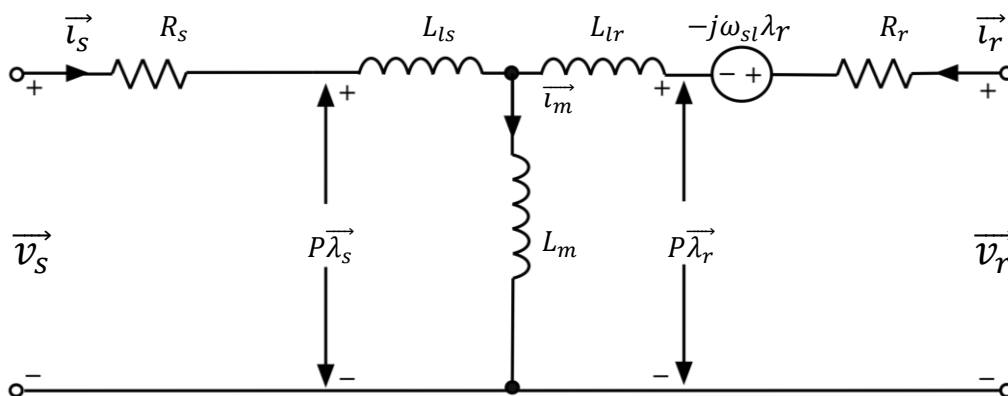
(b) IG model in the stationary frame

Figure 2.11 Space-vector models for induction generator in the synchronous and stationary reference frames.

Where:

$\vec{v_s}$, $\vec{v_r}$ - stator and rotor voltage vectors, respectively

$\vec{i_s}$, $\vec{i_r}$ - stator and rotor current vectors, respectively

$\vec{\lambda_s}$, $\vec{\lambda_r}$ - stator and rotor flux-linkage vectors, respectively

$\vec{R_s}$, $\vec{R_r}$ - stator and rotor winding resistances, respectively

ω – angular rotating speed of the arbitrary reference frame

ω_r - rotor electrical angular speed

p - derivative operator (p = d/dt)

L_s - stator self-inductance

L_r - rotor self-inductance

L_{ls}, L_{lr} - stator and rotor leakage inductances, respectively

L_m - magnetizing inductance

Chapter 2

The equations of the voltage of the generator's stator and rotor in the arbitrary reference frame can be expressed as:

$$\vec{v_s} = R_s \vec{\iota_s} + P\vec{\lambda_s} + j\omega\vec{\lambda}_s$$

$$\vec{v_r} = R_r \vec{\iota_r} + P\vec{\lambda_r} + j(\omega - \omega_r)\vec{\lambda}_s$$

(2.1)

The stator and rotor flux linkages equations are given by:

$$\vec{\lambda}_s = (L_{is} + L_m)\vec{\iota}_s + L_m\vec{\iota}_r = L_s\vec{\iota}_s + L_m\vec{\iota}_r$$

$$\vec{\lambda}_r = (L_{ir} + L_m)\vec{\iota}_r + L_m\vec{\iota}_s = L_r\vec{\iota}_r + L_m\vec{\iota}_s$$

(2.2)

In terms of the mechanical and electromagnetic torque, the motion equation that represents the dynamic behaviour of the rotor mechanical speed is given by

$$J\frac{d\omega_m}{dt} = T_e - T_m$$

(2.3)

$$T_e = \frac{3P}{2} Re(j\overrightarrow{\lambda_s}\overrightarrow{\iota_s}^*) = -\frac{3P}{2} Re(j\overrightarrow{\lambda_r}\overrightarrow{\iota_r}^*)$$

$$\vec{v_s} = v_{ds} + jv_{qs} \qquad\qquad \vec{v_r} = v_{dr} + jv_{qr}$$

$$\vec{\iota_s} = i_{ds} + ji_{qs} \qquad\qquad \vec{\iota_r} = i_{dr} + ji_{qr}$$

(2.4)

Chapter 2

$$\vec{\lambda_s} = \lambda_{ds} + j\lambda_{qs} \qquad\qquad \vec{\lambda_r} = \lambda_{dr} + j\lambda_{qr}$$

Using Eqn. (2.1) and Eqn. (2.4), the equations of the induction voltage of the generator in the *d-q-axis* can be derived as follows.

$$v_{ds} = R_s i_{ds} + P\lambda_{ds} + \omega\lambda_{qs}$$

$$v_{qs} = R_s i_{qs} + P\lambda_{qs} + \omega\lambda_{ds}$$

$$(2.5)$$

$$v_{dr} = R_r i_{dr} + P\lambda_{dr} - (\omega - \omega_r)\lambda_{qr}$$

$$v_{qr} = R_r i_{qr} + P\lambda_{qr} - (\omega - \omega_r)\lambda_{dr}$$

Substituting Eqn. (2.4) into Eqn. (2.2) of the stator and rotor flux linkages, the *d-q-axis* flux linkages are obtained as:

$$\lambda_{ds} = (L_{is} + L_m)i_{ds} + L_m i_{dr} = L_s i_{ds} + L_m i_{dr}$$

$$\lambda_{qs} = (L_{is} + L_m)i_{qs} + L_m i_{qr} = L_s i_{qs} + L_m i_{qr}$$

$$(2.6)$$

$$\lambda_{dr} = (L_{ir} + L_m)i_{dr} + L_m i_{ds} = L_r i_{dr} + L_m i_{ds}$$

$$\lambda_{qs} = (L_{ir} + L_m)i_{qr} + L_m i_{qs} = L_r i_{qr} + L_m i_{qs}$$

Chapter 2

The electromagnetic torque T_e can be calculated using currents and flux linkages of the *d-q axis* The most commonly torque models are given below[28]:

$$T_e = \frac{3P}{2} \, i_{qs}\lambda_{ds} - i_{ds}\lambda_{qs}$$

$$T_e = \frac{3PL_m}{2} \, i_{qs}i_{dr} - i_{ds}i_{qr} \tag{2.7}$$

$$T_e = \frac{3PL_m}{2L_r} \, i_{qs}\lambda_{dr} - i_{ds}\lambda_{qr}$$

The active and reactive power of the stator and rotor in the *d-q* reference frame can be expressed as:

$$P_r = v_{dr}i_{dr} + v_{qr}i_{qr}$$

$$Q_r = v_{qr}i_{dr} - v_{dr}i_{qr}$$

$$P_s = v_{ds}i_{ds} + v_{qs}i_{qs} \tag{2.8}$$

$$Q_s = v_{qs}i_{ds} - v_{ds}i_{qs}$$

Chapter 2

The steady state relationship between the mechanical power and the active power across the rotor and stator is shown in Figure 2.12, where P_m is the mechanical power produced by the turbine, P_r is the real power supplied by the rotor, $P_{air-gap}$ is the power at the generator air-gap, P_s is the power delivered by the stator and P_g is the total real power provided to the power network [29].
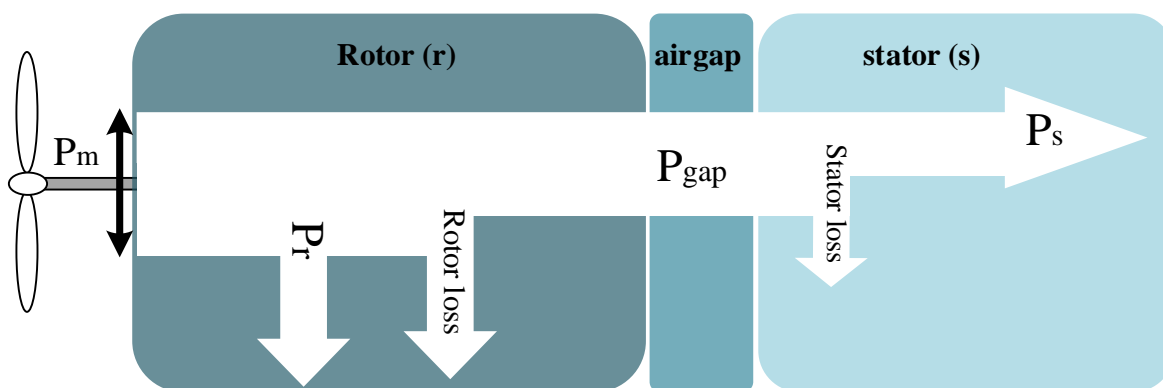
Figure 2.12 Power flow and loss in induction generator.

By neglecting the power losses in the stator and rotor:

$$P_{air-gap} = P_s = P_m - P_r \tag{2.9}$$

In terms of the electrical torque T, the above equation can be re-written as:

$$T_{\omega_s} = T_{\omega_r} - P_r \tag{2.10}$$

or

$$P_r = -T(\omega_s - \omega_r)$$

Accordingly, the rotor active power can be expressed as a function of the slip s as:

$$P_r = -sT\omega_s = sP_s \qquad (2.11)$$

The mechanical power, P_m, can be stated as

$$
\begin{aligned}
P_m &= P_s + P_r \\
P_m &= P_s - sP_s \\
&= (1 - s)P_s
\end{aligned}
\qquad (2.12)
$$

The total delivered power, P_g, is

$$P_g = P_s + P_r = (1 + s)P_s = \left(\frac{1+s}{1-s}\right)P_m \qquad (2.13)$$

The converter size of the DFIG is determined by the controllable range of the slip s. The maximum practical speed and slip range (between 0.7 and 1.2 pu) are limited by mechanical and other constraints [29].

Chapter 2

2.4.2.3.2   DFIG Control system:

A block diagram of a variable wind turbine equipped with a doubly fed induction generator (DFIG) is shown in Figure 2.13. The block diagram shows the wind turbine's aerodynamic and mechanical components, their control, and interaction with the power grid. In the generic model, the physical component of the wind turbine is represented as a block, and the arrows indicate the links between the different model blocks. Such links show the data exchange between the component blocks within the dynamic wind turbine model and the power flow between the generator and the power grid [24]. The main components of this model are:

- Dynamic wind

- Aerodynamic rotor

- Shaft system

- Induction generator

- Rotor side converter, including control

- Grid side converter, including control

- DC-link

- Pitch control

Chapter 2

WIND ENERGY CONVERSION SYSTEM
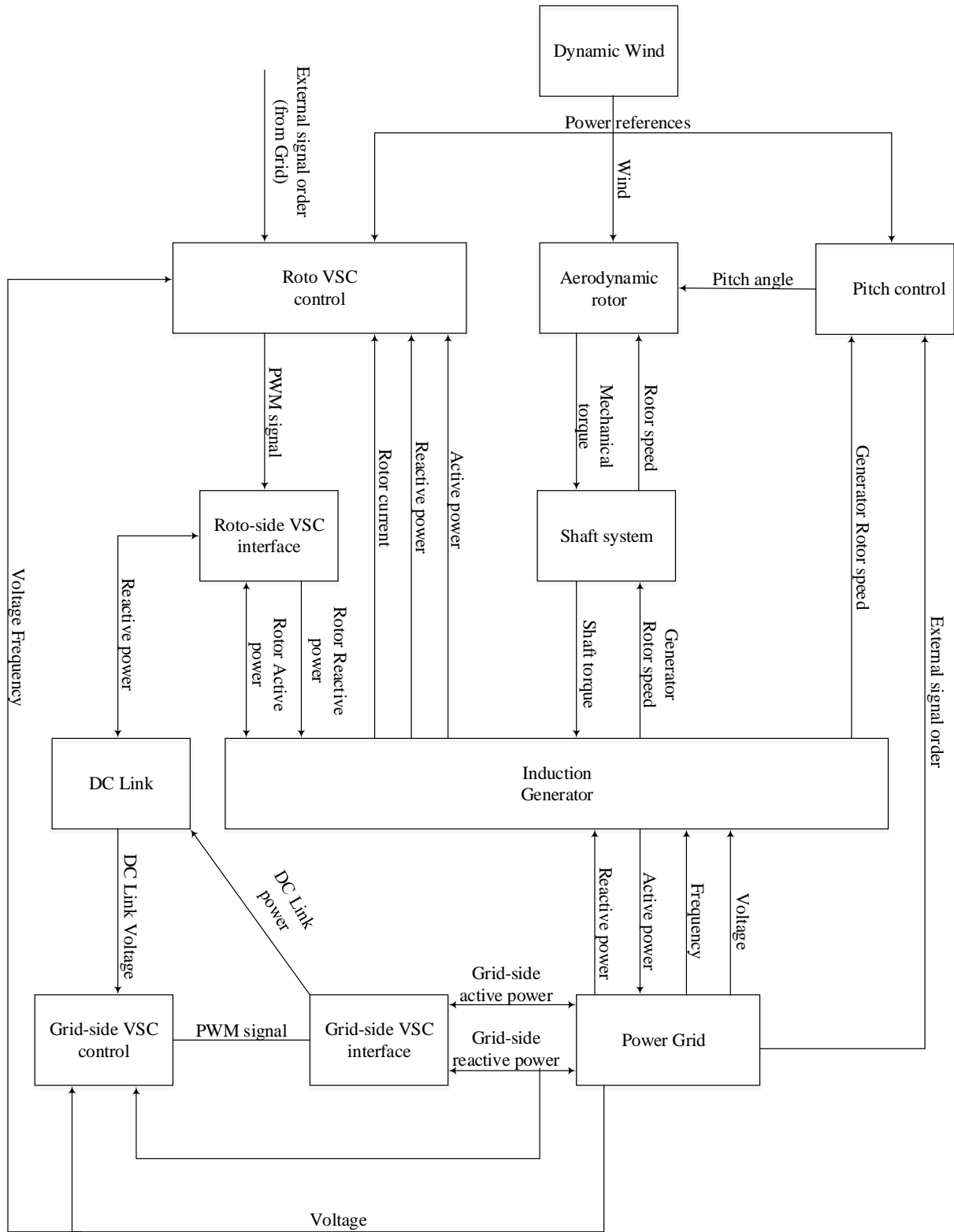
Figure 2.13Generic model for a wind turbine equipped with DFIG [24].
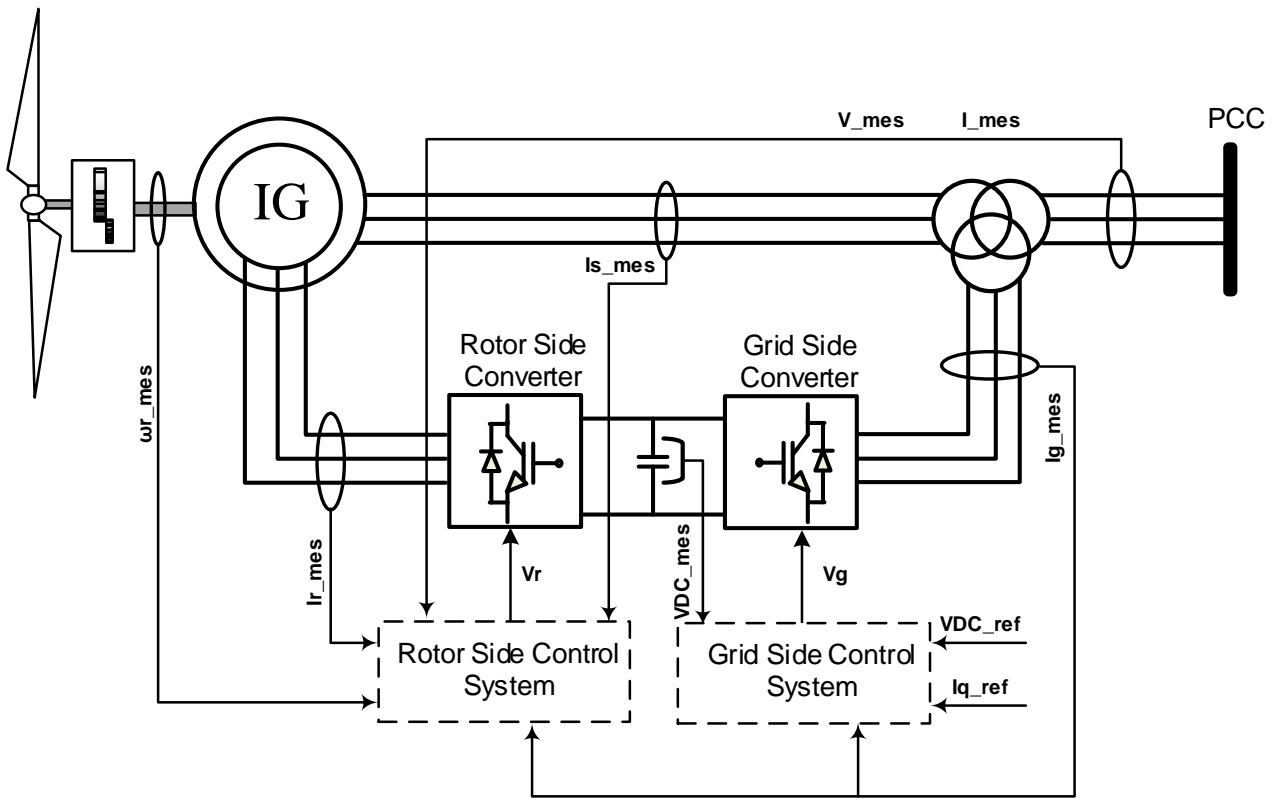
Figure 2.14 A DFIG control system scheme.

Figure 2.14 shows a schematic of a wind turbine equipped with a doubly fed induction generator and its overall control system. The converter station consists of two voltage source converters (VSC): one is connected to the grid side and called the grid side converter (GSC), and the other is connected to the rotor and called the rotor side converter (RSC). Both GSC and RSC are connected back to back via a dc link. The grid side converter controls the reactive power at the point of common coupling during disturbance events, by injecting or absorbing the reactive power if required. However, it does not exchange reactive power with the ac system during normal operation mode. Moreover, the grid side converter is responsible for regulating the dc

Chapter 2

voltage across the DC link capacitor. On the other hand, the rotor side converter controls the generated active and reactive power independently to improve the efficiency of the wind turbine output energy during wind gust fluctuations. The rotor circuit is excited through the rotor side converter control [24].

2.4.3   Impact of wind energy integration into electricity grid

The integration of wind energy into grid has been given more concern in recent years due to the significant increase in wind power generation level [30]. The high penetration of WECS into electricity grid leads to technical and power quality issues that need more concern and consideration by the system operators [30]. Some of these issues include:

- **Power variation**

Significant change in the power may occur because of the changing nature of the wind gust or the WECS tower shadow effects. Switching operation can also lead to power variation phenomena [31].

- **Harmonics**

The use of power electronic converter stations to interface wind turbine generator with the grid results in distorted voltage and current waveforms [32].

Chapter 2

- **Voltage fluctuation**

Voltage variation at the point of common coupling (PCC) connecting wind turbine generator with the grid may take place due to the intermittent nature of wind and if an adequate control scheme to regulate the voltage level is not adopted. Other causes of voltage variation include significant load changing and fault conditions [3].

- **Flickers**

Flickers may arise because of a rapid and continuous change in the wind generated power [32].

2.4.4   Fault ride through and grid code

Due to the significant increase in Wind turbine generators (WTGs) and the global trend to establish reliable smart grids, the transmission system operators (TSOs) require connection of WTGs with existing grids to provide power support during maintenance and fault circumstances of the latter. Accordignly, grid codes have been established in many countries to comply with these new requirements. There are many international codes related to the fault ride through (FRT) capability of WTGs [33-37]. The low voltage ride through (LVRT) grid codes for UK, Spain, Denmark, Germany, Australia, China and the US are shown in Fig2.15 as examples.

Chapter 2
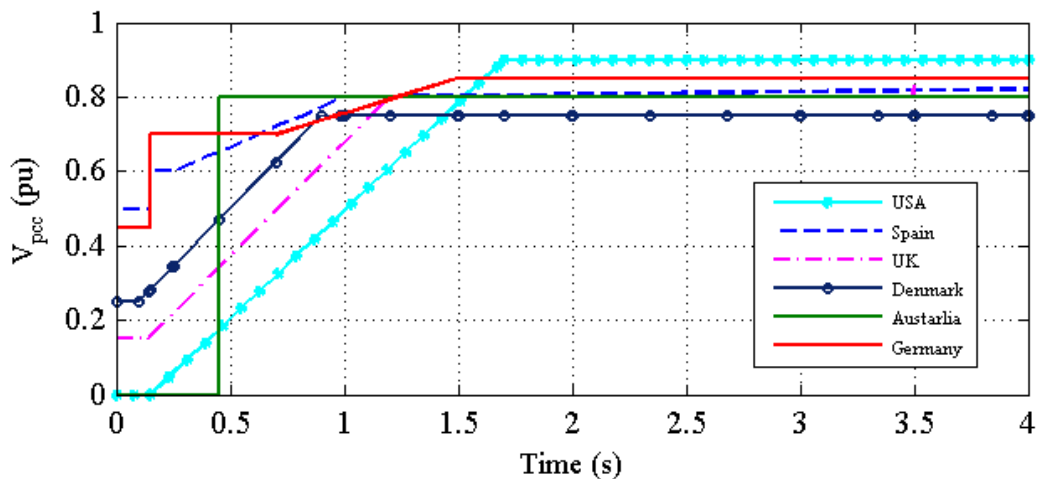
Figure 2.15 Nominated countries low voltage ride-through grid (LVRT) codes.

The allowed voltage sag at the PCC of the United States grid code is 0 pu, which lasts for a duration of 0.15s from the occurrence of the fault after which the LVRT profile increases linearly during the following 1.5s to 0.9 pu at which the voltage level is maintained [33].

The minimum acceptable voltages sag at the PCC for the Spanish grid code at the instant of fault occurrence is 0.5 pu, which lasts for 0.15s after which it increases to

Chapter 2   31

0.6 pu and lasts for 0.1s. The LVRT profile then ramps to 0.8 pu during the next 0.75s and remains at this level for 3s [33].

The Australian grid code requires WTG to withstand a PCC voltage level of 0 for 3s then LVRT increases to 0.8 pu [37]. WTGs are to be disconnected from the grid in case of voltage levels at the PCC fall outside the area bounded by the LVRT margins of the grid codes.
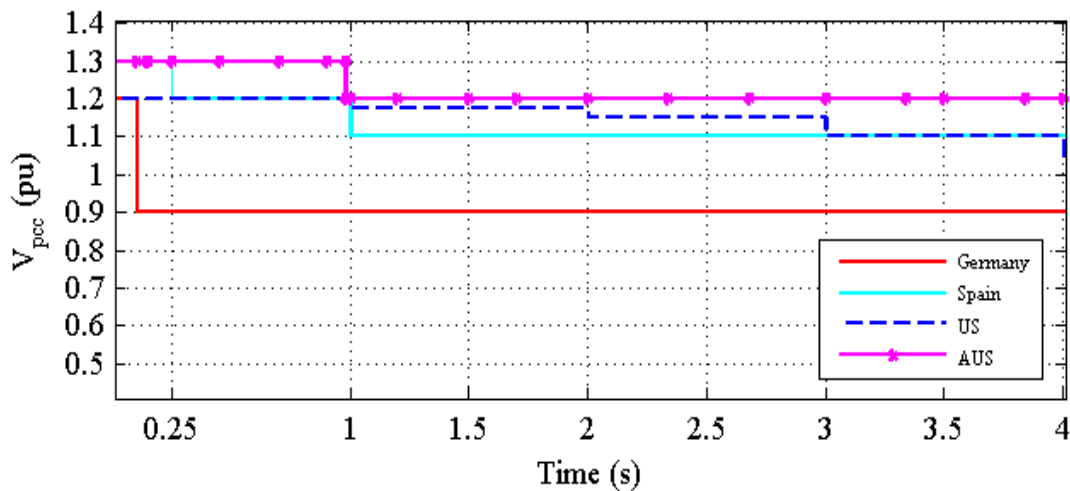
Figure 2.16 Nominated countries High voltage ride-through grid codes.

Figure 2.16. shows the technical requirements for the high voltage ride through (HVRT) capability of wind turbine generators in some countries. The allowed voltage swell at the PCC of the US grid code is 1.2 pu, whcih lasts for a duration of 1s from the fault occurrence. After that, the HVRT profile decreases by 0.05 pu every 1s during the following 3s, after which the voltage at the PCC has to be maintained within a safety margin of 0.05 pu from the nominal value [33].

Chapter 2

The maximum voltage rise at the PCC for the Spanish grid code at the instant of fault occurrence is 1.3 pu which remains for 0.25s after which it decreases by 0.1 pu, which lasts for 1 s. And then the voltage level at the PCC has to be maintained within a safety margin of 0.1 pu above the nominal value [33].

The Australian standard allows the voltage to increase by 1.3 pu for 0.98 second after that the voltage has to be limited to 1.2 pu [37].   Table 2.2 lists the LVRT and HVRT codes in 7 countries.

Table 2.2 Some parameters for Grid codes in some countries [34, 36, 37].

Country	LVRT				HVRT	
	During Fault		Fault Clearance		During Swell	
	V_{min} (pu)	T_{max} (s)	V_{min} (pu)	T_{max} (s)	V_{max} (pu)	T_{max} (s)
Denmark	0.25	0.1	0.75	0.5	NA	NA
Sweden	0.25	0.25	0.9	0.25	NA	NA
Germany	0	0.15	0.9	1.5	1.2	0.1
Spain	0	0.15	0.85	1	0.3	0.25
USA	0	0.15	0.9	1	1.2	1
Australia	0	0.45	0.8	0.45	1.3	0.98
China	0.2	0.625	0.9	3	NA	NA

Chapter 2

3

FLEXIBLE AC TRANSMISSION

SYSTEMS

3.1   Overview of FACTS Devices

The concept of FACTS (flexible ac transmission systems) was envisioned in the late of 1980s [38]. The technology consists of a variety of power electronic devices with the aim of controlling both power and voltage at a certain location of the electricity grids during disturbances. In general, the FACTS devices were invented to improve the existing transmission line capacity and provide a controllable power flow for a selected transmission direction [39].

Chapter 3

The FACTS devices are primarily divided into two groups. The first group involves quadrature tap-changing transformers, including conventional thyristor-switched capacitors and reactors, and the the second group involves voltage source converters based on gate turn-off (GTO) thyristor-switched converters [40]. The first group has introduced Thyristor-Controlled Phase Shifter (TCPS), Static Var Compensator (SVC) [41] and the Thyristor- Controlled Series Capacitor (TCSC) [42]. The second group has resulted in the Static Synchronous Series Compensator (SSSC) [42], the Static Synchronous Compensator (STATCOM) [43], the Interline Power Flow Controller (IPFC) [44] and the Unified Power Flow Controller (UPFC) [44]. Each generation of the FACTS devices has its own performance and characteristics [45].

Capacitor and reactor banks along with fast solid-state switches are used in the first group of FACTS devices, which can be connected in series or shunt with the power system to compensate for the reactive power at the PCC. However, real power exchange with the system is not possible with such systems.

The devices of the FACTS group that is based on voltage source converter (VSC) utilises self-commutated converters equipped with GTO thyristor switches. Through a proper control scheme, this group is able to generate capacitive and inductive reactance internally [40]. In addition to the independent reactive power control, the voltage source converter can be integrated with energy storage system to enable decoupled control of active and reactive power exchange with the system it is connected to [39]. Fig. 3.1 illustrates an overview of the main FACTS devices.

Chapter 3
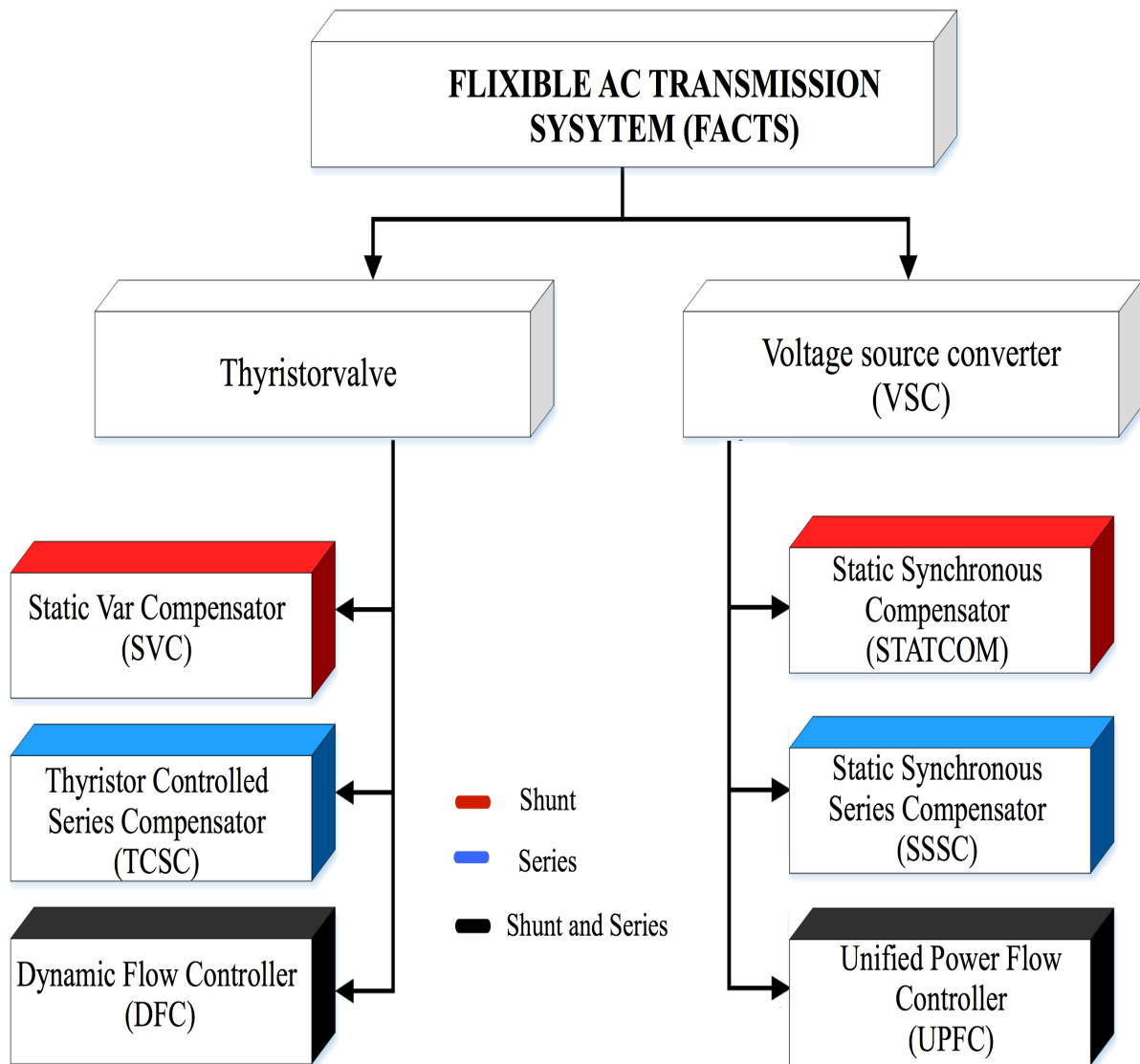
Figure 3.1 Overview of the main FACTS Devices

To explain the reactive power compensation process of a shunt FACTS, a shunt connected compensator (simulated as an ideal ac voltage source of voltage V_m) is

Chapter 3

connected to the middle of a lossless transmission line for the system shown in Figure 3.2.
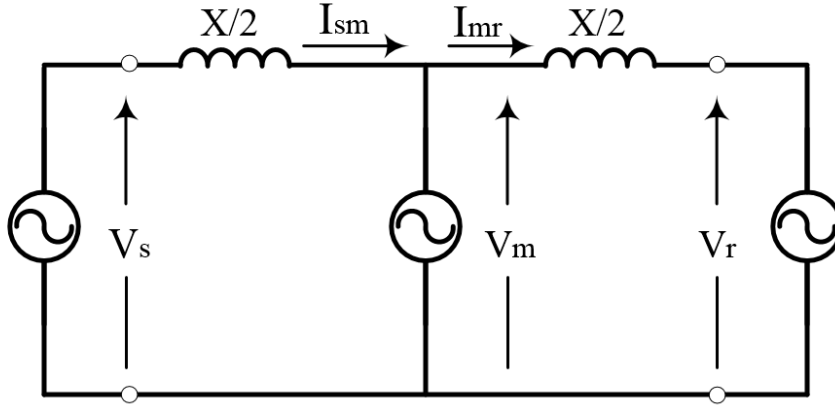
Figure 3.2 Two-machine system with shunt compensator

For an assumed lossless system, the real power can be written as :

$$V_{sm} = V_{mr} = V\cos\frac{\delta}{4} \quad ; \qquad\qquad I_{sm} = I_{mr} = I = \frac{4V}{X}\sin\frac{\delta}{4} \qquad (3.1)$$

The transmitted power is

$$P = V_{sm}I_{sm} = V_{mr}\,I_{mr} = V_m I_{sm}V\cos\frac{\delta}{4} \;=\; VI\cos\frac{\delta}{4} \qquad (3.2)$$

$$P = 2\frac{V^2}{X}\sin\frac{\delta}{2} \qquad (3.3)$$

Similarly

$$Q = VI\sin\frac{\delta}{4} = \frac{4V^2}{X}\left(1-\ \cos\frac{\delta}{2}\right) \qquad (3.4)$$

On the other hand, the basic function of the series compensation technique is to reduce the series inductive reactance of the transmission line. For simplicity, Figure 3.3 shows a two-machine power system with series capacitive compensation that is

Chapter 3

assumed to be composed of two identical parts. For the same end voltages, the magnitude of the total voltage across the series line inductance ($V_X = 2V_{X/2}$) is increased by the magnitude of the opposite voltage V_c, which is developed across the series capacitor, because of the increase in the line current.
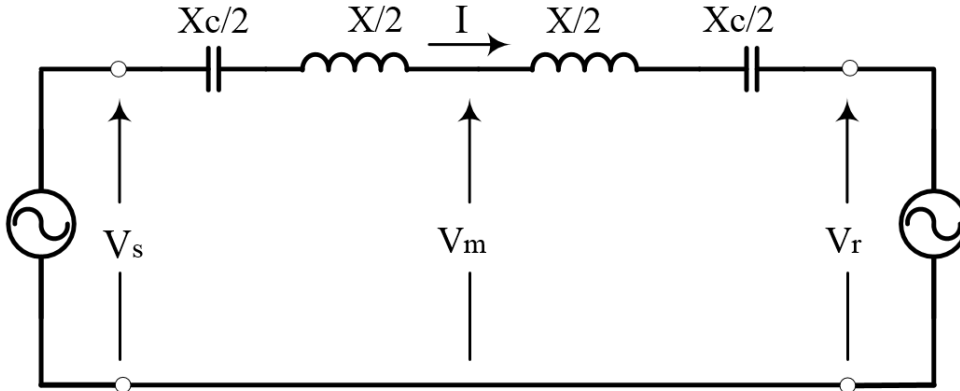
Figure 3.3 Two-machine system with series compensator

The effective transmission impedance X_{eff} with the series capacitive compensation is obtained from

$$X_{eff} = X - X_C \tag{3.5}$$

$$X_{eff} = (1 - K)\,X \tag{3.6}$$

where K is the amount of allowable series compensation

$$K = \frac{X_C}{X} \qquad 0 \le K < 1 \tag{3.7}$$

Assuming $V_s = V_r = V$ in Figure 3.7, the current in the compensated line, the corresponding real power transmitted and the reactive power delivered by the series capacitor can be written as follow

Chapter 3

$$I = \frac{2V}{(1-K)\,X}\,\sin\frac{\delta}{2} \tag{3.8}$$

$$P = V_m\,I = \frac{V^2}{(1-K)\,X}\,\sin\delta \tag{3.9}$$

$$Q_C = I^2\,X_C = \frac{2V^2}{X}\,\frac{K}{(1-K)^2}\,(1-\cos\delta) \tag{3.10}$$

FACTS devices introduce a wide operational range to increase the thermal limits of a power system and improve its stability. FACTS devices have been used for:

• Active and reactive Power control [46]

• Voltage control stability and Sub synchronous resonance mitigation [47]

• Power oscillation damping [48]

• Transients and dynamics stability [49]

• Fault current limiting [50]

• Flicker mitigation [51]

• Power system security enhancement [52]

Investments into such complex devices have to carefully consider many aspects such as the practical requirements and benefits of the application. Some FACTS devices can perform multi tasks as given in

Chapter 3

Table 3.1 FACTS Applications and cost Comparison

FACTS / Application	SVC	STATCOM	TSCS	SSSC	UPFC
Reactive power control	✗	✗	✗	✗	✓
Active power control	✗	✗	✗	✗	✓
Voltage control	✓	✓	✗	✗	✓
Voltage stability improvement	✓	✓	✗	✓	✓
Power oscillations damping	✓	✓	✓	✓	✓
Transients and dynamic stability	✓	✗	✓	✓	✓
Fault current limiter	✗	✗	✓	✓	✓
Var compensation	✓	✓	✗	✗	✓
Approximate Costs (US $) [53]	40/kVar	50/kVar	40/kVar	20/kVar	50/kVar

Chapter 3

Among the FACTS devices listed in Table 3.1, UPFC has the capability to cover all the listed applications due to its ability to control all the parameters affecting the transmission line power flow, including voltage, phase angle and impedance [44].

3.1.1 Static VAR compensator (SVC)

Static VAR compensator is a shunt reactive power compensation device that modulates reactive power at the connection point, by exchanging the needed reactive power with the system [38]. The first SVC was introduced in 1960s; before the introduction of such device, the reactive power compensation was performed using a synchronous generator [40]. Figure 3.4 shows the basic configurations of the static VAR compensator [43].
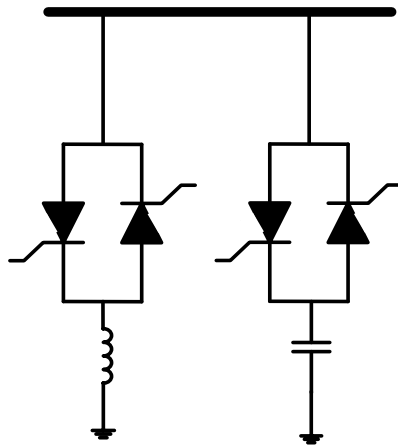
Figure 3.4 SVC basic configrations

Chapter 3

The SVC is designed to operate in both inductive and capacitive modes to facilitate bidirectional reactive power compensation with the grid. The voltage current characteristic of SVC is illustrated in Figure 3.5 [43].
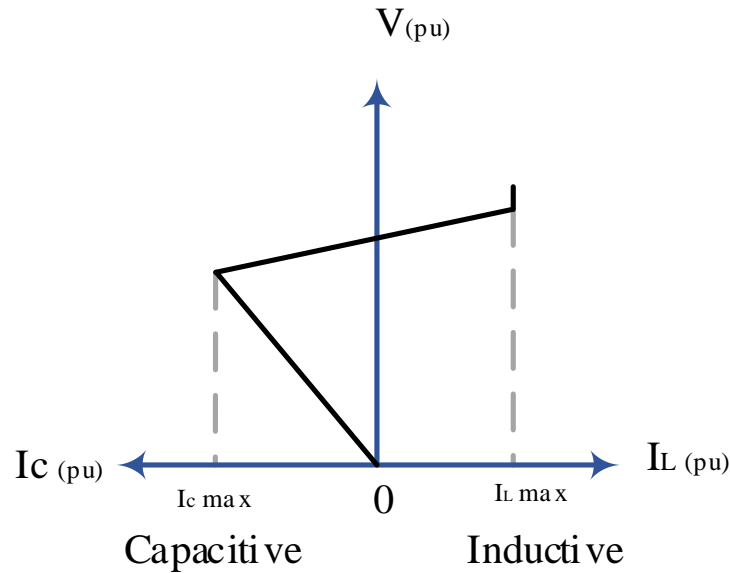
Figure 3.5 SVC V-I charactrastics

A number of studies investigated the use of SVC to increase the power system quality and stability [54-56]. Li et al. studied the use of SVC to improve the integration of an offshore wind farm and a marine current farm [56]. The application of SVC to improve an induction motor performance was demonstrated in [54]. Application of SVC for damping power system oscillations was studied in [55].

Chapter 3

3.1.2 Static synchronous compensator

Static synchronous compensator (STATCOM) is a shunt connected reactive power compensation controller. The advancements in power electronics, in particular the GTO thyristor, enabled implementation of such technology as a competitive alternative to conventional SVC [57]. A schematic configuration of STATCOM is shown in Figure 3.6.
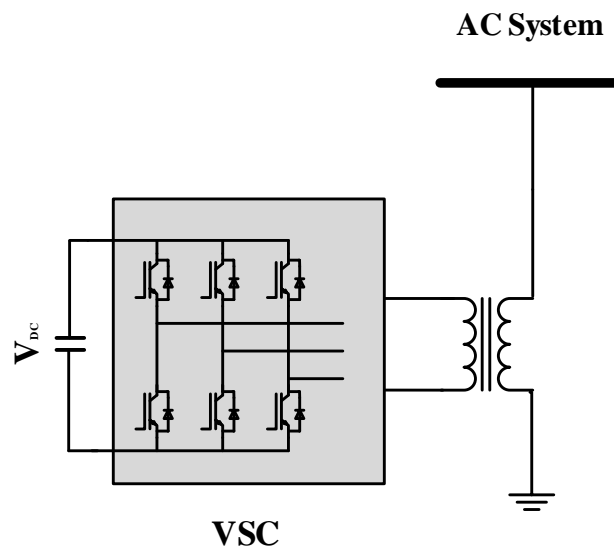
Figure 3.6 Basic configration of STATCOM

The interaction between the AC system voltage and the voltage at the STATCOM AC side terminals provides the control of the reactive power flow. If the voltage at the STATCOM terminals is higher than the system voltage, reactive power will be

Chapter 3

injected from STATCOM to the system and will therefore behave as a capacitor. When the voltage at the STATCOM is less than the AC voltage, STATCOM will behave as an inductor and the reactive power flow will be reversed. Under normal operating conditions, both voltages will be equal and there will be no power exchange between the STATCOM and the system [58]. Figure 3.7 shows the characteristics of the STATCOM voltage and current.
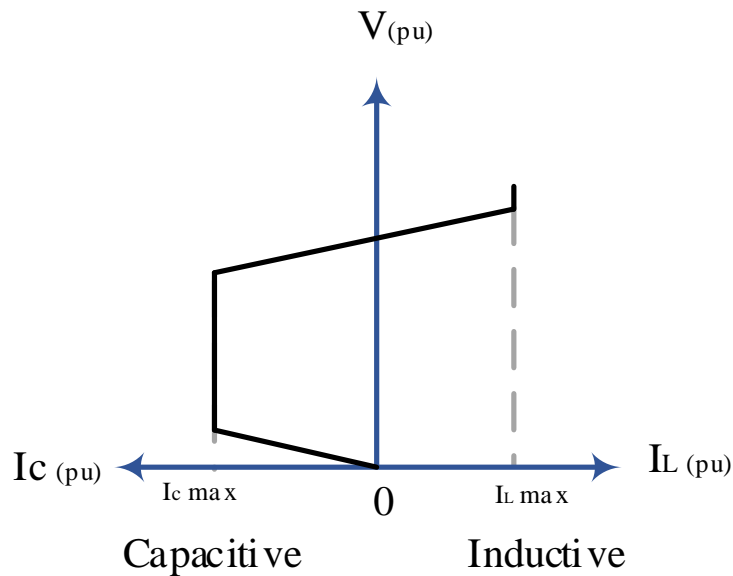
Figure 3.7 STATCOM V-I charactrastics

Several studies proved that STATCOM is capable of improving power system dynamics and system stability for renewable energy applications [59-66]. STATCOM was introduced for flicker mitigation in [65], while the application of STATCOM in mitigating the effects of sub synchronous response in wind farms based on a series compensated induction generators was investigated in [63]. More

Chapter 3

studies were conducted to investigate the application of STATCOM with wind turbine generators and its integration with the ac grid [60-62, 64, 66].

3.1.3 Thyristor- controlled series capacitor

Thyristor controlled series capacitors (TCSC) is a series controller device that was proposed in 1986 [42]. Figure 3.8 shows the basic configurations of TSCS, which consists of a Thyristor Controlled Reactor in parallel with a compensating capacitor [42].
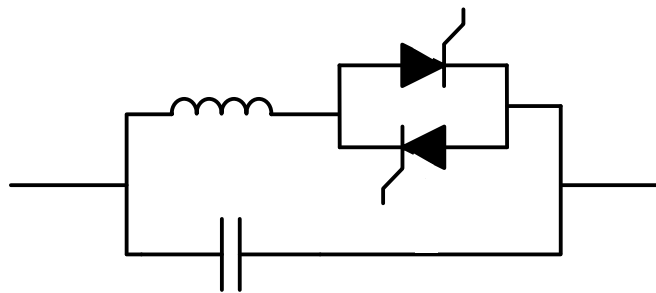
Figure 3.8 Basic confogration of TCSC

The TCSC voltage and current characteristics is shown in Figure 3.9. In the capacitive region, the minimum delay angle (α) sets the limit for the maximum compensating voltage (up to a value of the line current) at which the maximum rated voltage constrains the operation until the rated maximum current is reached. In the inductive region, the maximum delay angle (alpha) limits the voltage at a low line current and the maximum rated thyristor current at high line currents [42].

Chapter 3
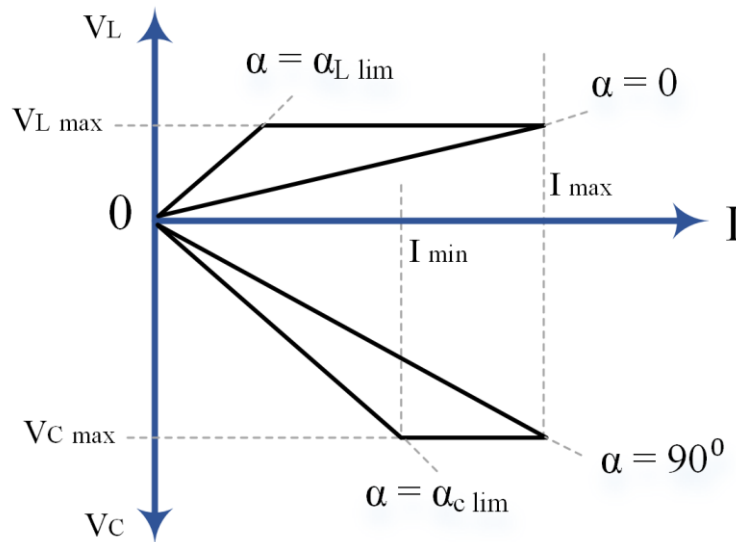
Figure 3.9 TCSC V-I charactrastics

Studies in the literature have introduced the TCSC for power quality enhancement [67-72]. The application of TCSC to improve transmission capacity and mitigate sub synchronous resonance has been introduced in [67, 72]. The impact of using TCSC to reduce the effect of in rush current of a transformer and to enhance power system quality is investigated in [71]. The application of TCSC in improving system stability including wind turbine generators performance has been studied in [68-70].

Chapter 3

3.1.4 Static synchronous series compensator

Static synchronous series compensator (SSSC) is a series connected FACTS device that was introduced in 1989 [42]. The basic configuration of SSSC is shown in Figure 3.10. It consists of a voltage source converter coupled to a dc voltage source and connected with the ac system via a series transformer.
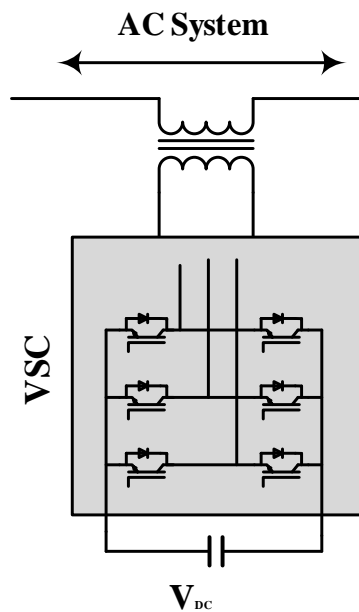
Figure 3.10 Basic configration of SSSC

Figure 3.11 shows the voltage and current characteristics of the SSSC during voltage control operation. The SSSC has the capability to deliver capacitive or inductive compensating voltage independent of the transmission line current and up to the rated current limits. Therefore, during the voltage control mode the SSSC maintains the capacitive or inductive compensating voltage during the change in the line current from zero to I_{max}.

Chapter 3
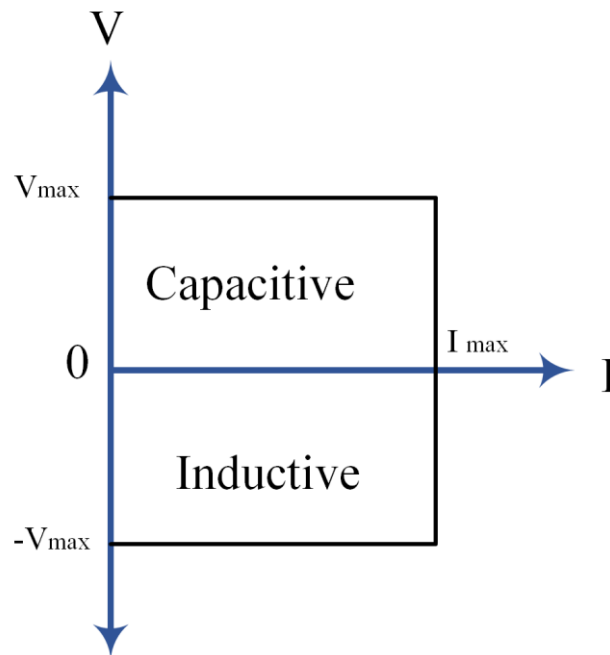
Figure 3.11 SSSC V-I charactrastics

SSSC has been involved in several studies to investigate its applications for stability improvement [73-77]. Damping of Sub-Synchronous resonance by installing static synchronous series compensator was presented in [74, 75]. The application of SSSC to dampen the low frequency oscillations of the power system in [76]. The power flow control and stability improvement of integrating wind farm with an ac grid was presented in [77]. Moreover, the Application of a SSSC to improve stability of a SG-based power system with an offshore wind farm is introduced in [73].

Chapter 3

3.2 Unified power flow controller

The unified power flow controller (UPFC) is a complex power electronic device that was developed to control and optimize the power flow in electrical power transmission systems [41]. Gyugyi introduced the UPFC in 1991 as a versatile device capable of controlling all the parameters affecting the power flow in the transmission line, including voltage, impedance and phase angle [44]. As shown in Fig. 3.12 a UPFC is mainly a combination of a static compensator (STATCOM) and a static synchronous series compensator (SSSC) coupled through a common dc link. The application of the UPFC to power systems has been extensively considered by the power industry due to its many advantages, which include smooth control of both active and reactive power of the system at the PCC and its rapid and independent performance in four quadrant operational moods [38], [78].

Bus A   Bus B

Series   Shunt
Converter   Converter
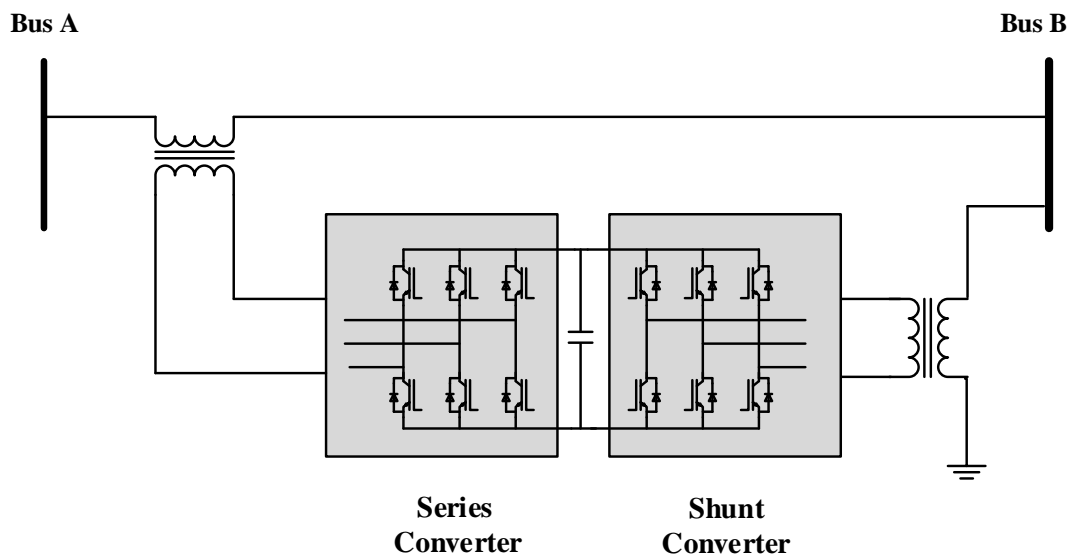
Figure 3.12 Basic configration of UPFC.

Chapter 3

3.2.1 The basic voltage source converter concept
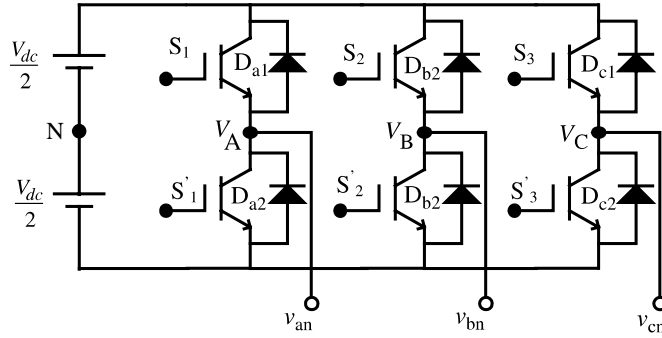
Figure 3.13 Basic configuration of voltage source converter

A basic configuration of a three-phase, IGBT-based voltage source converter is shown in Figure 3.13, in which the voltages across the converter legs are represented by V_A, V_B, and V_C and the load voltage is represented by v_{an}, v_{bn}, and v_{cn}. Assuming a star connected load, the relationship between the voltage across the converter legs and the phase to the neutral load voltage can be expressed as [79]:

$$V_A(t) = v_a(t) + v_{nN}(t)$$
$$V_B(t) = v_b(t) + v_{nN}(t) \quad\quad\quad (3.11)$$
$$V_C(t) = v_c(t) + v_{nN}(t)$$

where

Chapter 3

v_{nN} is the voltage difference between the negative point of the voltage (N) across the dc bus and the load's star common point n.

The values of the line voltages along with the sequence of VSC switches are listed in table 3.1.

Table 3.2 Line voltages for six-step mode of operation

Switching mode	Switches ON	Line Voltage v_{ab}	Phase voltage v_{bc}	Phase voltage v_{ca}
1	S_1, S'_2, S_3	V_{dc}	$-V_{dc}$	0
2	S_1, S'_2, S'_3	V_{dc}	0	$-V_{dc}$
3	S_1, S_2, S'_3,	0	V_{dc}	$-V_{dc}$
4	S'_1, S_2, S'_3	$-V_{dc}$	V_{dc}	0
5	S'_1, S_2, S_3	$-V_{dc}$	0	V_{dc}
6	S'_1, S'_2, S_3	0	$-V_{dc}$	V_{dc}

The basic function of a VSC-based reactive power compensator is to exchange the reactive power with the system it is connected to, according to the difference in the voltage level at the VSC and system terminals. When the AC (OR ac?) voltage of the converter behind the leakage reactance lower than the AC bus voltage, the compensator acts as an inductance connected to the AC system terminals, where it absorbs the reactive power from the system. On the other hand, if the AC voltage of the converter behind the leakage reactance is higher than the AC bus voltage, the compensator will act as a capacitance, where it injects the reactive power to the AC system. During normal operation, the voltage at the terminal of the converter and the AC bus system voltage are equal and no reactive power exchange between the VSC and the system takes place [80]

Chapter 3

By adjusting the switching angle of the VSC valves, the magnitude of the voltage across the converter terminals can be controlled according to the reactive power requirement of the system. On the other hand, adjusting the phase angle of the converter terminal voltages controls the active power could flow from or to the converter [80].

3.2.2 Shunt converter
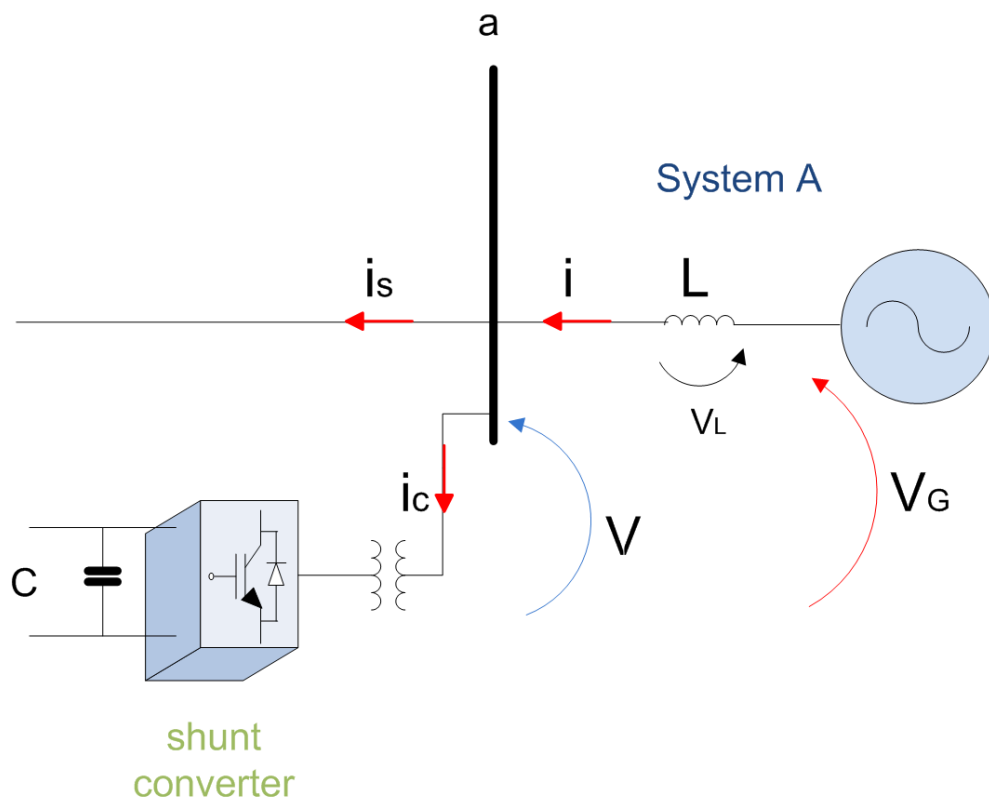
Figure 3.14 Configurations of the UPFC shunt converter and voltage compensation technique.

Chapter 3

To compensate for the voltage of the ac network controlled bus, the shunt converter shown in Fig. 3.14 is used to produce a controlled imaginary current that lags or leads the fundamental component of the voltage by 90°. Inductive current (ic) produces a positive value of the reactive power (i.e. $q_1 > 0$) in order to reduce the magnitude of the voltage across the ac bus, as shown in Fig. 3.15; this mode of operation takes place when there is a surplus reactive power generated as a result of significant load shedding that leads to voltage swell in the system. On the other hand, capacitive current (ic) produces negative reactive power (i.e. $q_1 < 0$) in order to increase the amount of the voltage across the ac network bus. This operational mode takes place in case of voltage sag and short circuit faults.
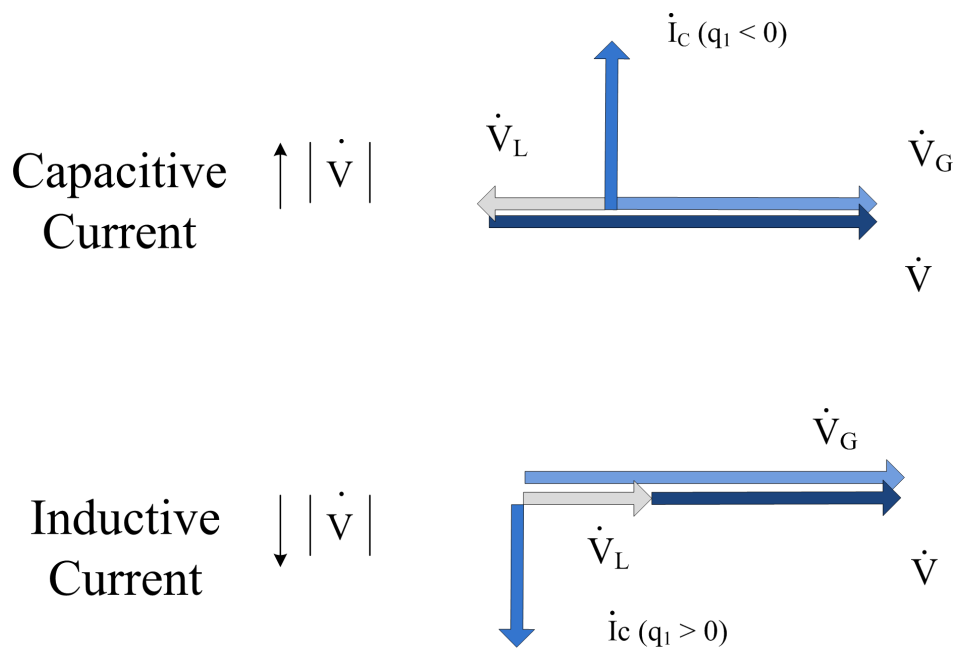
Figure 3.15 Phasor diagram of the voltage compensation mode by the UPFC shunt converter

Chapter 3

3.2.3 Series converter
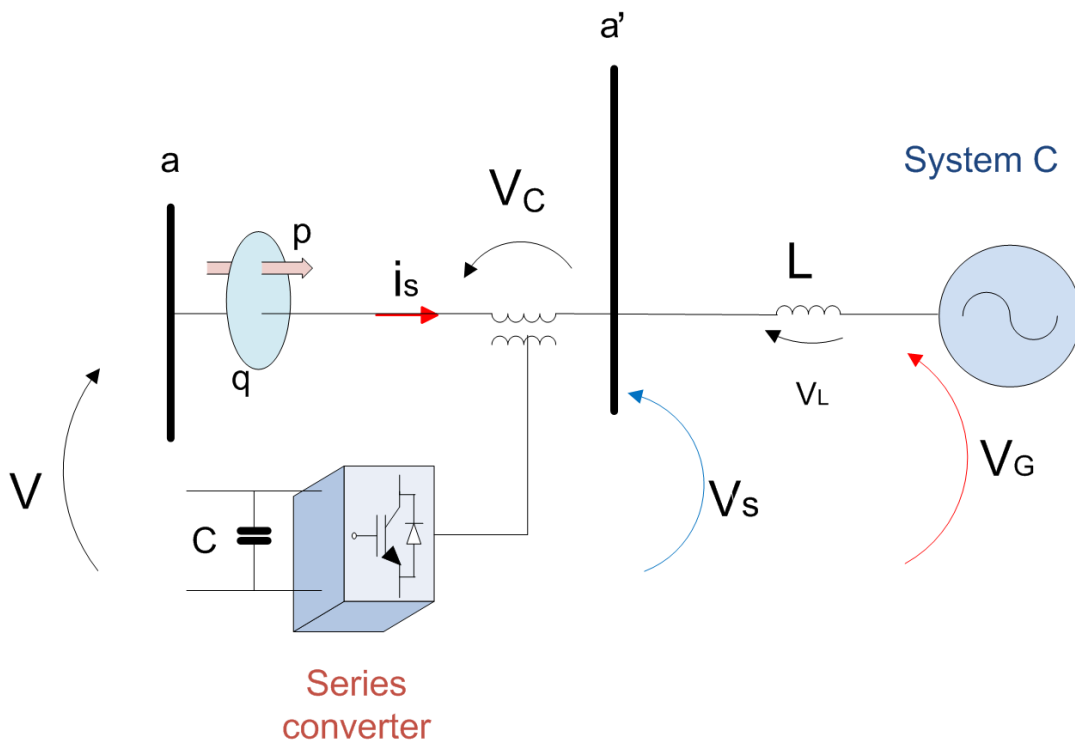
Figure 3.16 Power flow control by the series converter of the UPFC.

The UPFC series converter controls the active and reactive power by controlling the voltage at the ac network bus and the current (is) of the transmission system. The voltage at the generator bus (v_s) is regulated by controlling the series voltage (v_c), which in turn will regulate the magnitude of the current (i_s) to meet the required active power reference P_{REF} and reactive power reference Q_{REF} (Fig. 3.16).

Chapter 3
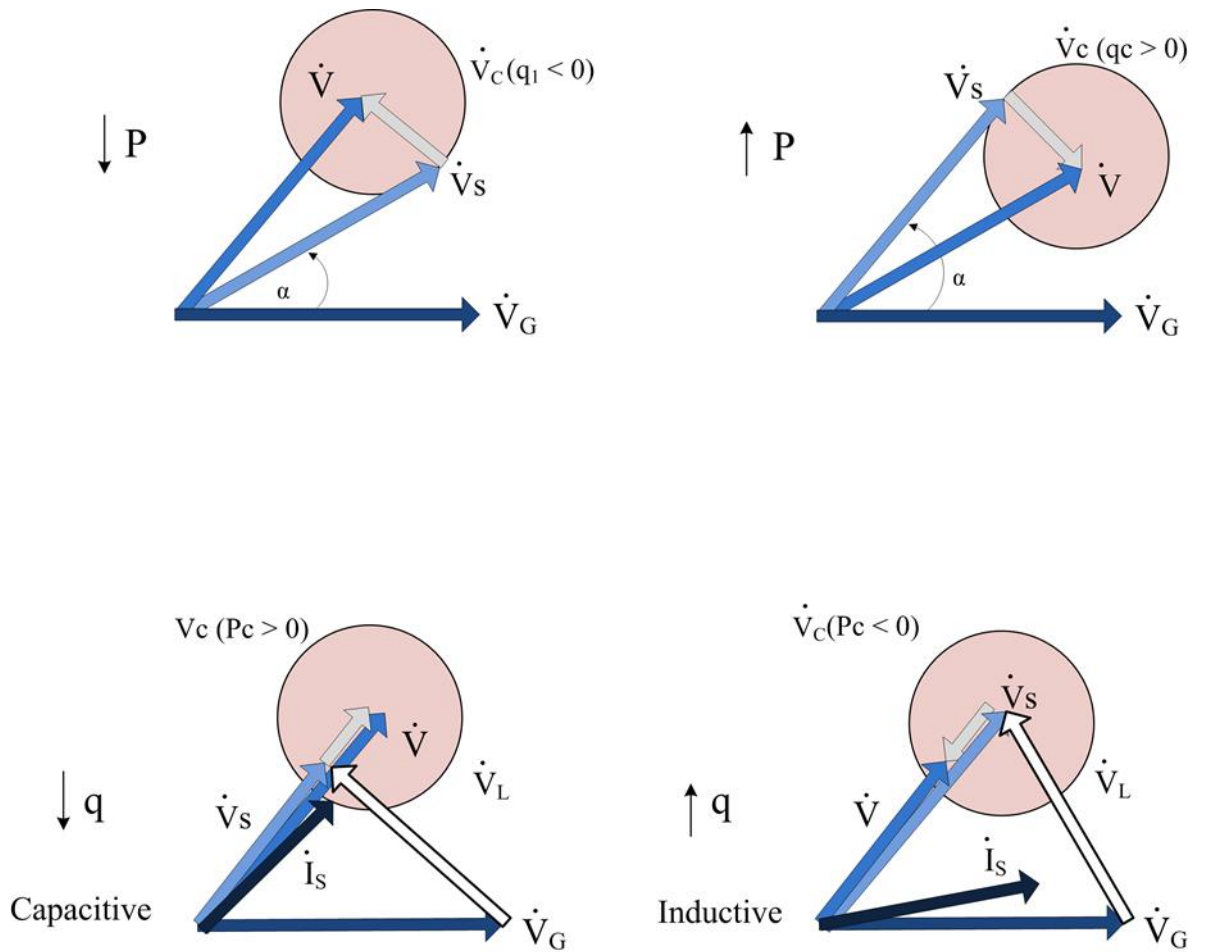
Figure 3.17 Phasor diagram of the UPFC's series converter in the operational mode of active and reactive power control.

To produce the required demand of the active P_{REF} and the reactive Q_{REF} power, the UPFC controls the voltage components $V_C(q_C)$ and $V_C(p_C)$ in series with the transmission line, which in turn control p and q, as shown in Fig 3.17. The real power P decreases when the voltage component V_C (q_C) leads the voltage V by $90°$, while the opposite occurs when the voltage V_C (q_C) lags the voltage component V by $90°$. In

Chapter 3

contrast, the reactive power decrease and the current phasor I_S becomes more capacitive when the compensating voltage is greater than zero, V_C ($p_C > 0$), whilst the reactive power increases and the current phasor I_S becomes more inductive when the compensating voltage is less than zero, V_C ($p_C < 0$).

3.2.4 UPFC Control System

In [81] an adaptive neuro-fuzzy controller was designed for UPFC. The results show that the settling time and amplitude of the low frequency oscillations are reduced by the proposed adaptive neuro-fuzzy controller. A Lyapunov-based adaptive neural controller was proposed in [82] for the UPFC to improve the transient stability of the studied system. In this study, the dynamic characteristics of the UPFC were investigated and a supplementary control system was developed to suppress power swings. Damping of the power system oscillation using UPFC based on a simple PI controller was presented in [83]. The fuzzy-logic control scheme was presented in [84] to improve the power system stability during transient conditions. In [85], application of UPFC based on nonlinear PID and tracker controller was introduced. Table 3.2 summaries the various applications of the UPFC along with the proposed controllers that are published in the literatures.

Chapter 3

Table 3.3 Summary of the applications of UPFC along with the proposed controllers published in the literatures.

	Controller	Application	Ref.
1	Neuro Fuzzy	Damping Low Frequency Oscillations	[81]
2	Gravitational Search Algorithm (GSA)		[86]
3	Lyapunov	Transient Stability Enhancement	[82]
4	Neuro Controller	Damping Power System Oscillation	[87]
5			[83]
6	PI controller	Power-Flow Control Performance Analysis of UPFC	[88]
7		Real and Reactive Power Coordination for a UPFC	[89]
8	Radial Basis Function Neural Network (RBFNN)		[90]
9	Nonlinear Variable-gain Fuzzy Controller		[84]
10	Nonlinear PID (NLPID) Controller		[85]
11	Feed-Back Linearization Controller (FBLC)	Improving Transient Stability Performance of Power System	[91]
12	Nonlinear Optimal Predictive Controller		[92]
13	Based on H_2 method	Damping of Oscillation in Distribution System	[93]

Chapter 3

3.2.4.1 Proposed control system

IGBTs-based converters are implemented in the proposed UPFC due to its advantages over GTOs, since IGBT has a higher switching frequency range (2-20 kHz), compared with GTO (1 kHz [94]). In the proposed system, the shunt and the series converters of the UPFC are controlled using a hysteresis current controller (HCC) and a proportional Integral controller (PI), respectively, as will be elaborated below. The widely used park's transformation or the so-called dq transformation that was introduced by Park in 1929 [95] is used in the controller proposed herein. It is a mathematical transformation that can be applied to any arbitrary three-phase system to calculate the two equivalent components in the dq reference frame; this arrangement has the advantage of transforming the main component of waveform to a constant DC term under steady state conditions. The transformation equation is given below:

$$\begin{bmatrix} x_d \\ x_q \\ x_0 \end{bmatrix} = \sqrt{2/3} \begin{bmatrix} cos\theta_d & cos(\theta_d - 2\pi/3) & cos(\theta_d + 2\pi/3) \\ -sin\theta_d & -sin(\theta_d - 2\pi/3) & -sin(\theta_d + 2\pi/3) \\ 1/\sqrt{2} & 1/\sqrt{2} & 1/\sqrt{2} \end{bmatrix} \begin{bmatrix} x_a \\ x_b \\ x_c \end{bmatrix} \quad (3.12)$$

Chapter 3

Quantities in the dq reference frame can be transferred to three-phase using the inverse transformation of (3.12) as:

$$\begin{bmatrix} x_a \\ x_b \\ x_c \end{bmatrix} = \sqrt{2/3} \begin{bmatrix} cos\theta_d & -sin\theta_d & 1/\sqrt{2} \\ cos(\theta_d - 2\pi/3) & -sin(\theta_d - 2\pi/3) & 1/\sqrt{2} \\ cos(\theta_d + 2\pi/3) & -sin(\theta_d + 2\pi/3) & 1/\sqrt{2} \end{bmatrix} \begin{bmatrix} x_d \\ x_q \\ x_0 \end{bmatrix} \qquad (3.13)$$

Where

$$\theta_d = \omega_d + \theta$$

ω_d is the angular velocity of the signals to be transformed

θ is the angle of the initial state.

3.2.4.1.1 Hysteresis current controller

The hysteresis current control (HCC) method has the advantages of being effective and simple, in addition to the fact that it does not require complex processor to implement. The main concept of the HCC is that switching pattern generated by the convertor, which is effected by comparing the actual values of the phase current with a fixed tolerance band around the reference value of the current associated with that phase. Figure 3.18 shows the HCC scheme in the position where the measured load current is maintained within the hysteresis band by controlling the switching state of the respective converter node voltage. However, the other two phases can affect this

Chapter 3

type of band control, which may give rise to high frequency in the switching signal in consequence of the interference between the phases (referred as inter-phases dependency) [96]. Inter-phases dependency can be reduced by applying the phase-locked loop technique to keep the converter switching at a fixed predetermined frequency level [97].
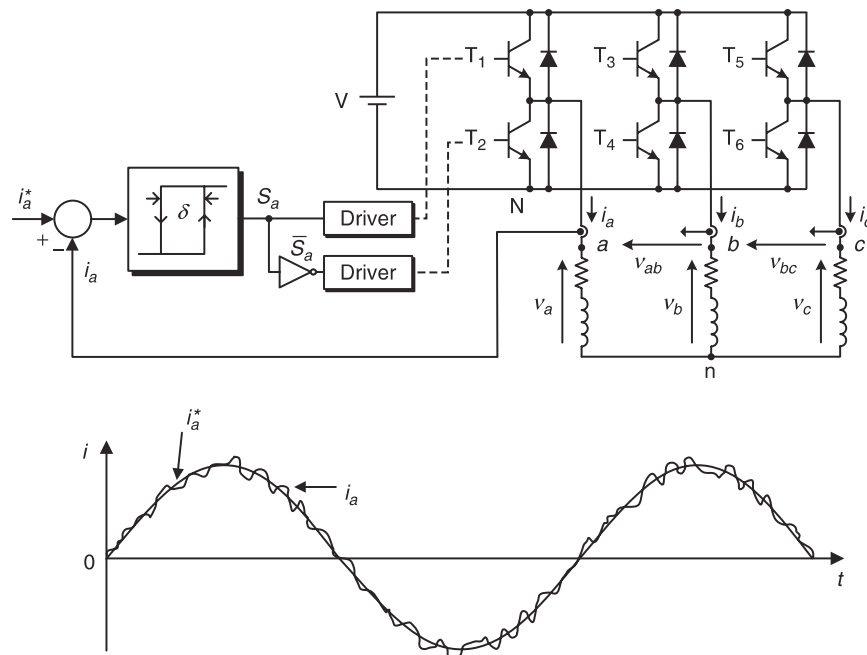
Figure 3.18 Basic concept of Hysteresis current control for a three phase converter

As shown in Fig. 3.19, the deriving signals for the switches of the UPFC shunt converter are generated by comparing the values of the reference currents ($I_{abc}*$) with the three-phase line currents (I_{abc}), which are derived using I_d* and I_q* references. The values of I_d* and I_q* are generated based on the error values of the voltage across the dc-link capacitor (V_{DC}) and the generator terminal voltage (V_g) by a

Chapter 3

traditional proportional integral (PI) controller. The values of I_d* and I_q* are

converted using the Park transformation (*dq0-abc*) to create the reference values of

the current ($I_{abc}*$).
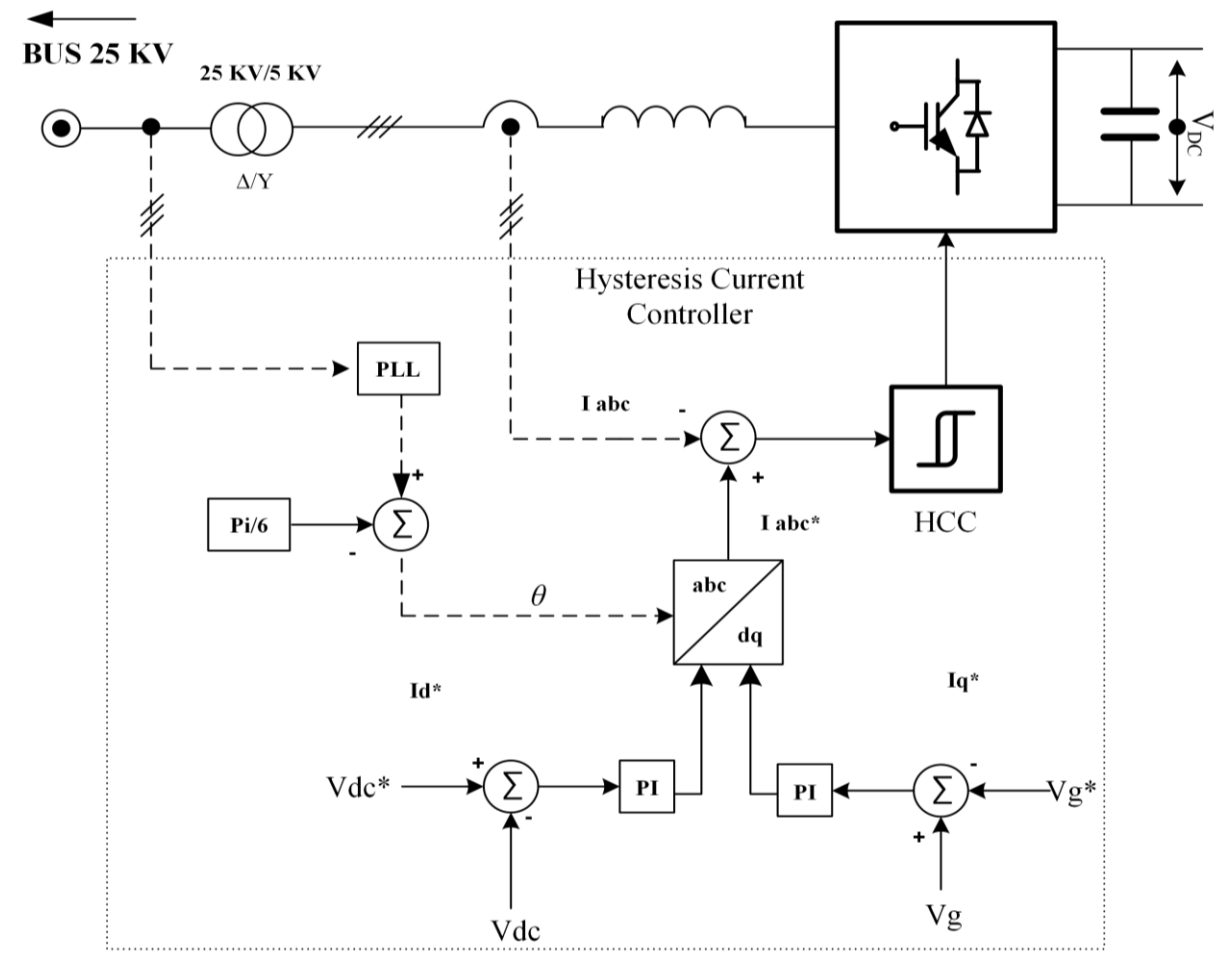
Figure 3.19 Shunt converter HCC system

Chapter 3

3.2.4.1.2 The proportional integral controller

The main role of the UPFC series converter is to control the active and reactive power flow through the transmission line, by inserting a compensated voltage with controllable magnitude and phase in series with the transmission line. The a-b-c components at the point of common coupling (PCC) and the transmission line current are converted to the d-q reference frame using the Clarke-Park transformation technique. As shown in Figure 3.20 the differences between the generator active and reactive powers and their pre-set values are used as input signals to the PI controllers, which are tuned to generate the reference voltage values in the d-q reference frame (V_d^* and V_q^*) required for controlling the series converter switches using pulse width nodulation (PWM). The active power P and reactive power Q in the d-q reference frame can be calculated as follows [32]:

$$P = V_d\, I_d + V_q\, I_q \qquad (3.14)$$

$$Q = V_q\, I_d - V_d\, I_q \qquad (3.15)$$

Chapter 3
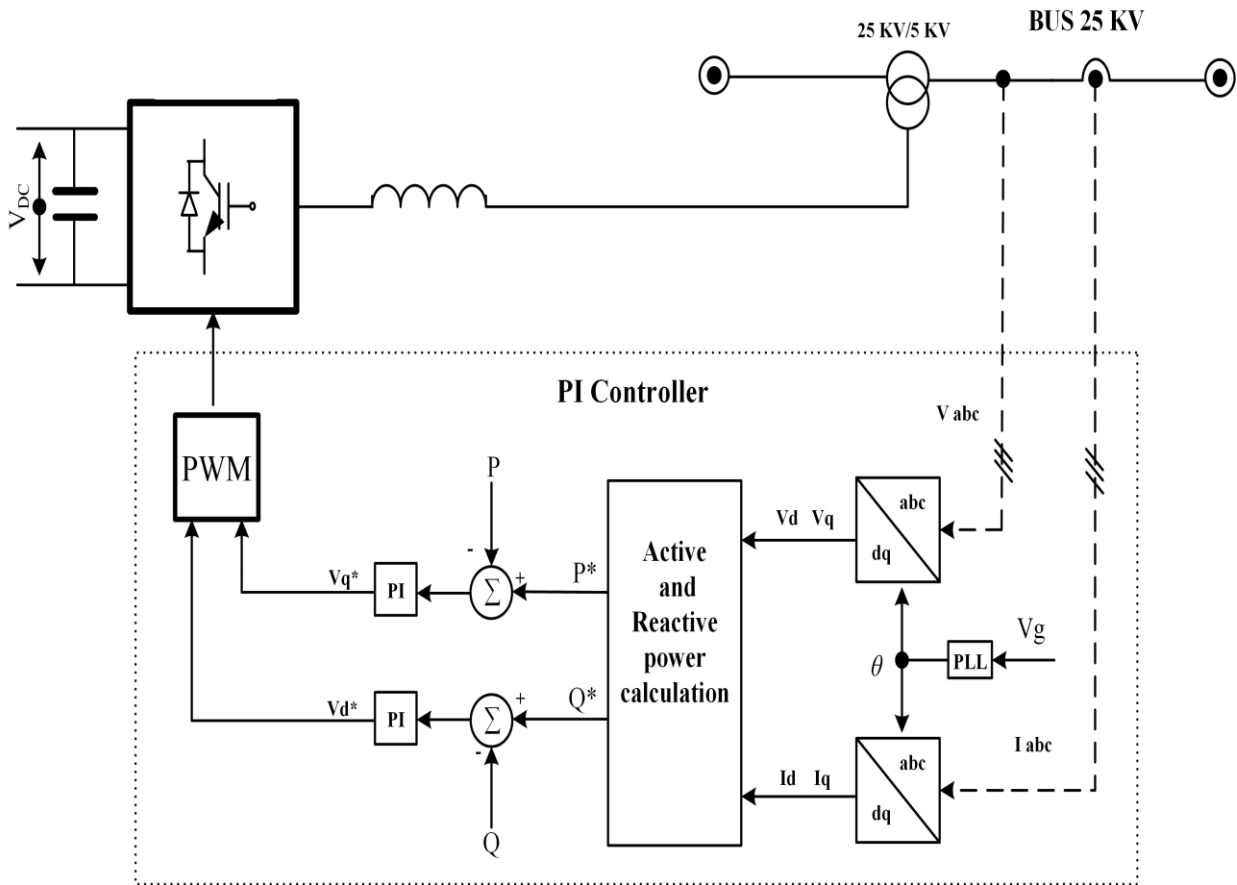
Figure 3.20 Series converter control system

Chapter 3

4

Application of UPFC to Improve the Overall Performance of a DFIG-based WECS during Grid Side Faults

---

4.1 Introduction

In a Doubly Fed Induction Generator (DFIG)-based Wind Energy Conversion System (WECS) as shown in Fig. 4.1, the DFIG stator circuit is connected directly to

the ac network at the point of common coupling (PCC) via a transformer, whereas rotor circuit is connected to the PCC via a back-to-back partial-scale voltage source converter (VSC) and the coupling transformer. The voltage source converter facilitates the variable [24] speed operation of the DFIG [98],[99]. During the initial stage of introducing WECS to the electrical energy market, the disconnection of a wind turbine generators (WTGs) from the grid during a fault event at the ac network side was allowed to protect the wind turbine and the converter switches form any possible damages [36]. Currently, the developed grid codes require WTGs to ride-through intermittent fault conditions to remain connected, thereby supporting the grid under such events. This will assure sustainable power delivery to the grid during faults and abnormal operating conditions [36]. Improving DFIG fault ride through (FRT) capability can be achieved by implementing new control schemes for WECS to make them comply with the various grid codes that have been established by transmission system engineers as shown in the literature [100-104]; however this approach is only effective for new WECS installations. A cost effective approach to improve the FRT capability of the existing WECS is by connecting flexible ac transmission system (FACTS) device to the PCC [105]. A proper FACTS controller can also aid in overcoming some of the drawbacks of the DFIG (which include its high sensitivity to grid faults [23, 106]). Reference can be made to previous studies on the low voltage ride through capability of the DFIG-based WECS [100-104]. Unfortunately, the problem of voltage swell has not been investigated thoroughly in the literature, despite the fact that its occurrence can cause a surge in the the voltage at the point of common coupling and consequently violate the upper safety margin of

Chapter 4

the grid code requirements [107-109]. If not carefully mitigated, these faults may lead to voltage fluctuation across the terminal of the DFIG, high current within DFIG converter switches and voltage swell within the dc link capacitor of the converter station.

As previously mentioned in Chapter 3 application of the UPFC in power systems was investigated by many researchers [9, 38, 78, 83, 85, 110-118]. However, studies concerning application of UPFC to WECS are limited. Moreover, majority of the existing studies limit the use of UPFC to smoothen the output power of fixed speed WECS during wind speed fluctuation to avoid system instability [110].

Following on from the limitations discussed above concerning UPFC, this chapter introduces new applications of it to improve the overall performance of DFIG-based WECS during fault events at the grid side. A new UPFC control approach that combines the hysteresis current control (HCC) and proportional integral control (PI), as explained in Chapter 3 is proposed herein. Simulation was carried out using the Simulink/Matlab software and the results obtained are analysed to examine the performance of WECS with and without the connection of UPFC.

Chapter 4

66
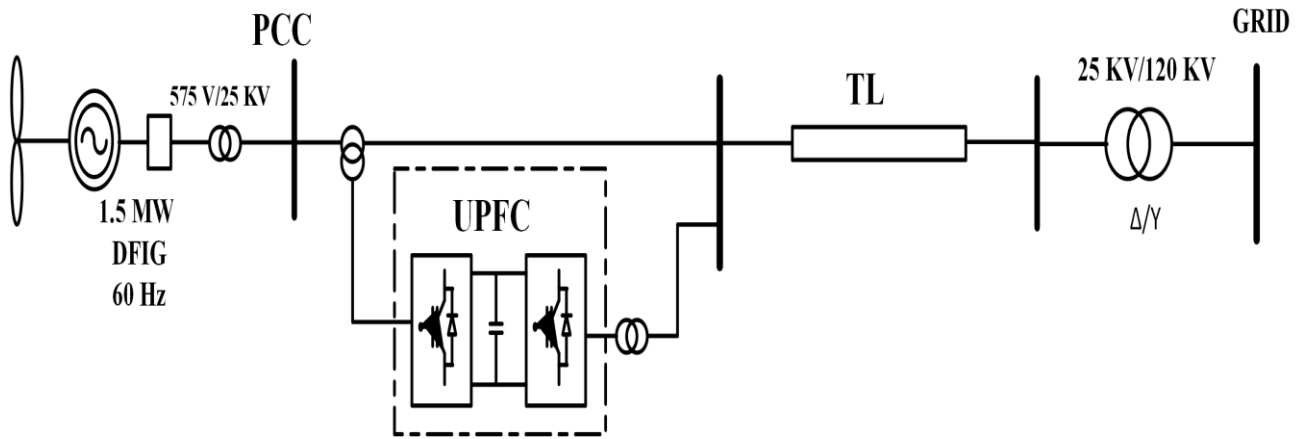
Figure 4.1 Schematic of the Proposed System

Fig. 4.1 shows the proposed system, which consists of a wind farm of six DFIG-based wind turbines integrated with the ac grid at the point of common coupling (PCC), with each DFIG being rated at 1.5 MW. The DFIG rotor winding is connected to a bi-directional back to back voltage source converter, while the stator winding is connected directly to the ac network via a step up transformer. The wind turbines are connected to the grid via a 30 km transmission line and a step up transformer. During modelling, the ac network is simulated as an ideal three-phase voltage source of constant frequency and voltage. Under normal operating conditions, the reactive power delivered by the DFIG is controlled at zero MVar to maintain a unity power factor connection at the PCC. In the proposed case study, the average wind speed is assumed to be 15 m/s and the generator's nominal speed is 1.2 pu, while output active power of the turbine is 1.0 pu. The proposed UPFC is connected to the PCC bus.

Chapter 4

4.2   Case study 1: Low Voltage Ride Through

A significant voltage drop of 0.4 pu of the nominal value is assumed at the grid side of the proposed system (Fig. 4.1) at t = 6s, and this drop is assumed to last for 5 cycles. The simulation results shown in Figure. 4.2, indicate that the voltage across the PCC will decrease to 0.43 pu when the UPFC is not connected. On the other hand, this voltage drop is regulated to a value of 0.87 pu by connecting the UPFC to the PCC bus. Based on the grid codes requirements, the regulated voltage (using UPFC) is assumed to work provide a safety margin by wind turbine designers, as can be seen in Fig. 4.2 [106]. Fig. 4.3 shows that, during the voltage drop and with the presence of UPFC, the reactive power support provided by the DFIG to the grid is decreased by an amount equivalent to that compensated for by the UPFC. Consequently, the steady state condition is reached faster, compared with the system without UPFC. In the absence of UPFC, the active power delivered by the wind turbine generator is significantly decreased by about 0.45 pu during the sag event as shown in Fig. 4.4, while with the presence of the UPFC, the active power can be also modulated and the settling time reduces. The DFIG power reduction results in acceleration of the shaft to stabilize the imbalance in the delivered power as can be seen in Fig. 4.5. However, with the presence of the UPFC, the drop in the power generated by the DFIG decreases, which leads to a reduction in both the speed overshooting and settling time. The voltage across the dc link capacitor of the DFIG (V_{DC}) experiences an oscillation of 60 Hz frequency during and upon the fault clearance, as shown in Fig. 4.6. With the UPFC being connected at the PCC, voltage overshooting across the capacitor of the dc link decreases.

Chapter 4

Figure 4.2 Voltage at the PCC with and without UPFC during voltage sag

Figure 4.3 DFIG reactive power response with and without during voltage sag

Figure 4.4 DFIG active power response with and without UPFC during voltage sag

Chapter 4

69
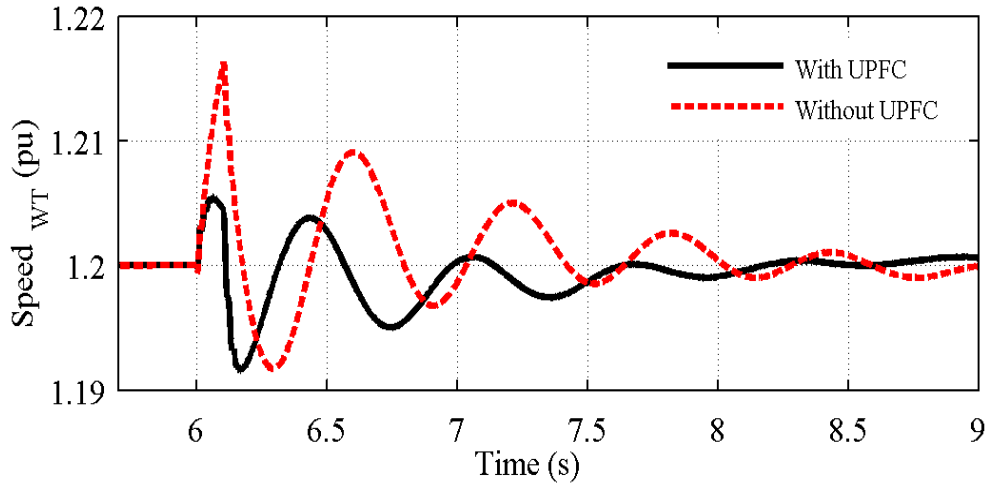
Figure 4.5 DFIG shaft speed response with and without UPFC during voltage sag
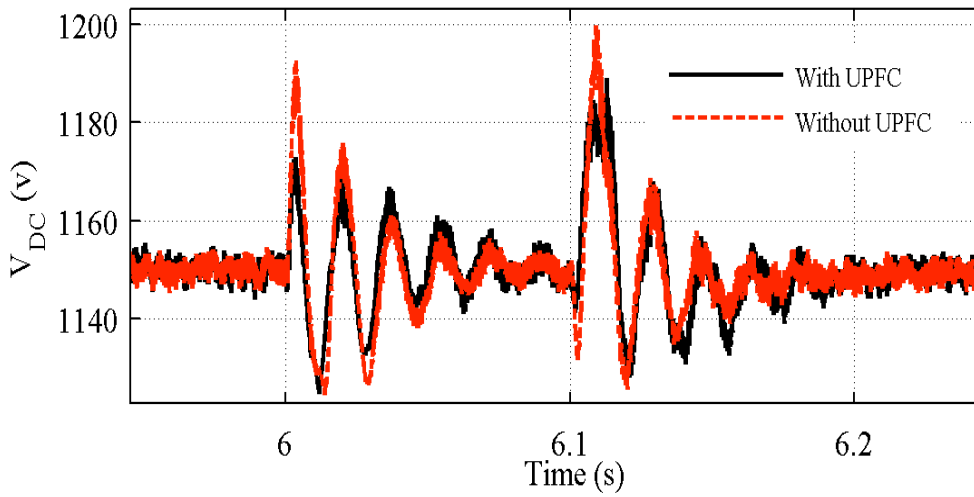
Figure 4.6 DC Voltage link of DFIG with and without UPFC during voltage sag

Chapter 4

4.3   Case Study 2: High Voltage Ride Through

Voltage swell occurs due to switching on a large capacitor bank or switching off a large load. A 1.4 pu voltage swell was simulated at the grid terminals and was assumed to last for 5 cycles, starting at t = 6s. Fig. 4.7 reveals that this fault causes the voltage at the PCC to increase by more than 30% without the connection of the UPFC, while this voltage is settled to a level less than 1.1 pu when the UPFC is connected to the PCC. Without UPFC, the voltage at the PCC is compensated by the DFIG, as it absorbs the excessive reactive power as shown in Fig. 4.8. By the connection of the UPFC to the PCC bus, the reactive power profile of the DFIG is significantly improved and the unity power factor operation is almost maintained. The delivered power by the DFIG will increase during the voltage swell fault event and will be decreased when the fault is cleared, as can be seen in Fig. 4.9. The maximum power overshooting and settling time are substantially reduced when the UPFC is connected to the system. Due to the increment of DFIG generated power during a voltage swell event, the generator shaft speed is slightly retarded through fault duration and settles at a lower steady state level than the pre-set level (1.2 pu), as shown in Fig. 4.10. This figure also shows that the generator shaft speed profile is significantly improved with the connection of the UPFC. As can be seen in Fig. 4.11, the voltage across the dc link capacitor of the DFIG exhibits significant overshooting and oscillations during the voltage swell event when the the UPFC is not connected to the system. This overshooting may eventually result in blocking of the converters [106]. It is noted that, with the proposed UPFC controller, the voltage overshooting levels are significantly reduced.
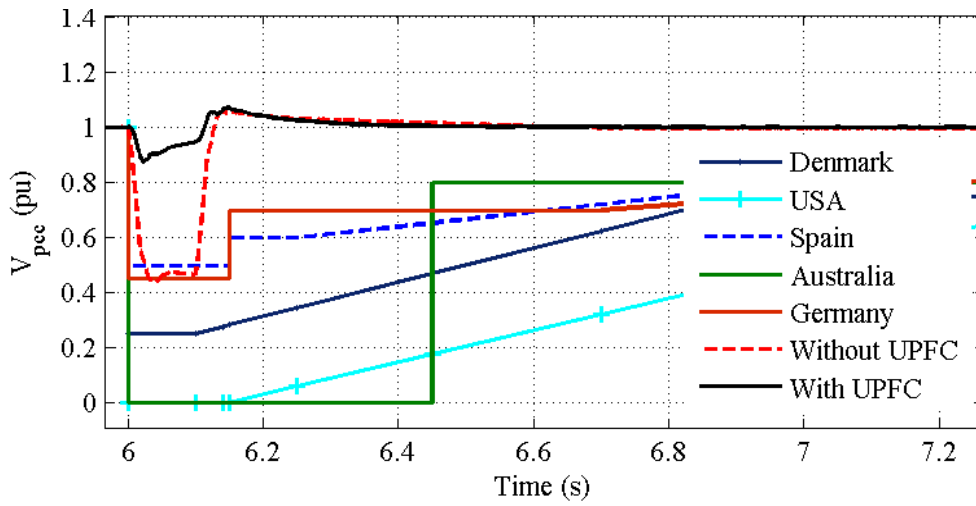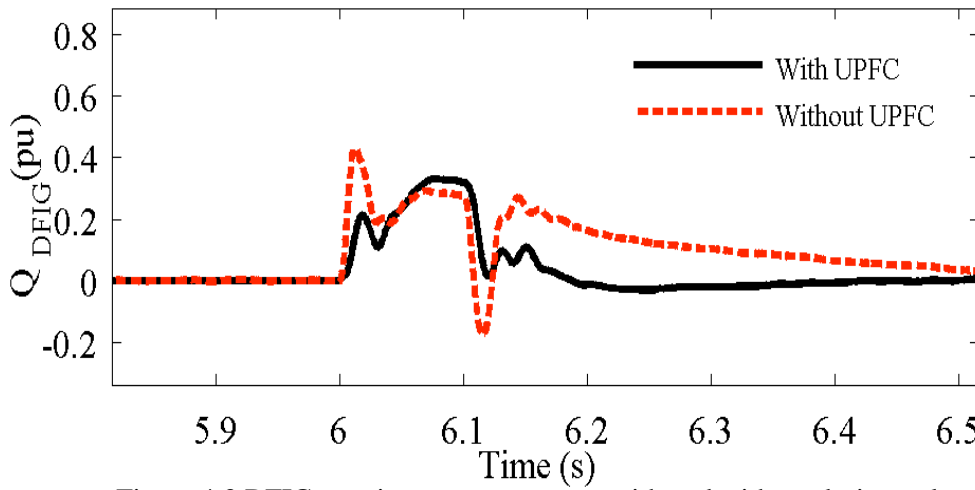
Chapter 4
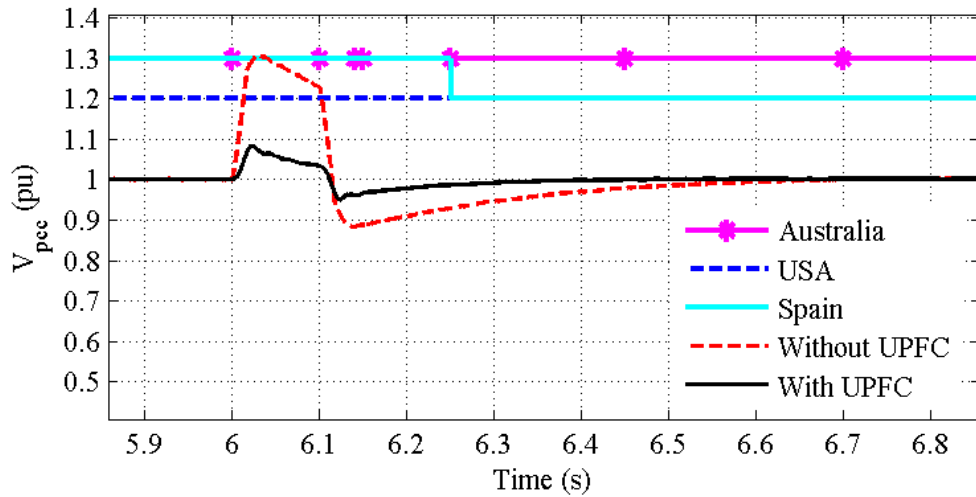
Figure 4.7 Voltage at the PCC with and without UPFC during voltage swell
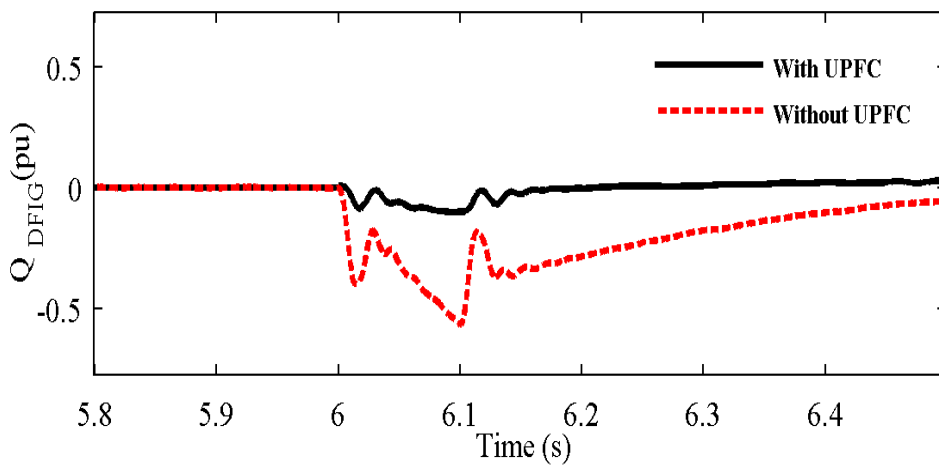
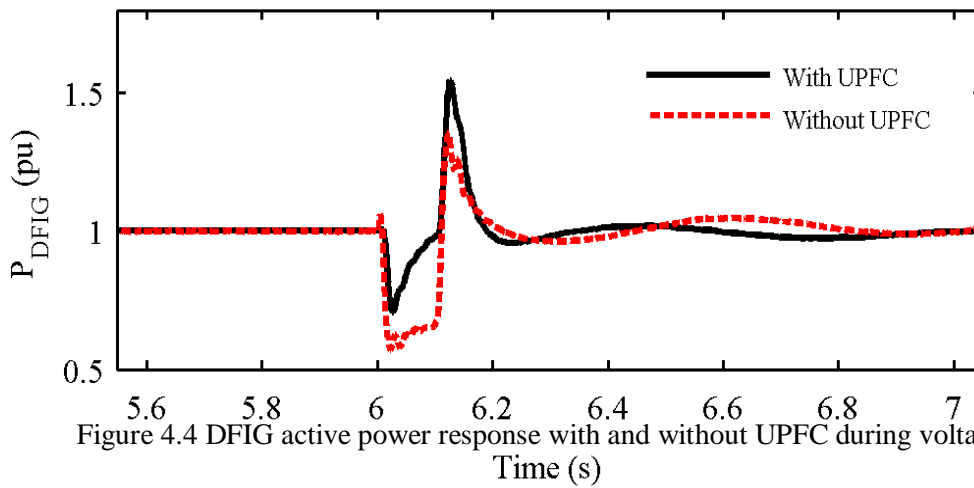Figure 4.8 DFIG reactive power response with and without during voltage swell

Figure 4.9 DFIG reactive power response with and without during voltage swell

Chapter 4

72

Figure 4.10 DFIG shaft speed response with and without UPFC during voltage swell
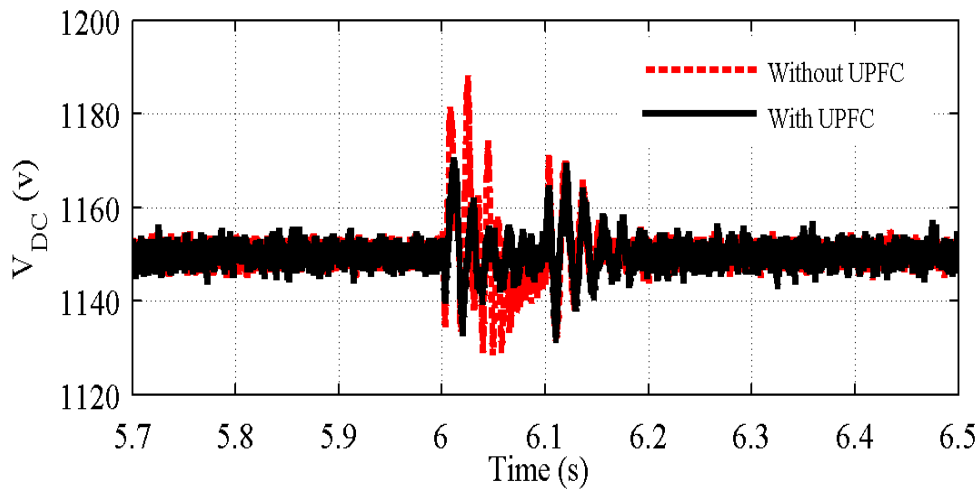
Figure 4.11 DC link Voltage of DFIG with and without UPFC during voltage swell

4.4   Case Study 3: Three Phase Short Circuit

A fault of a three-phase short circuit is simulated at the grid side of the system under study at t = 6 s and is assumed to last for 3 cycles. Figs. 4.12 through Figure 4.16 show the dynamic response of the DFIG with and without the connection of the UPFC. The voltage magnitude at the PCC drops to 0.1 pu in the case when the UPFC is not connected, as shown in Fig. 4.12. On the other hand, when the UPFC is connected, the voltage drop at the PCC is modulated to 0.8 pu, which is attributed to the reactive power

Chapter 4   73

support of the UPFC as clearly seen in Fig. 4.13. In fact, the DFIG output active power is significantly reduced due to the short circuit fault at the grid side (when the UPFC is not connected) and this gets improved with the connection of the UPFC, as shown in Fig. 4.14. Due the drop in the generated power (if the UPFC is not connected), the DFIG shaft speed is accelerated to compensate for the power imbalance and the shaft will experience oscillations; these otherwise oscillations are substantially reduced when the proposed UPFC controller is connected (Fig. 4.15). The voltage across the DFIG dc link capacitor is affected during the three-Phase short circuit event (in the base case of no UPFC), as shown in Figure 4.16. When the UPFC is connected to the system, the voltage overshooting is reduced through fault duration.
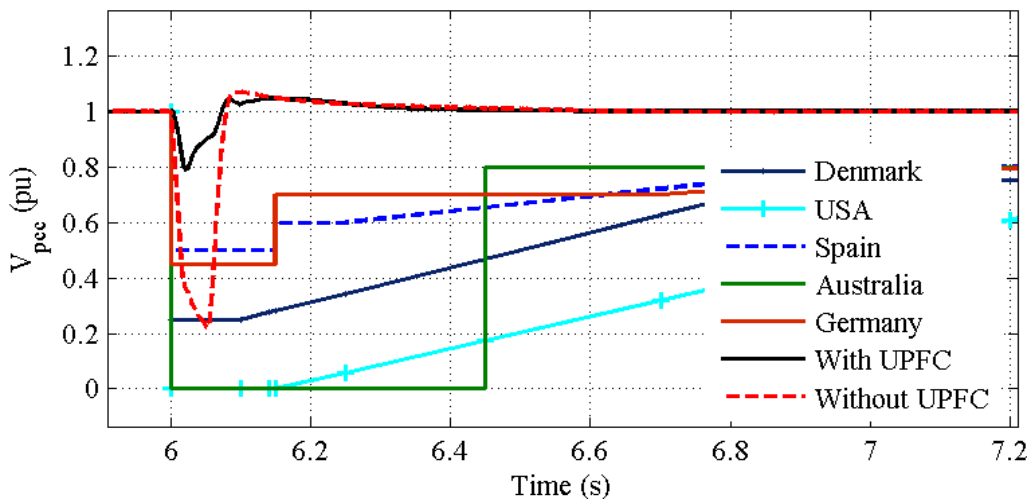
Figure 4.12 Voltage at the PCC with and without UPFC during 3Phase SC

Chapter 4

74
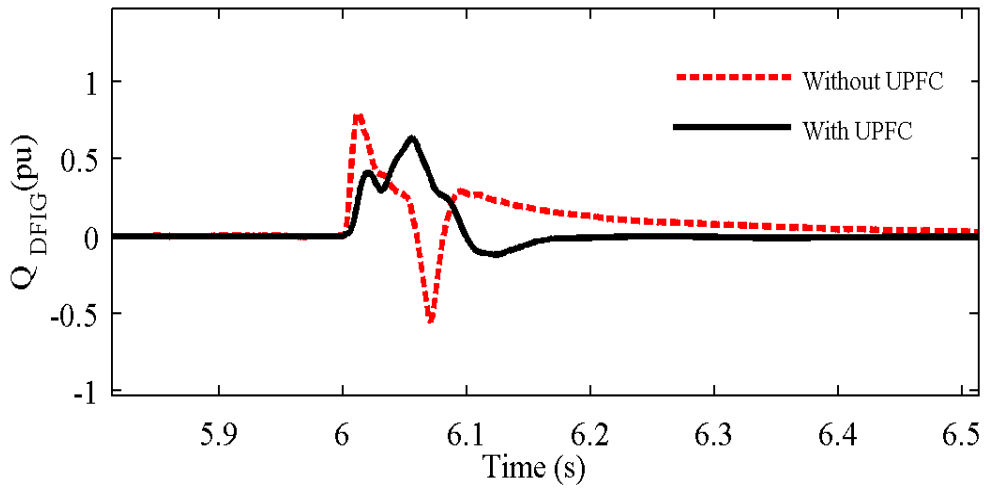
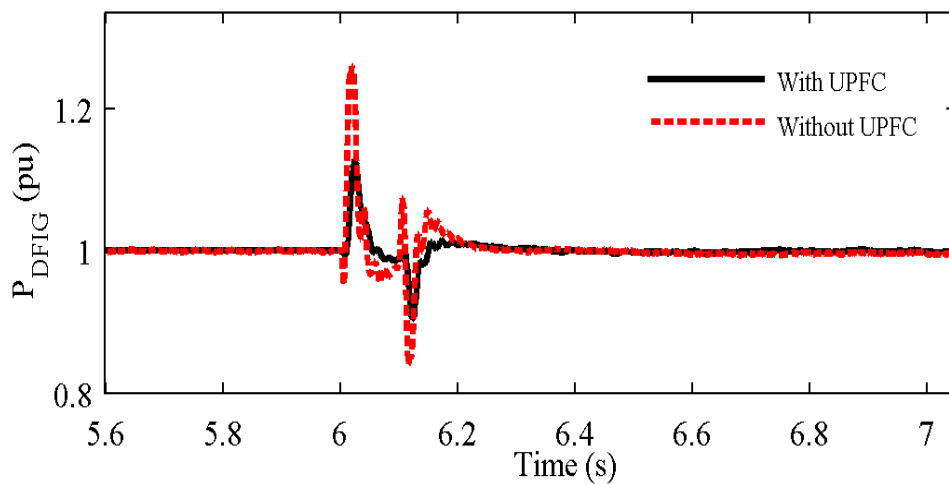Figure 4.13 DFIG reactive power response with and without during 3Phase SC
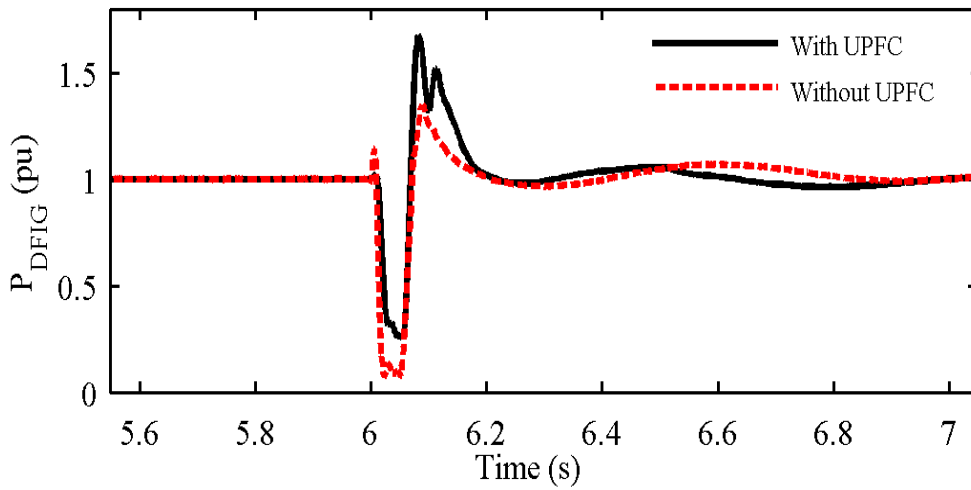
Figure 4.14 DFIG active power response with and without UPFC during 3Phase SC
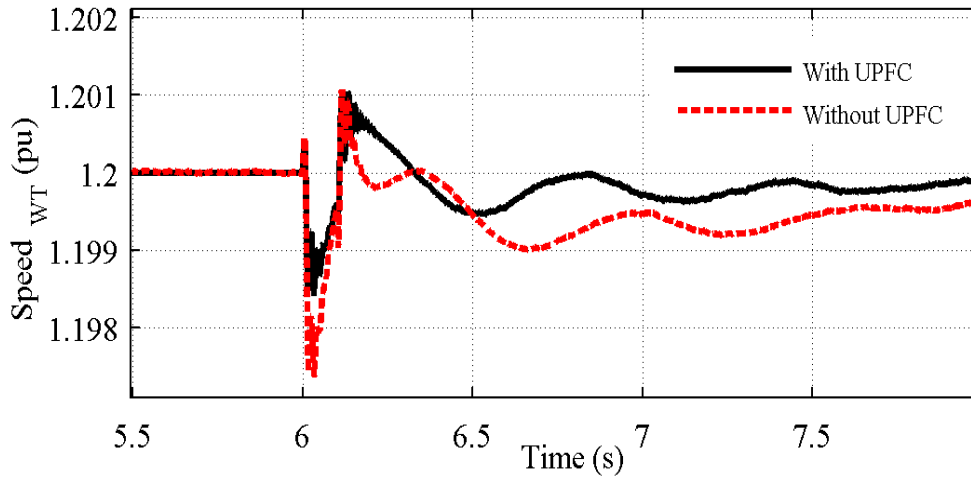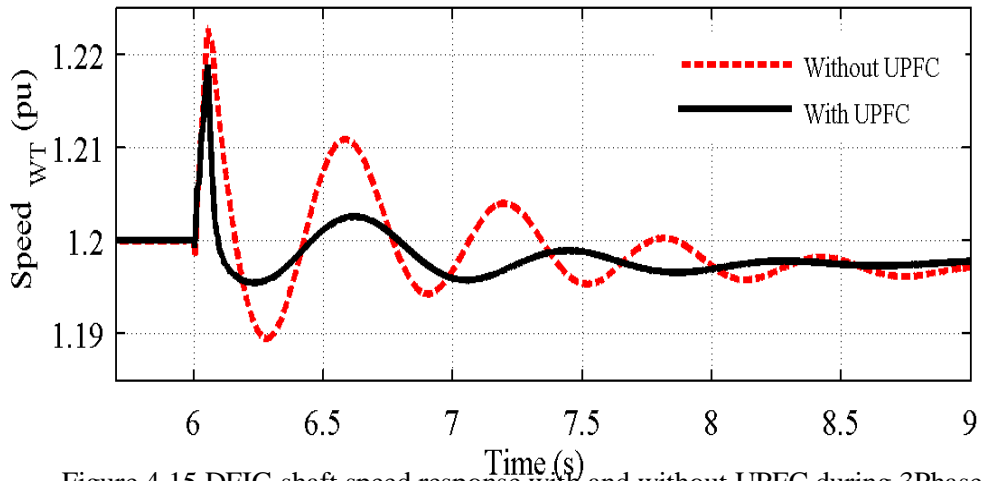

Figure 4.15 DFIG shaft speed response with and without UPFC during 3Phase SC

Chapter 4

75
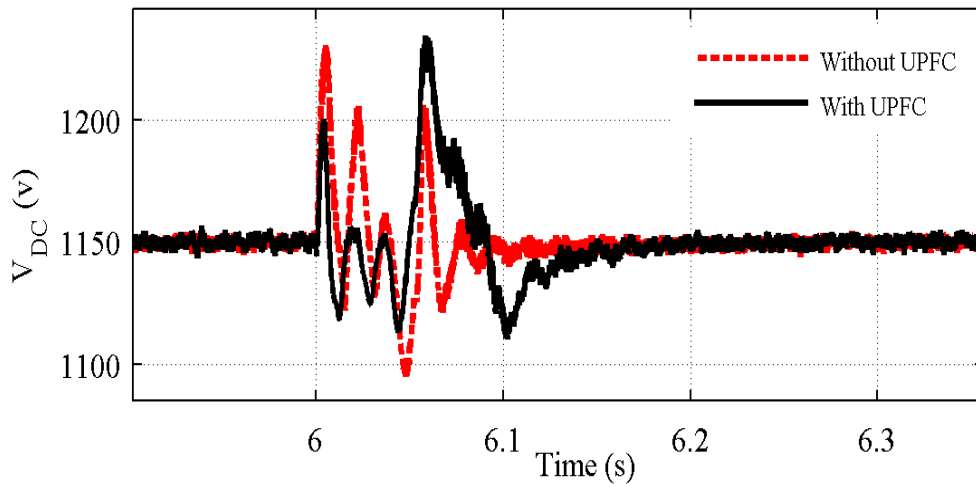
Figure 4.16 DC link Voltage of DFIG with and without UPFC during 3Phase SC

4.5   UPFC Response during fault events

Depending on the fault type, UPFC has three modes of operation, as explained below.

Standby mode: this mode of operation occurs during normal operating conditions, where there will be no energy exchange between the system and the UPFC.

Capacitive operating mode: this mode of operation occurs during voltage sag and short circuit faults at the grid side. When the voltage drop takes place at the PCC at t = 6 s in the studied cases, the UPFC is function in a capacitive mode, where the UPFC terminal current leads the bus voltage, as shown in Fig. 4.17 and Fig. 4.20. As a result, the reactive power is instantly injected by the UPFC to support the grid and to regulate the voltage at the PCC, as shown in Figs. 4.18. As the shaft speed will be

Chapter 4

slightly impacted during and upon the clearance of the voltage sag fault, the UPFC aids in improving the active power profile at the PCC, as can be seen in Figure 4.19. The active power modulation is substantially higher in the case of the three phase short circuit fault, as shown in Fig. 4.22. The phase angle and magnitude of UPFC current and voltage control the amount of active and reactive power support. After clearing the fault, the UPFC controller acts to retain the standby mode of operation by reducing its current to zero level as shown in Figs. 4.17.

Figure 4.17 UPFC terminal voltage and current during voltage sag
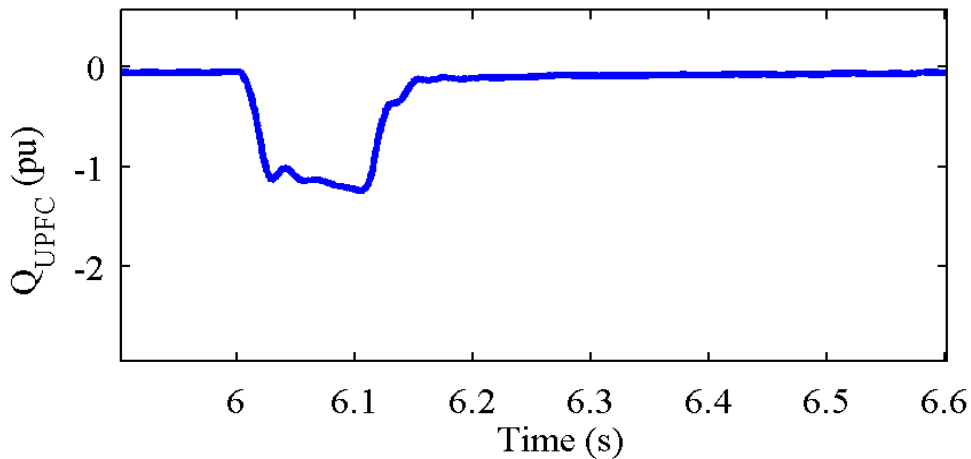
Figure 4.18 UPFC reactive Power during voltage sag

Chapter 4
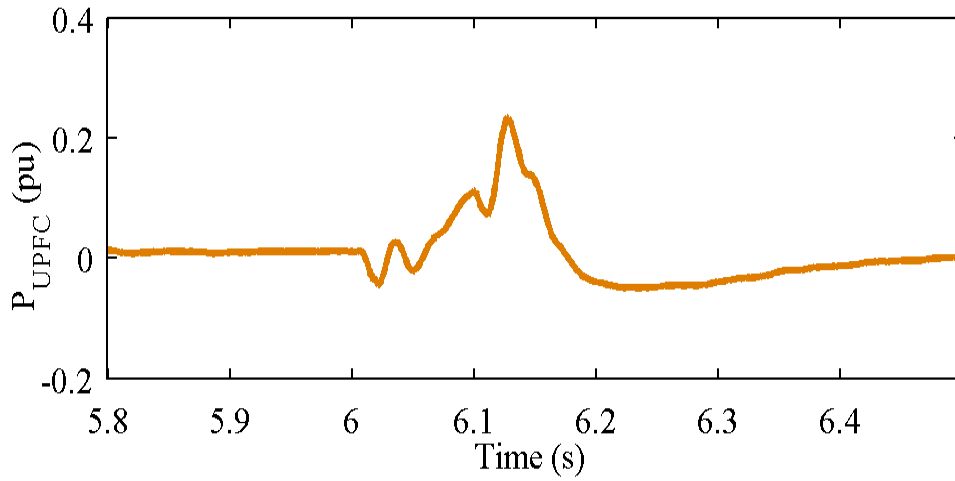
Figure 4.19 UPFC active Power during voltage sag
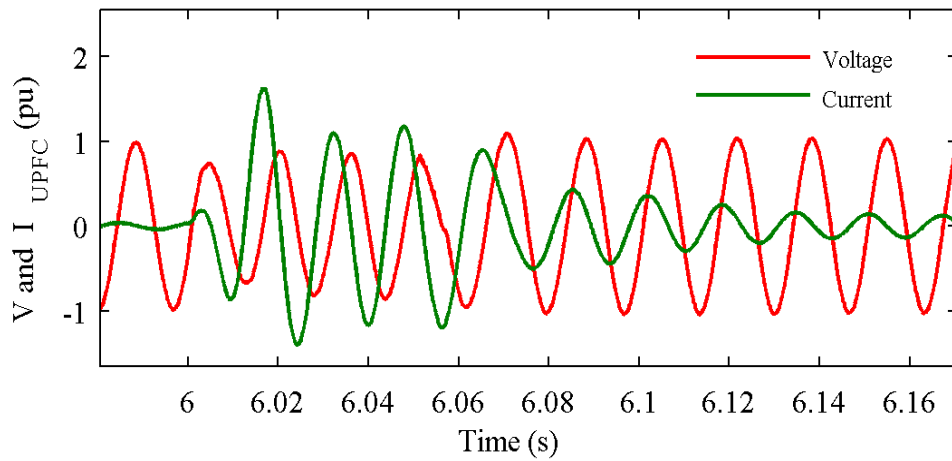
Figure 4.20 UPFC terminal voltage and current during three-phase short circuit
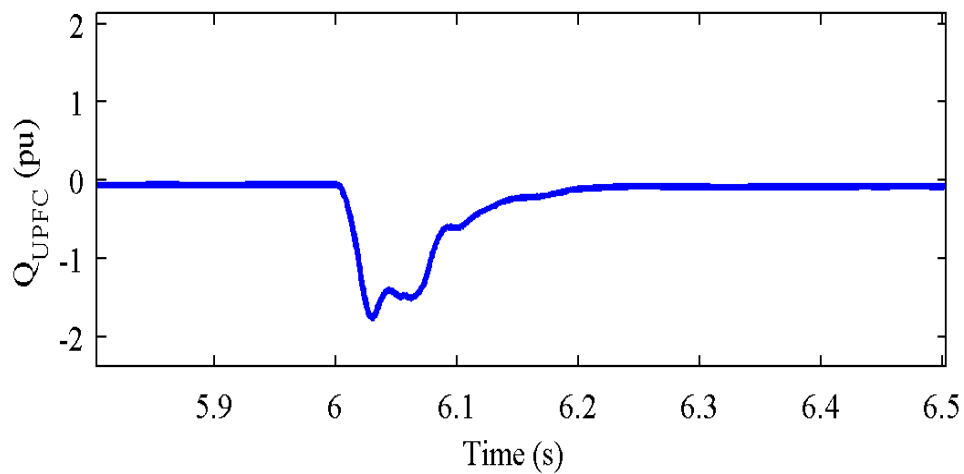
Figure 4.21 UPFC reactive Power during three-phase short circuit

Chapter 4
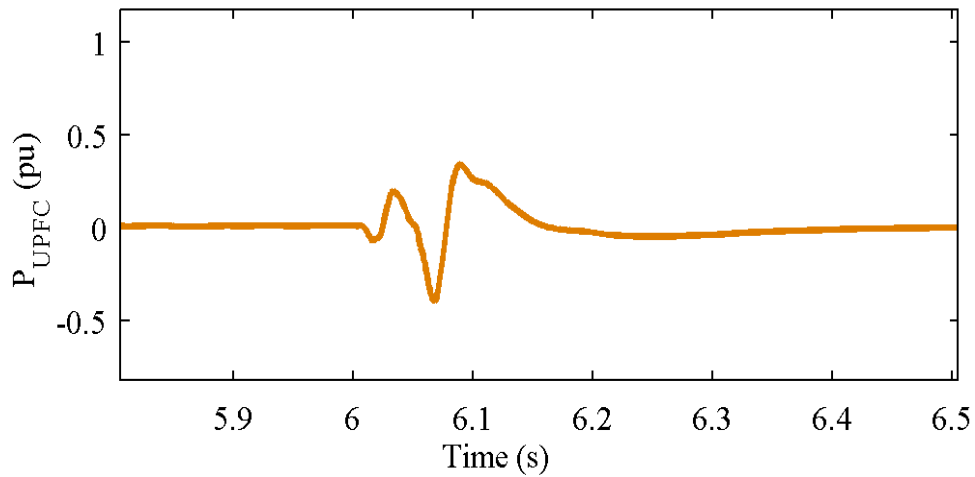
Figure 4.22 UPFC active Power during three-phase short circuit

Inductive operating mode: this mode is activated when voltage swell disturbance occurs at the grid side. During a voltage swell event, the UPFC controller acts to absorb the excessive amount of the reactive power from the grid to maintain the voltage constant at the PCC within pre-determined safety margins. In this mode of operation, the UPFC terminal current lags the terminal voltage, as shown in Fig. 4.23, and this facilitates transfer of the reactive power from the PCC to the UPFC, as can be observed in Fig. 4.24. Also, active power modulation will occur due to the impact of the voltage swell on the generator shaft (Fig. 4.25).

Chapter 4
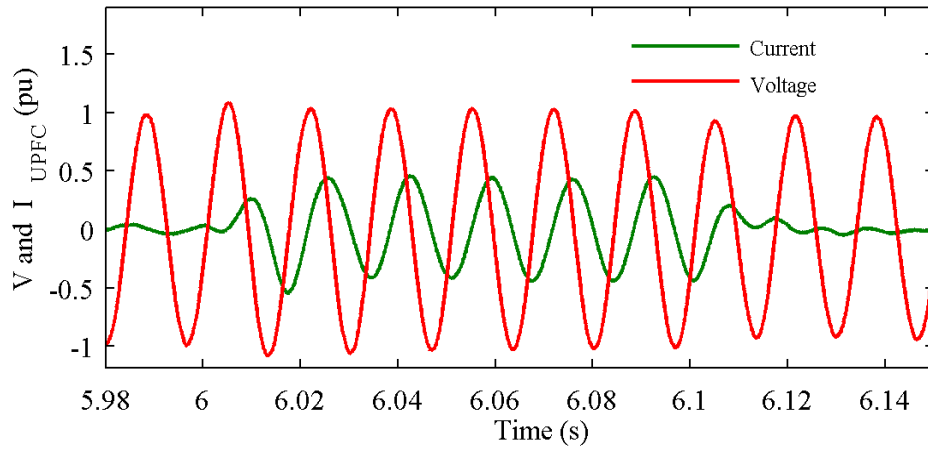
Figure 4.23 UPFC terminal voltage and current during voltage swell
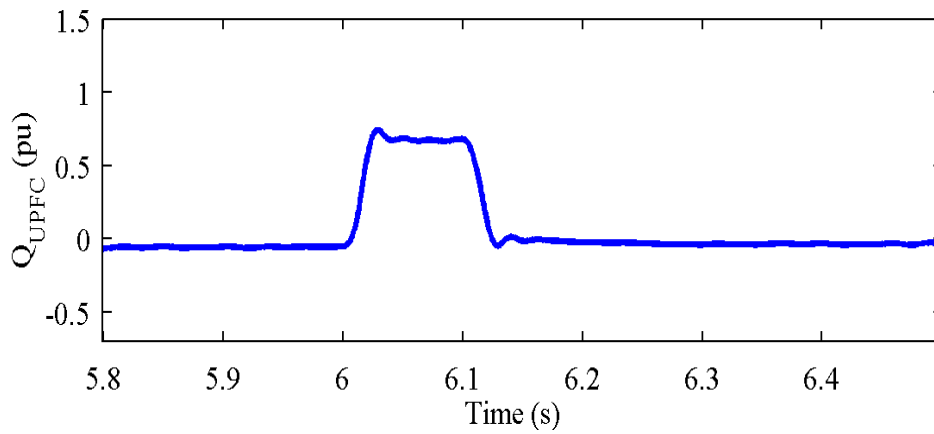
Figure 4.24 UPFC reactive Power during voltage swell

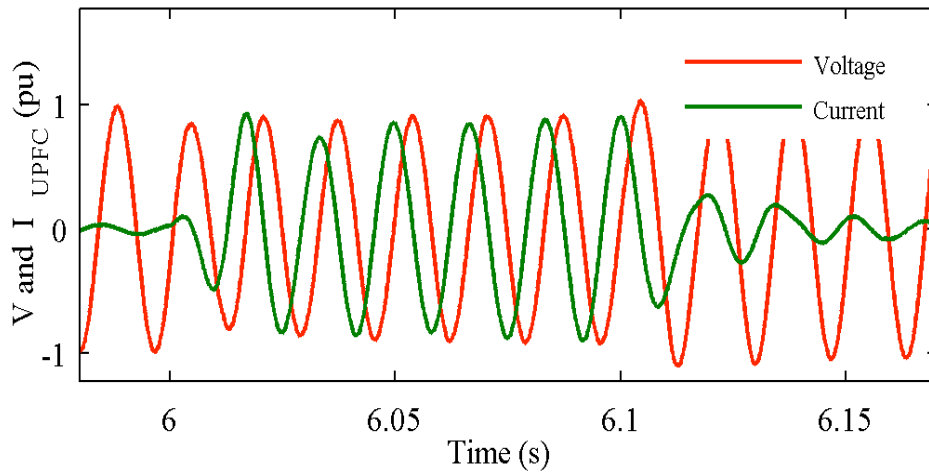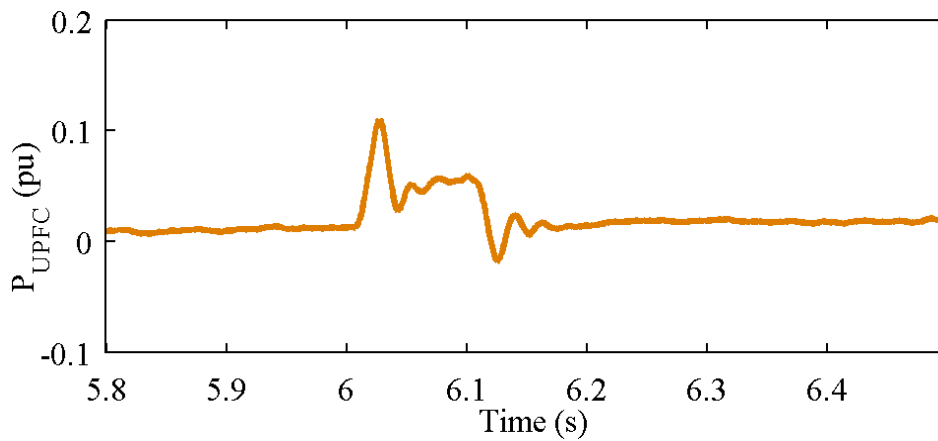Figure 4.25 UPFC active Power during voltage swell

Chapter 4

80

4.6   Case Study 4: Sub-Synchronous Resonance

Power systems are becoming larger and more interconnected, and as a consequence, the transient stability problem has become more serious. If the stability is lost, network collapse may occur with annihilating economical losses and severe power grid damages that may lead to overall blackout [119, 120]. Stability problems can occur due to the increase in the power demand with overloading the transmission lines; therefore, transmission line operators are required to increase the power transfer capability of the existing transmission lines. In this context, they have two options: the first one is to build an additional parallel transmission line, which is not a cost effective, especially for long transmission lines. The second option is to use a series capacitor as a partial compensation reactance to the transmission line, which has been extensively used as a very effective method to increase power transfer capability of transmission systems and improve the steady state and transient stability limits of a power system [121, 122]. Series capacitor is, however, not without problems, as it may cause sub-synchronous resonance (SSR) when the mechanical frequency of the generator mechanical shaft and the electrical frequency of the transmission system are added to the power frequency [123]. There are three ways in which a system and generator can interact with sub-synchronous effects: induction generator effect, torsional interaction and transient torques [123]. SSR due to transient torque can be developed if the electrical resonant frequency of the network

Chapter 4

is complementary to any of the natural torsional oscillating frequencies of the turbine-generator shaft during system disturbance events. The electric resonance of the transmission system and the torsional oscillations of the mass-spring system of the turbine generator will be mutually excited and might get augmented, causing serious shaft oscillations and shaft fatigue and possibly damage and failure [124]. The first two shaft failures due to SSR occurred at the Mohave power station in 1970 and 1971, respectively [125-127]. It is important to investigate the sub-synchronous resonance when planning to include series capacitors for new or existing transmission lines. Extensive research was undertaken to increase the damping of the torsional mode and many countermeasures were suggested to dampen the SSR. Some suggested solutions include use of the synchronous-machine-based Energy Storage System (ESS) [128], static var compensator (SVC) [129, 130], superconducting magnetic energy storage (SMES) unit [131-134], Static Synchronous Compensator (STATCOM) [135], shunt reactor controller [136, 137], Thyristor-controlled dynamic resistance braking [126, 138], excitation control of synchronous generator [139, 140], and gate controlled series capacitors [141, 142].

The case study presented in this section investigates the use of Unified Power Flow Controller (UPFC) to enhance transient stability and to dampen the SSR of a steam turbine-generator connected to a large interconnected AC grid via a series capacitor compensated transmission line.

Chapter 4
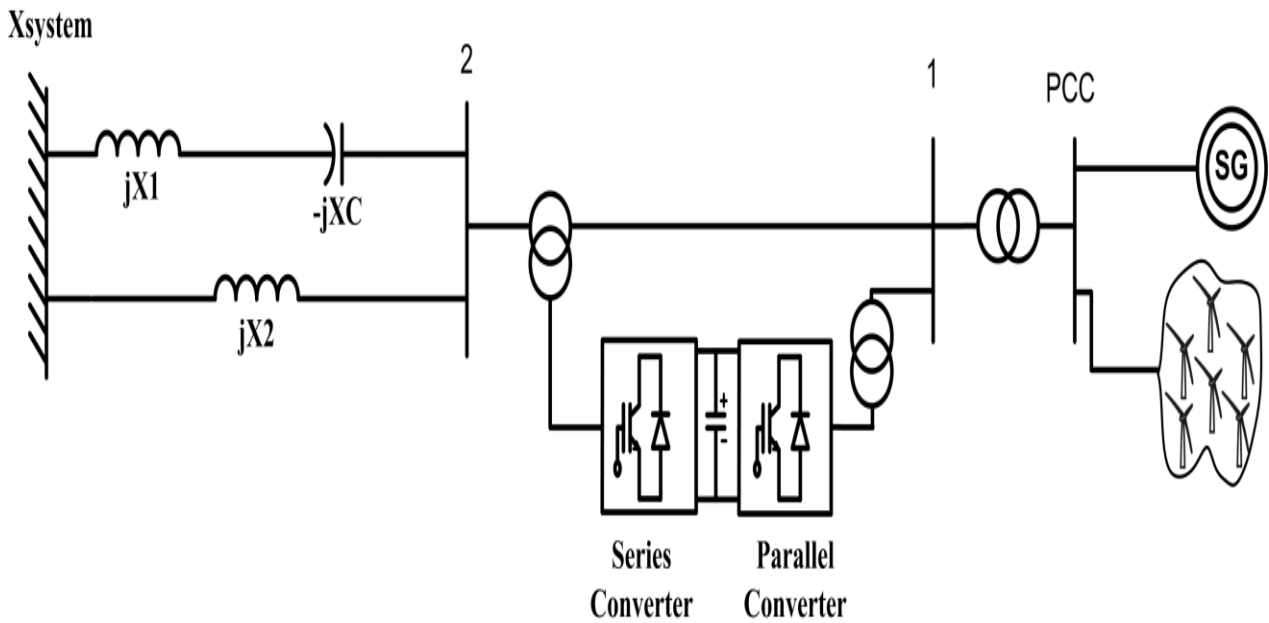
Figure 4.26 The system proposed in this study

The system proposed in this study is modified to the one shown in Fig. 4.26. It consists of a synchronous generator and wind farm that includes 6 wind turbines of type D connected to the grid (simulated as infinite bus via a Y/Δ step down transformer) and two parallel transmission lines: one of which is series compensated. The UPFC is connected to bus-1 between the compensated transmission lines and the generators to provide adequate damping for the turbine generator set.

The shaft system of the turbine generator set consists of four masses; a high-pressure turbine (HP), a low-pressure turbine (LP), a generator rotor (Gen) and an exciter (Ex). The system is simulated with inclusion of all non-linearities, such as

Chapter 4

exciter ceiling voltage limit. A three phase short-circuit fault is simulated at bus-2 at t = 12 s and is assumed to be cleared at t = 12.035 s. The compensation degree (X_c/X_l) is assumed to be 55%. Figure 4.27 to Figure 4.35 show the dynamic response of the studied system with and without the UPFC. The effect of the SSR and the UPFC controller is investigated through time domain waveforms of various system variables such as the synchronous generator speed deviation, deviation in torsional torque induced on the shaft sections between the high- pressure, low-pressure turbines ($T_{HP\text{-}LP}$) and the low-pressure turbine and generator ($T_{Gen\text{-}LP}$), the DFIG electromechanical torque (T_{em}), the PCC voltage, the DFIG converter DC voltage and the DFIG speed.

Without the UPFC and due to lack of damping, the system is unstable as evinced by the high torsional forces induced in the generator mechanical shafts and the significant increment in the shaft speeds, as can be seen in Fig 4.27.
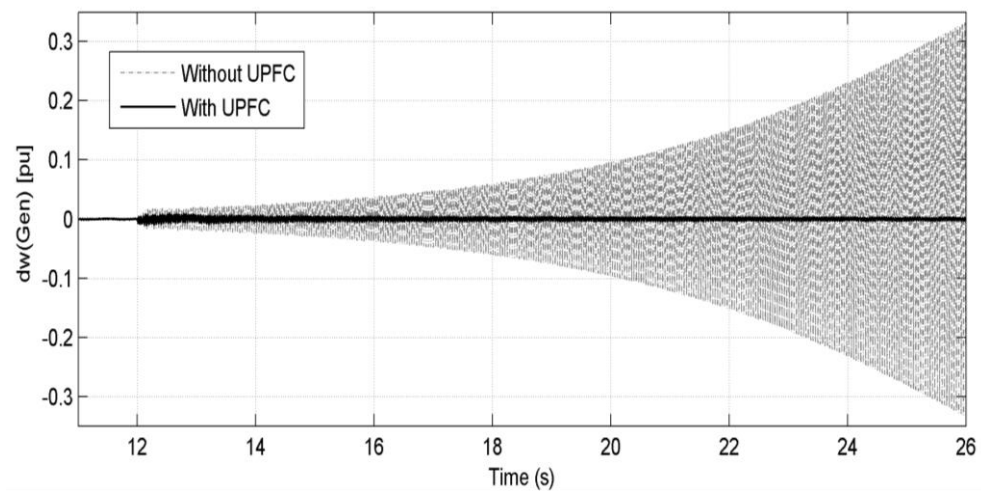
Figure 4.27 Deviation of the generator speed deviation for the cases with and without UPFC

Chapter 4
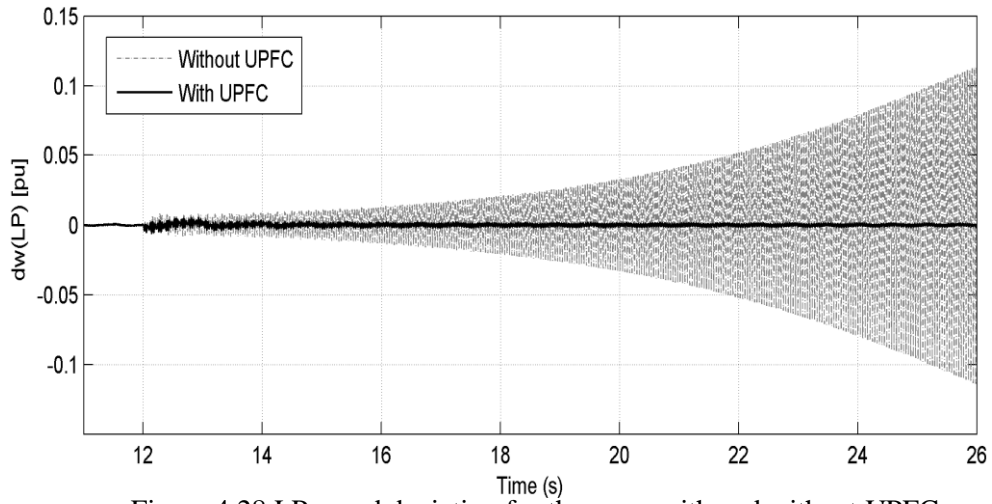
Figure 4.28 LP speed deviation for the cases with and without UPFC
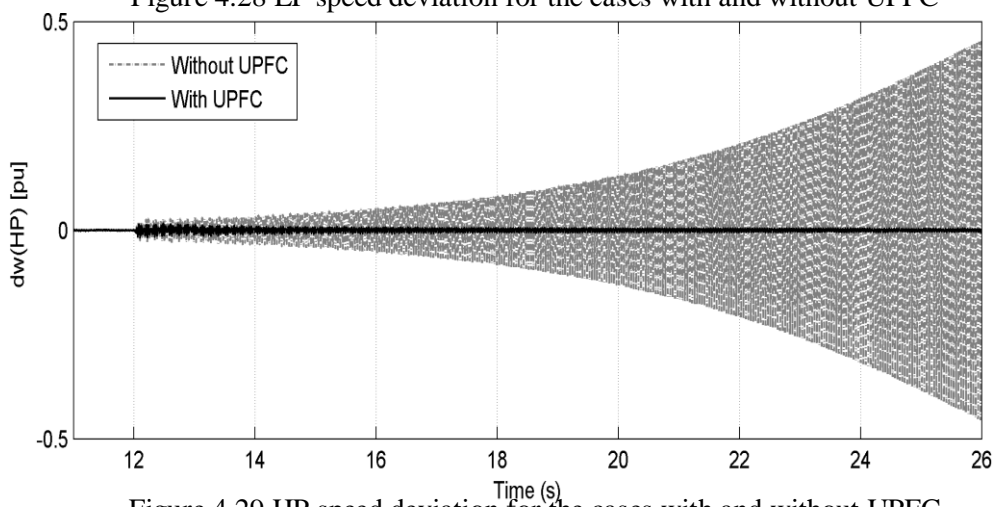
Figure 4.29 HP speed deviation for the cases with and without UPFC
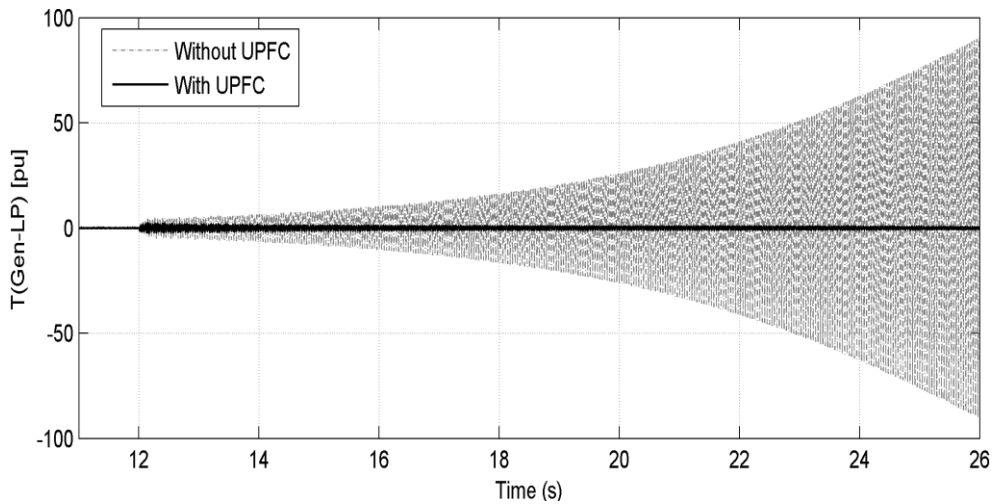
Figure 4.30 LP to Gen Torque deviation with and without UPFC

Chapter 4
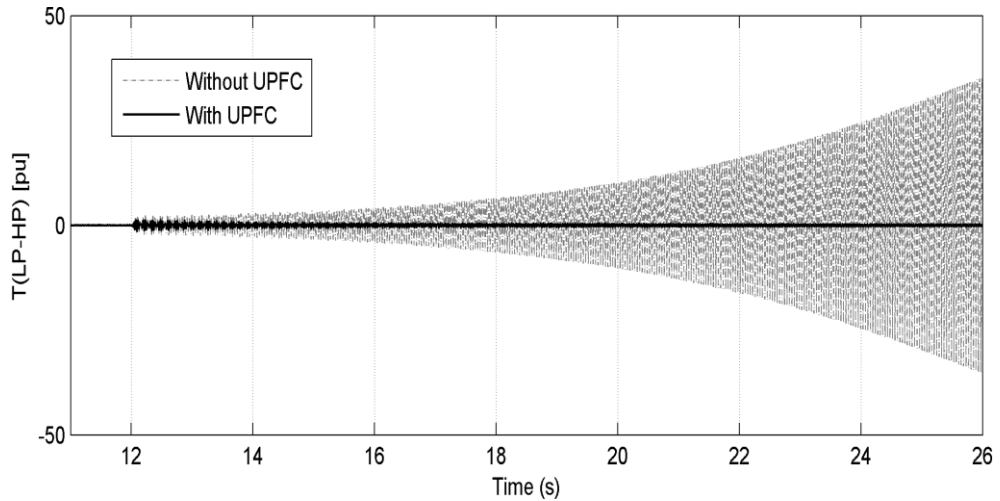
Figure 4.31 HP to LP Torque deviation for the cases with and without UPFC

When the UPFC is connected, damping of the synchronous generator and the DFIG is greatly enhanced and the stability margin can be extended, as shown in the Figure 4.32 to Figure 4.35. It can also be shown that using a UPFC unit reduces the high torsional forces on the turbine-generator shaft sections approximately to the normal steady state values; it also decreases the settling time substantially. Connecting the UPFC also reduces the generator shaft speed oscillations and maintains the speed at the nominal value, as clearly shown in Fig4.35.
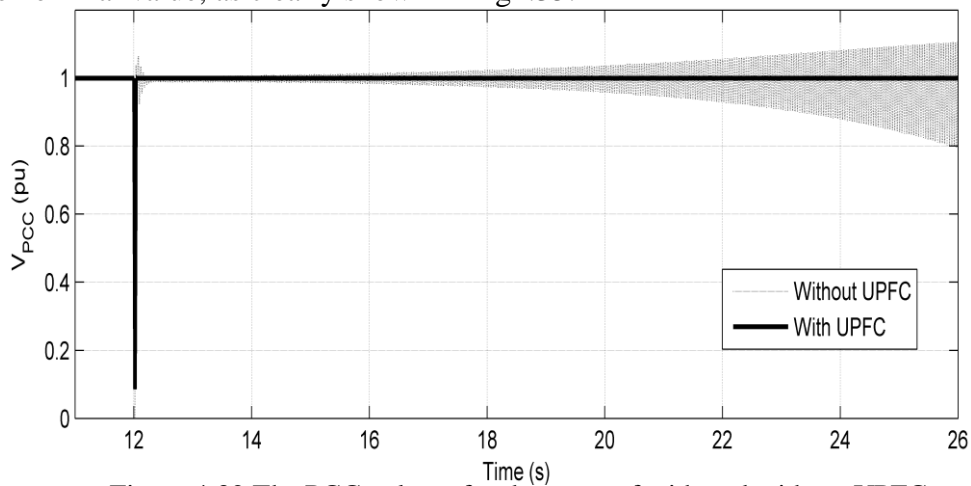
Figure 4.32 The PCC voltage for the cases of with and without UPFC
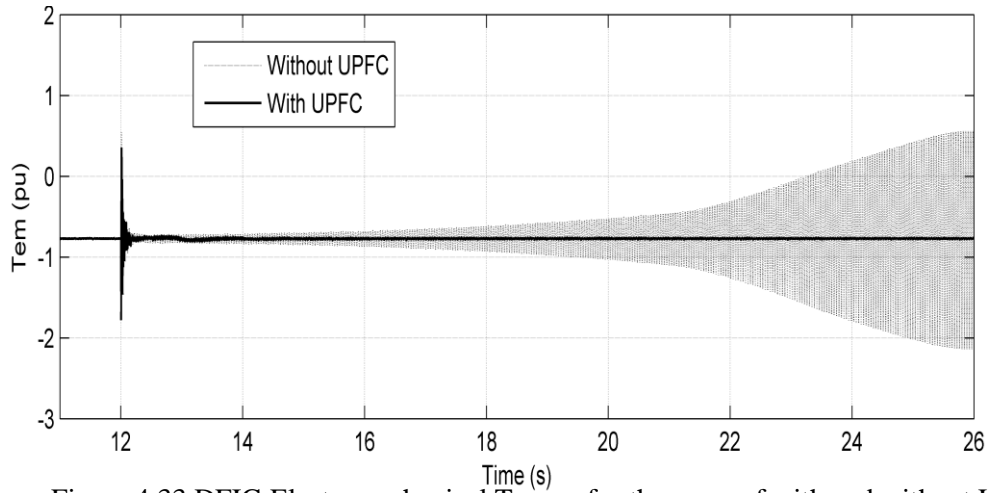
Chapter 4

Figure 4.33 DFIG Electromechanical Torque for the cases of with and without UPFC
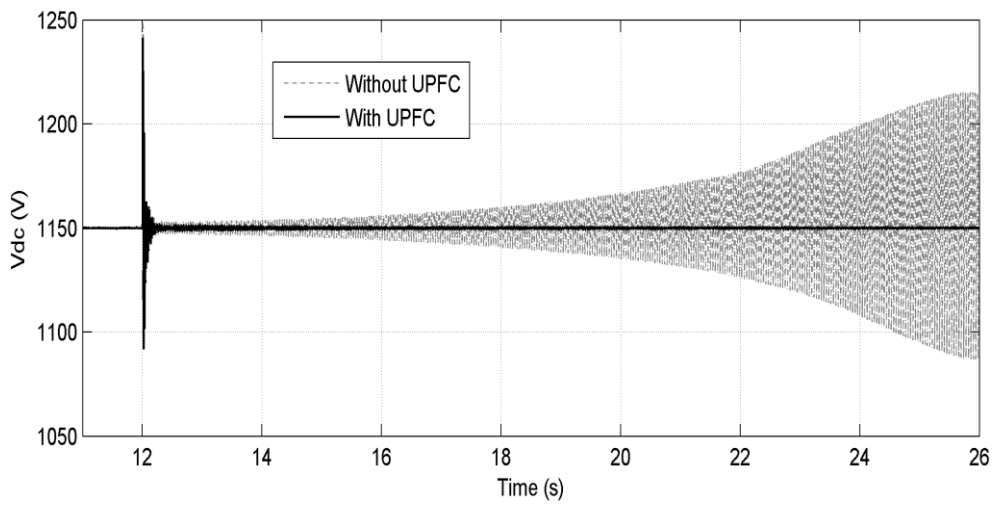
Figure 4.34. DFIG VDC response for the cases of with and without UPFC
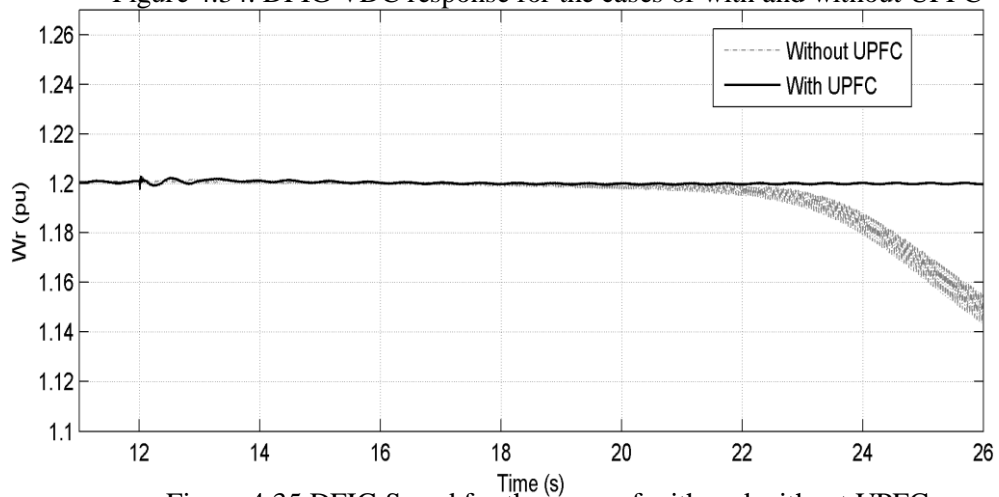
Figure 4.35 DFIG Speed for the cases of with and without UPFC

Chapter 4

4.7   Summary

In this chapter, new applications for UPFC have been proposed to improve the overall performance of a DFIG-based WECS during voltage sag/swell and short circuit faults at the grid side. Results from simulation work show that the proposed UPFC controller succeeded to improve the dynamic performance of the studied DFIG-based WECS during various fault events. The proposed control algorithm is simple, easy to implement and is able to improve the fault ride through the DFIG. Moreover, the chapter has investigated application of the UPFC to stabilize multi-mode torsional oscillations of sub-synchronous resonance. The simulation results indicated that the proposed UPFC controller is actually very effective in damping all SSR modes of the proposed system and in minimizing the potential disconnection of the wind farm during the studied faults.

Chapter 4

5

Application of UPFC to Improve the Performance of DFIG During Converter Station Faults

5.1   Introduction

While there are some studies about the effect of internal converter station faults (such as misfire and fire-through) on the performance of high-voltage direct-current systems [143, 144], only limited attention has been given to investigation of the impact of such faults on the overall performance of the DFIG-based WECS and the compliance of the DFIG with the recent developed grid codes during such faults [145, 146]. Misfire is the failure of the converter switch in taking over conduction at a scheduled programmed conducting period. On the other hand, fire through is the failure of the converter switch to block during a scheduled, non-conducting period [147]. These internal converter faults are caused by various malfunctions in the control and firing equipment [148]. Industrial survey about failure distribution in the converter stations that interface HVDC lines with ac network shows that converter faults due to malfunctions within the control circuit represent about 53.1% while about 37.9% of the converter faults are attributed to converter power parts (Figure 5.1) [149, 150].
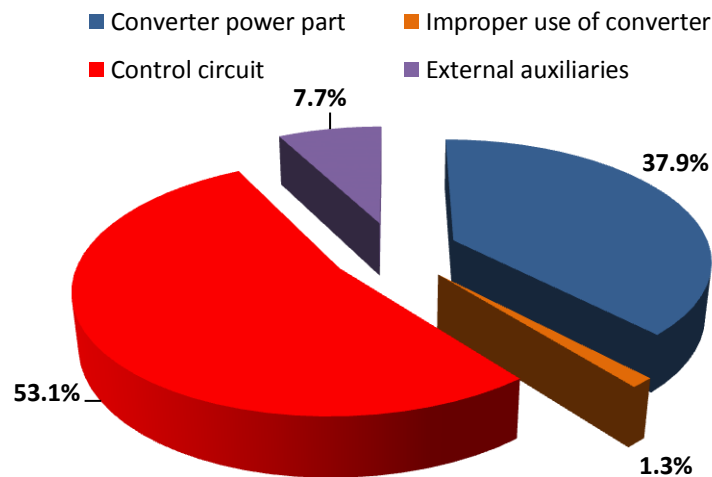
Figure 5.1 Distribution of failure types in the converters [150].

Chapter 5

Some of the converter faults are self-clearing if the causes are of transient nature; however, they can still have a detrimental impact on the system, particularly when they occur within the inverter station rather than within the rectifier station [151]. The use of an the use of insulated-gate bipolar transistor (IGBT) in both DFIG converters is preferred due to it is switching frequency advantages when compared with gate turn-off thyristor (GTO), as previously mentioned in Chapter 3 [94]. When a malfunction occurs on the IGBT-based converter station, it can cause catastrophic breakdown to the device, if the fault remains undetected [152].
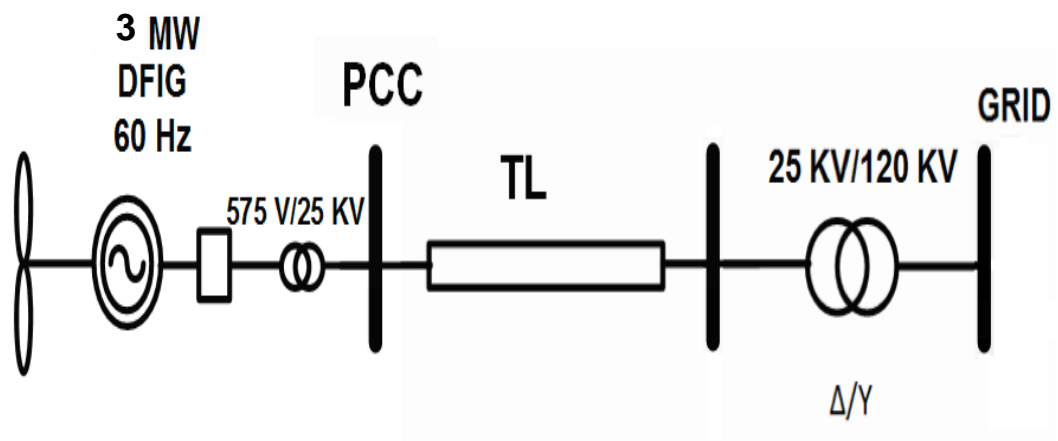
Figure 5.2 Proposed System

5.2 Faults within Rotor Side Converter

In this section, the DFIG dynamic performance under misfire and fire-through fault intermittent faults within the RSC are investigated. The two aforementioned faults

Chapter 5

are assumed to take place on switch S1 within the RSC at 4.1 s and cleared at 4.15 s, as shown in Fig. 5.3.
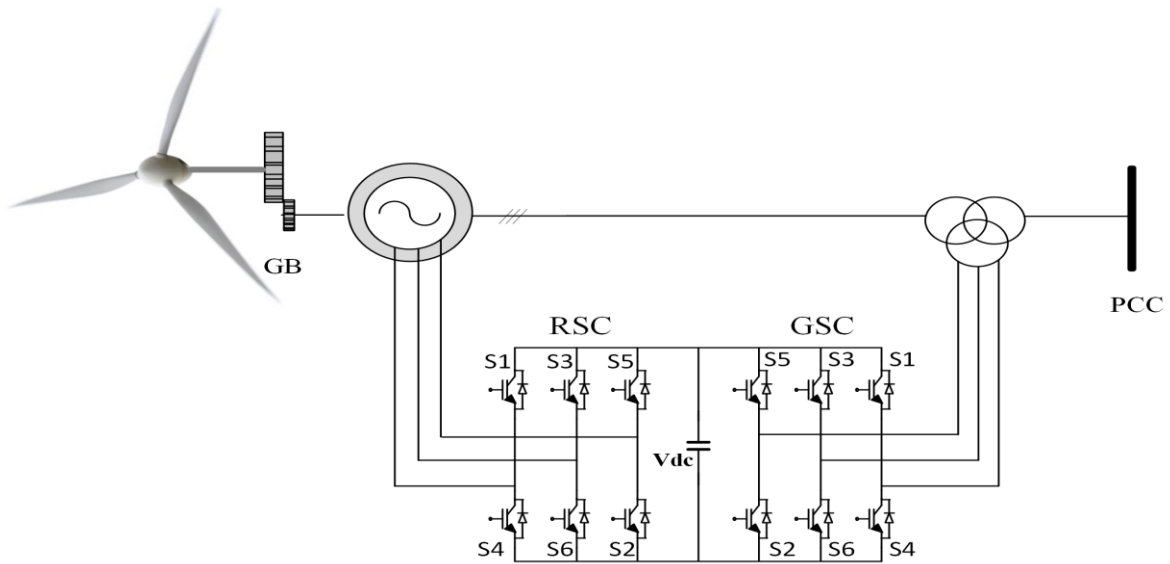
Figure 5.3 Basic configuration of wind turbine based on DFIG
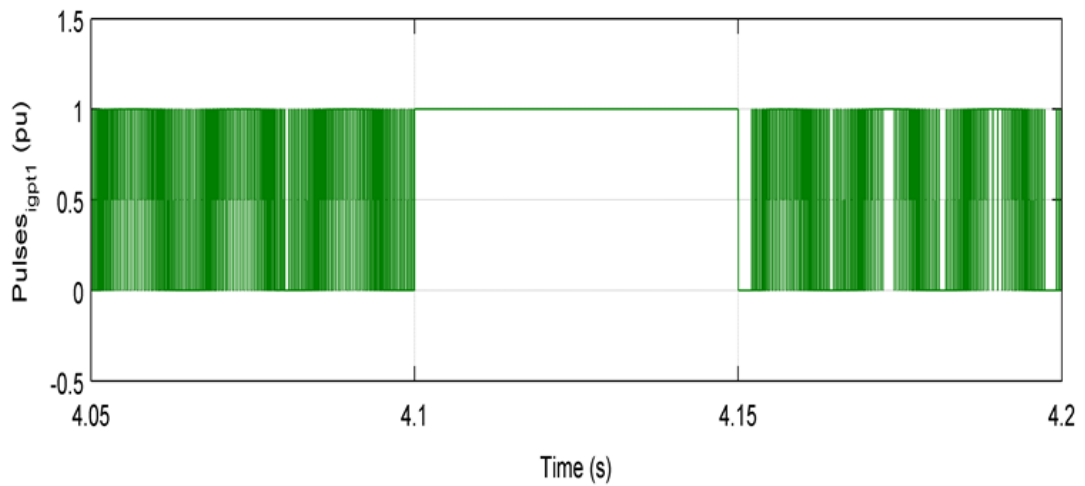
Figure 5.4 Fire-through fault in IGBT-1

Chapter 5
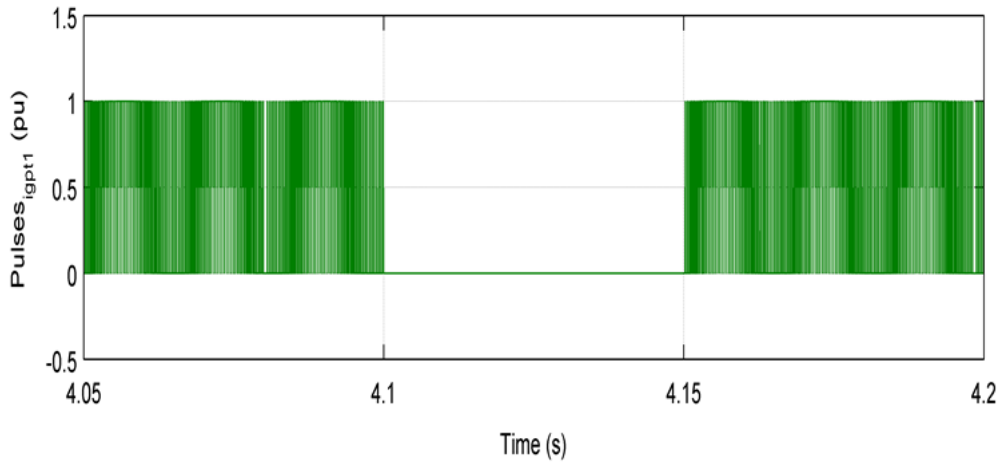
Figure 5.5 Misfire fault in IGBT-1

Figs. 5.6 shows the dynamic performance of the DFIG during the two switch faults. As can be seen in Fig. 5.6(a), the fire-through fault causes the voltage at the PCC to drop to 0.45 pu, while the misfire fault impact on the voltage at the PCC is insignificant. During steady state condition, DFIG delivers 1 pu active power and 0 pu reactive power to the ac network, as shown in Figs 5.6 (b) and (c). However, when the fire-through fault takes place in one of the switches, a significant drop in the delivered active power will occur and the reactive power will be absorbed from the grid. On the other hand, the impact on DFIG power is insignificant when misfire fault takes place. The shaft speed behaviour can be seen in Fig. 5.6 (d), where the shaft speed will experience oscillations and overshooting during the two faults; the impact is more pronounced in the case of fire-through fault. As can be observed in Fig. 5.6 (e), the fire through fault will cause short circuit across the DC capacitor

Chapter 5

when switch S4 takes over conduction along with the faulty switch (S1), and as a result, the voltage across the DC capacitor link will drop to zero level. The impact of misfire on this voltage is insignificant. The voltage cross the capacitor is designed with safety requirements set by the designers; in [24] this safety level is between 0.25 pu and 1.25 pu. If this safety level is violated, the converter station protection system must act to disconnect the converter to avoid possible damages to the switches.

Chapter 5
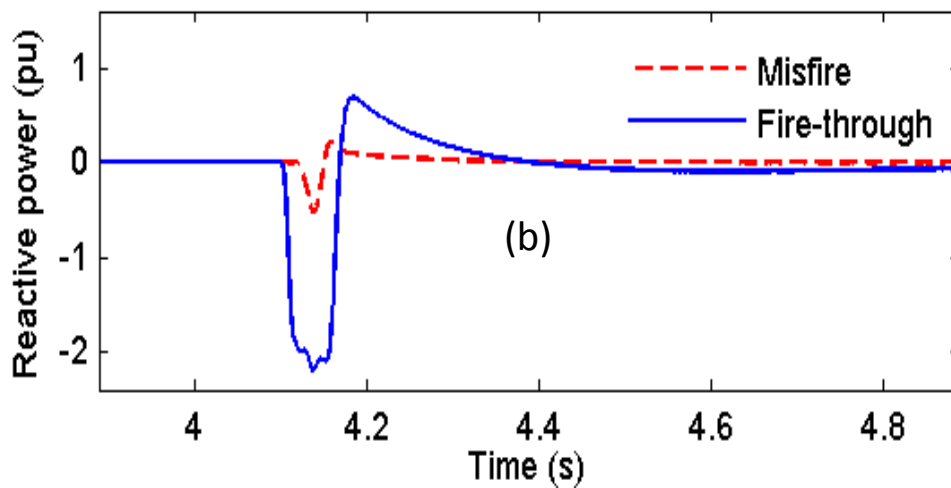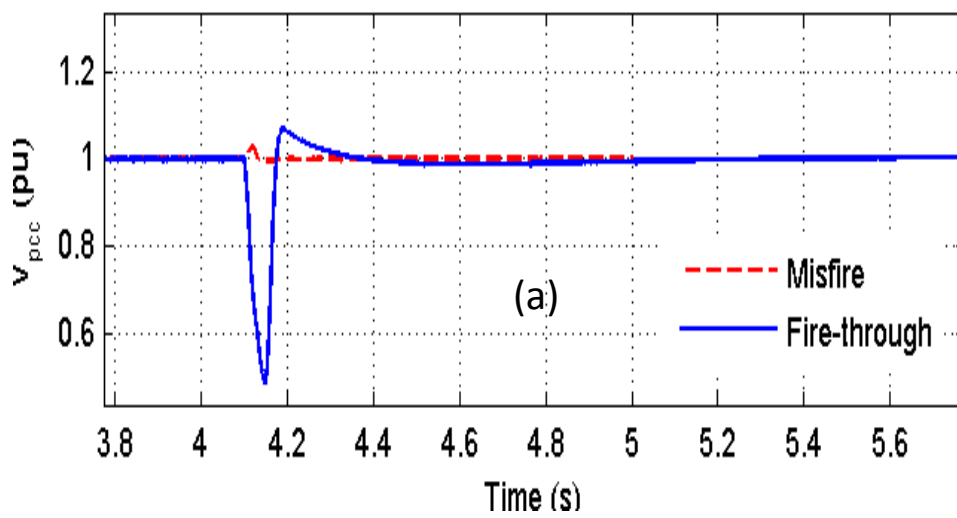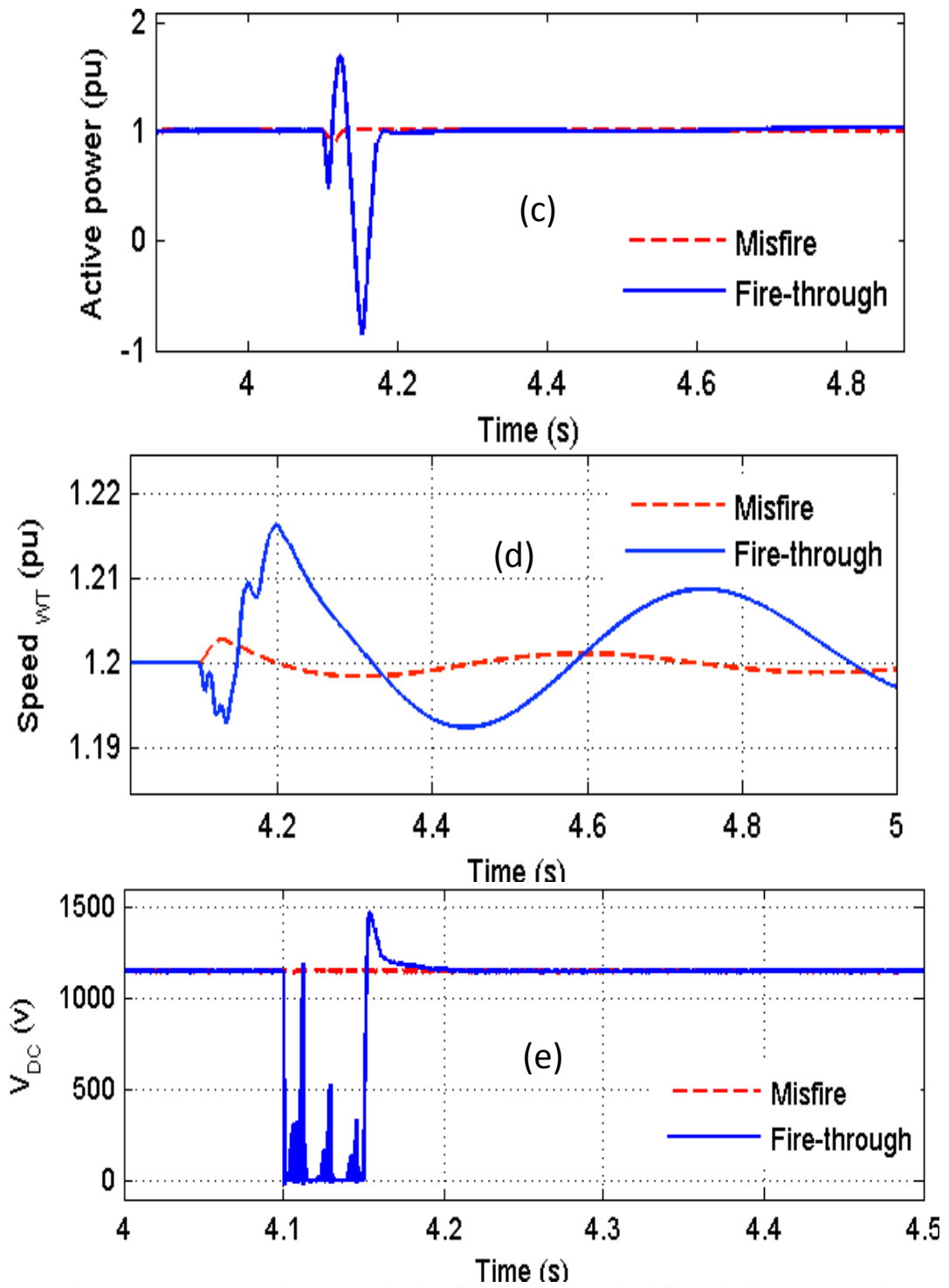
Figure 5.6. DFIG performance during fire-through and misfire within the rotor side converter: (a) PCC voltage, (b) reactive power, (c) active power (d) shaft speed, and (e) DC link Voltage of DFIG.

Chapter 5

The impact of misfire and fire-through faults on converter terminal voltages is shown in Fig. 5.7. Spikes are introduced to the converter terminal voltages when switch S1 of the RSC experiences misfire. However, the fire-through fault on switch S1 causes short circuit across the converter terminals, causing the voltage to drop to zero level during the fault.

Chapter 5
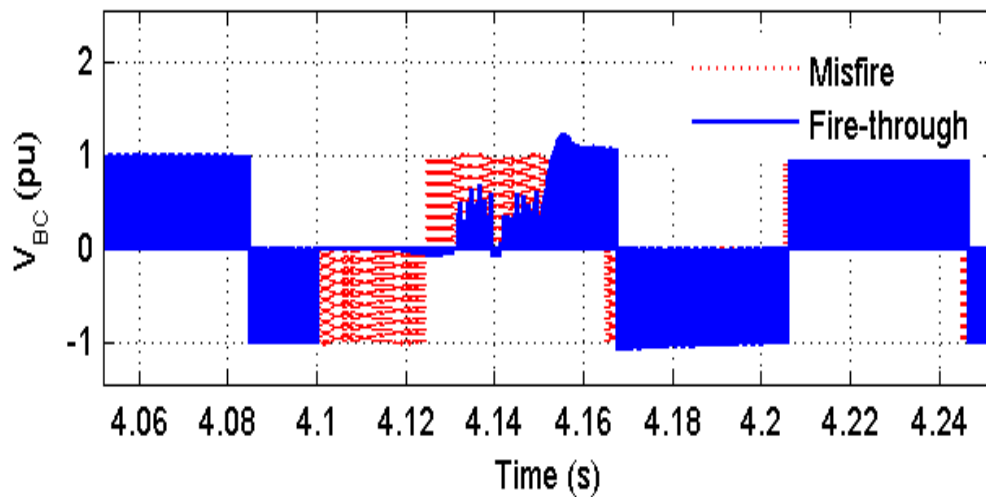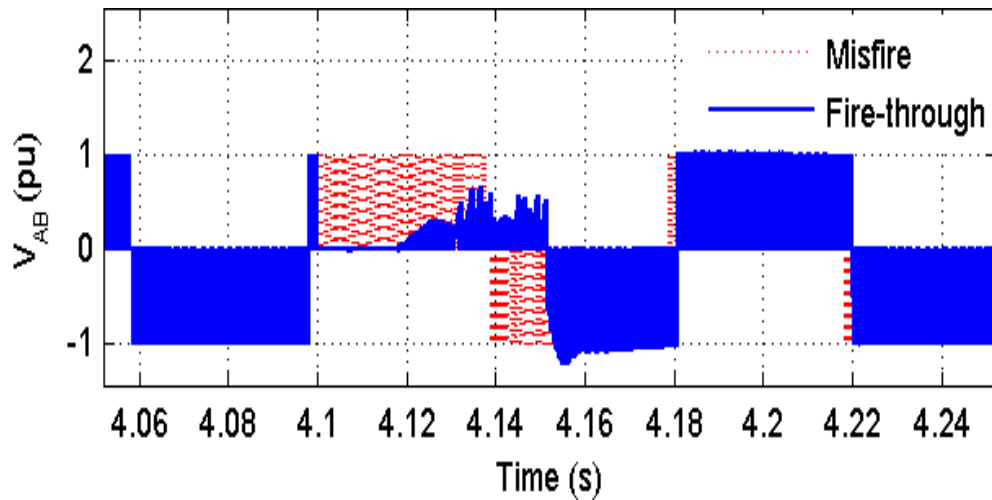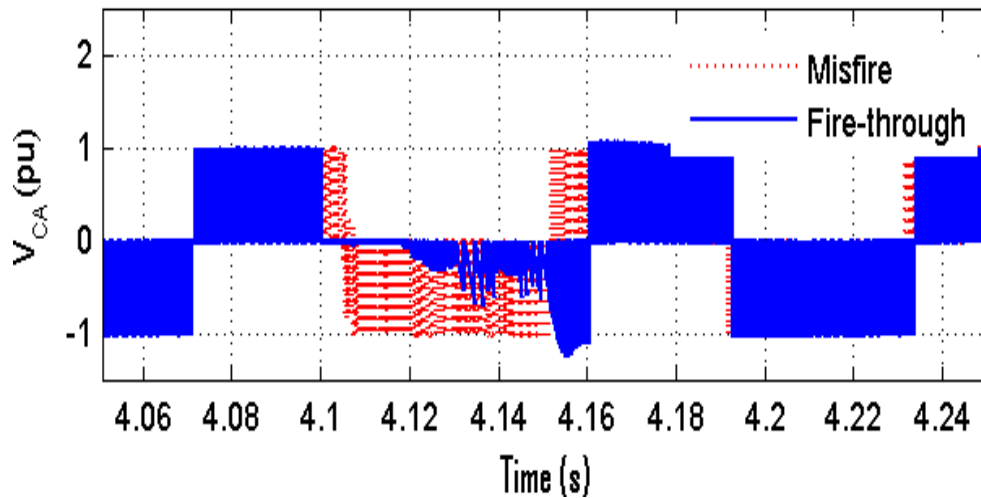
Figure 5.7 Voltage change across RSC terminals during fire-through and misfire in S1 within RSC

5.3 Faults Within the Grid Side Converter

In this case study, the GSC switch S1 is assumed to experience misfire and fire-through within the period 4.1 s to 4.15 s. As shown in Fig.5.8 (a), due to the fire-through fault, the voltage at the PCC decreases by 0.55 pu, whereas the impact of misfire fault is negligible. During the event of fire-through the DFIG will absorb a significant amount of the reactive power from the ac network and the real power produced by the DFIG will be significantly decreased, as shown in Fig. 5.8 (b) and 5.8 (c), respectively. In contrast, both the reactive and active powers are slightly affected during the misfire fault event. The DFIG power drops cause acceleration to the shaft speed to compensate for the power imbalance during the fire-through fault, as can be shown in Fig.5.8 (d), with no impact due to the misfire fault. It can be seen from Fig.5.8 (e) that the fire-through fault causes the DC voltage across the capacitor

Chapter 5

to drop to zero level; while in the case of misfire, the dc voltage experiences slight

fluctuation.

Chapter 5
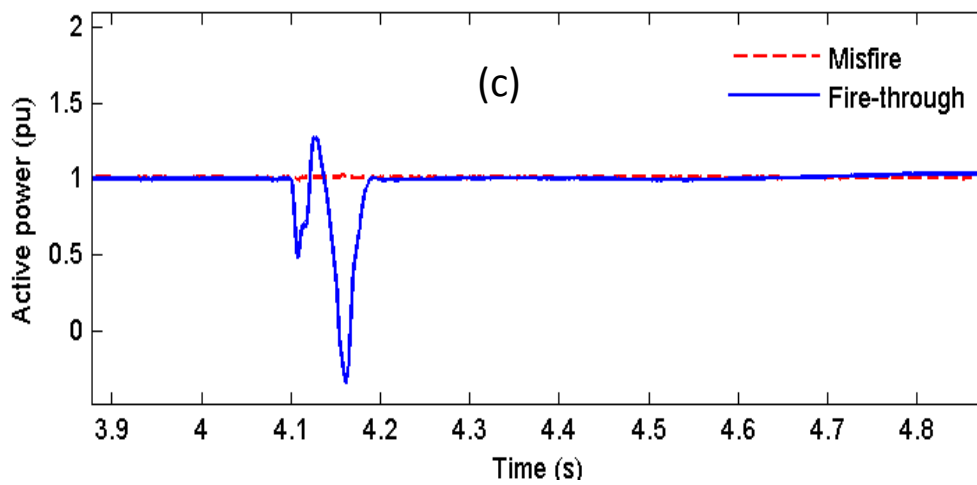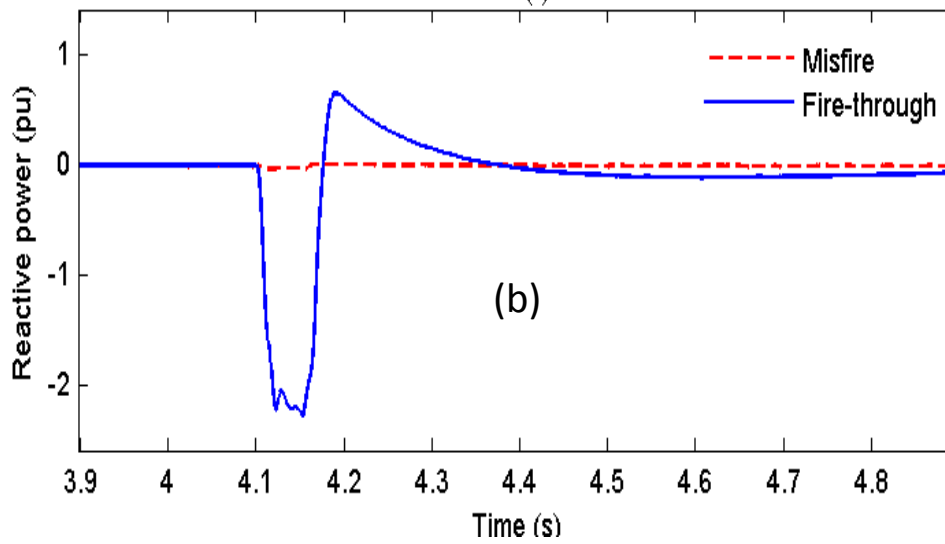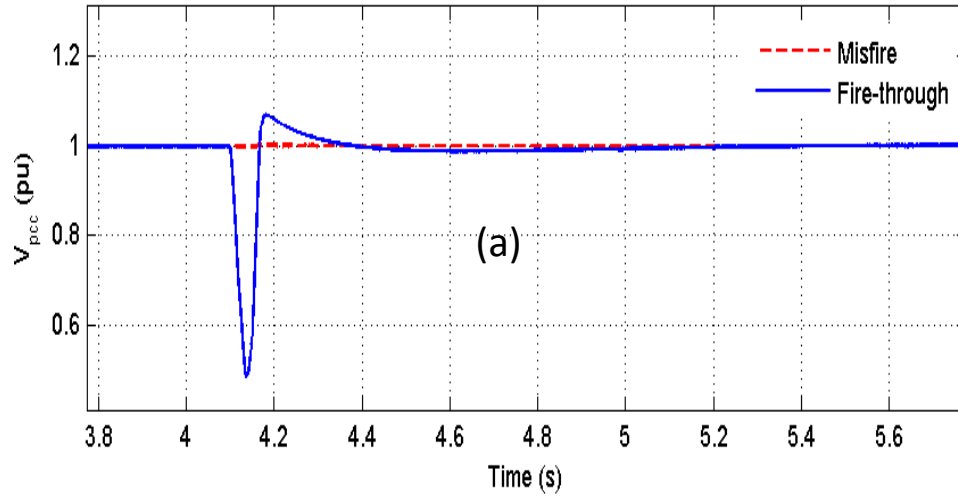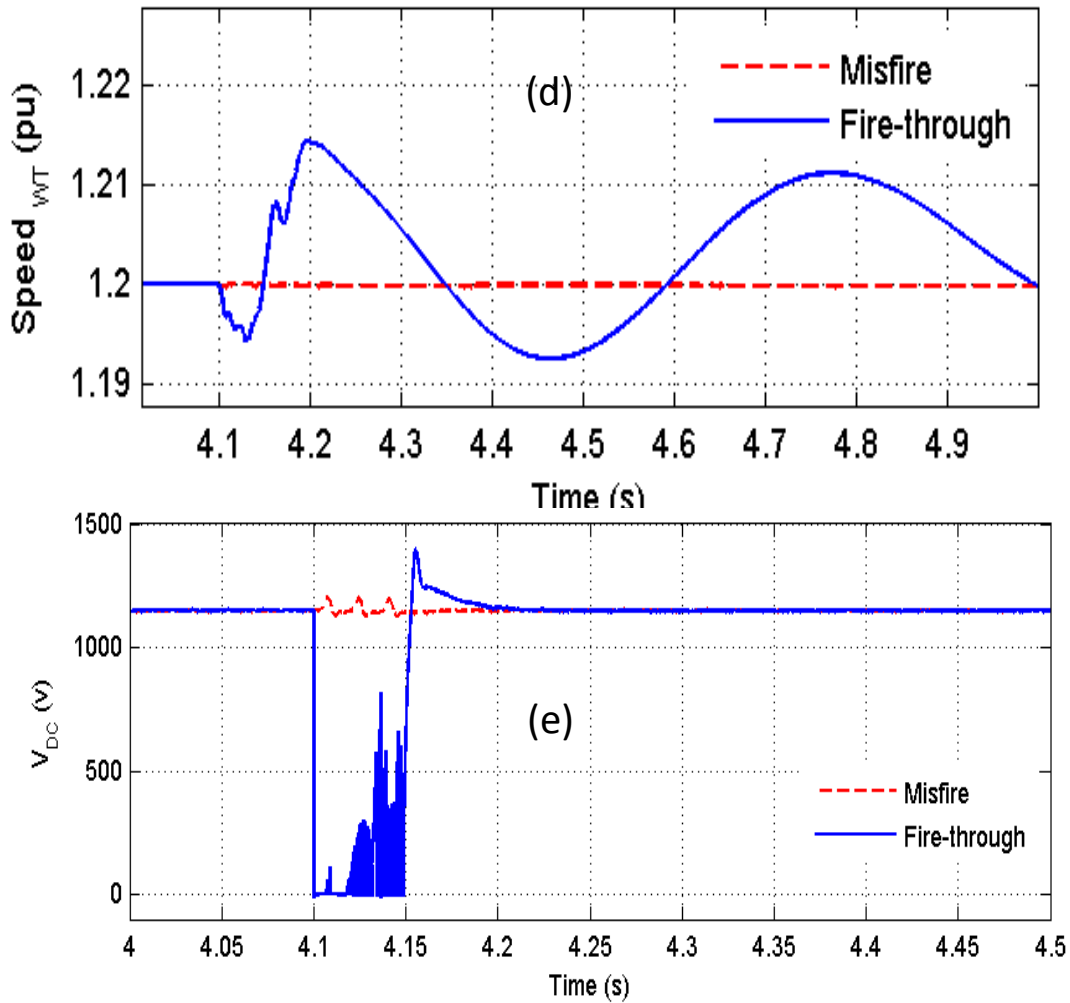
Figure 5.8 DFIG performance during fire-through and misfire within the grid side converter; (a) PCC voltage, (b) reactive power, (c) active power (d) shaft speed, and (e) DC link voltage of DFIG.

The fire-through fault causes a voltage collapse to zero level across the converter terminals, as shown in Fig 5.9. Similar to RSC, the impact on the converter terminal voltages is negligible when the misfire fault takes place on switch S1 of the GSC.

Chapter 5

Figure 5.9. Voltage change across GSC terminals during fire-through and misfire in S1 within GSC

Chapter 5

Chapter 5

Figure 5.10. Voltage change across converter switches during fire-through in switch S1.

Chapter 5

Chapter 5
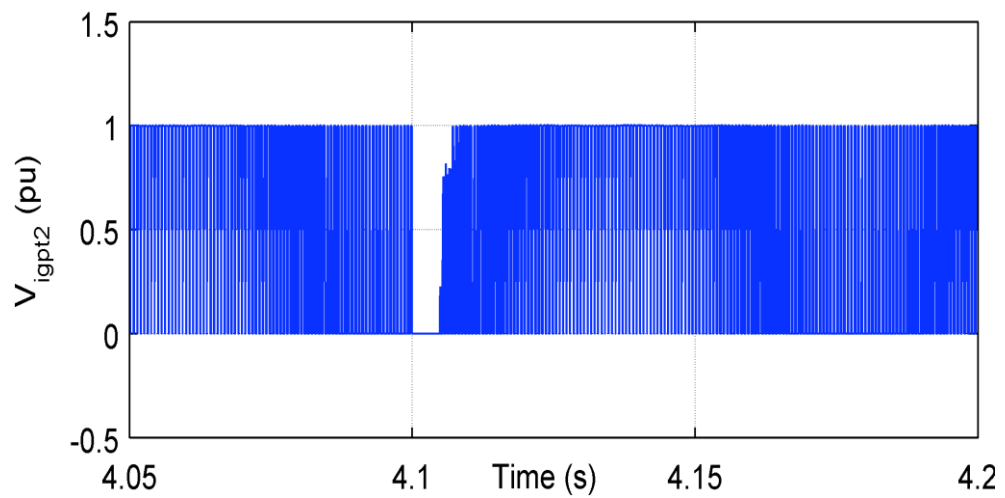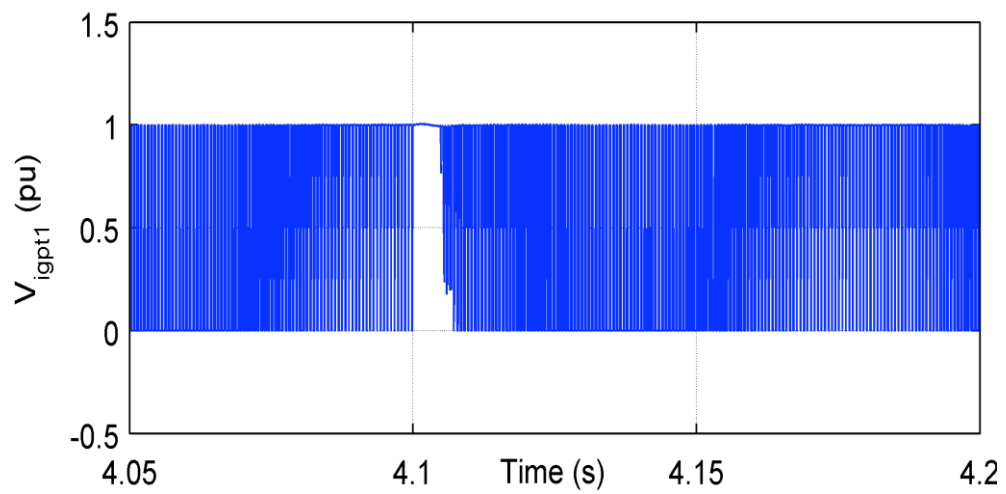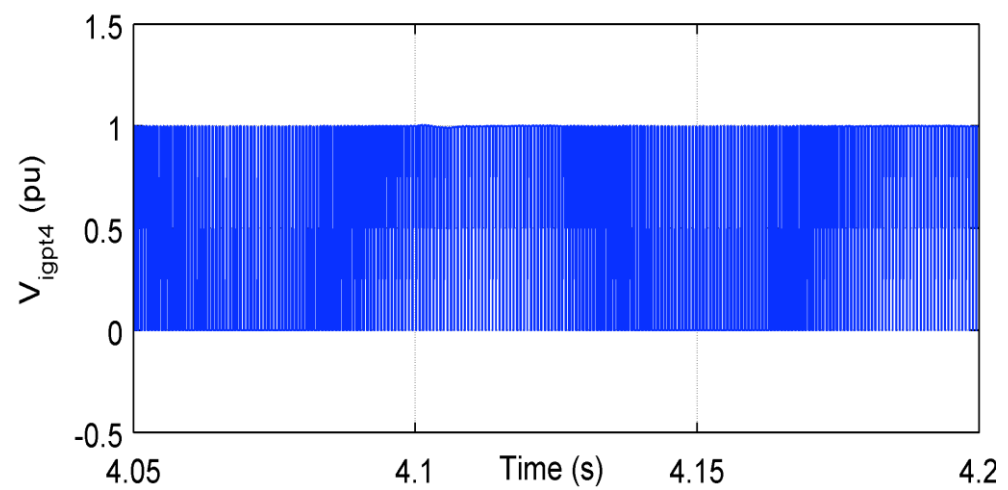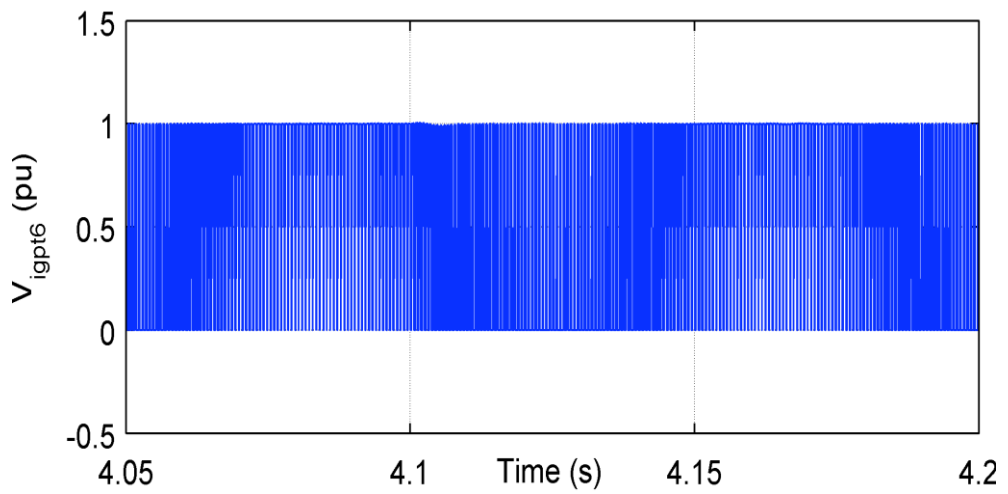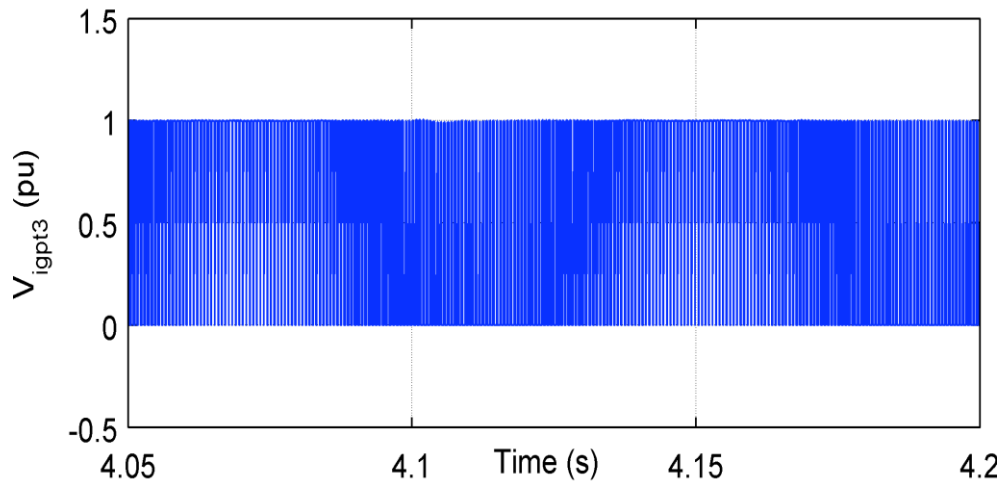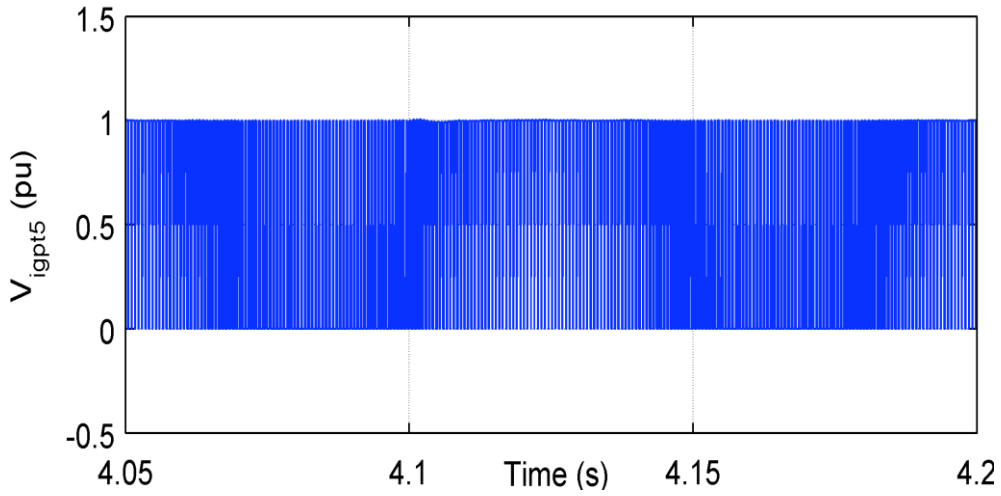
Figure 5.11. Voltage change across converter switches during misfire in switch S1.

5.4   Impact of UPFC During Converter Station Faults
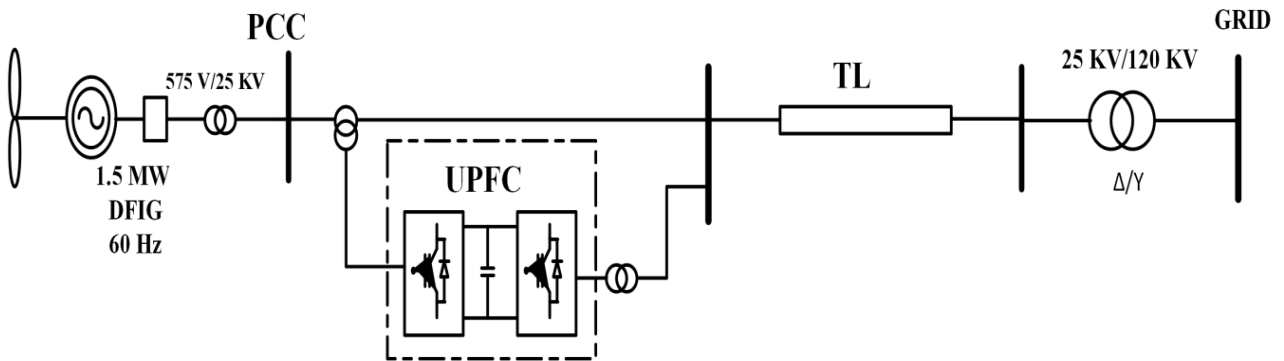
Figure 5.12 Proposed System with UPFC

To mitigate the adverse impacts of fire-through faults on the DFIG performance, the UPFC is connected to the PCC, as shown in Fig.5.12. As the misfire fault has

Chapter 5

insignificant impact, it is not included in this section. Fire-through fault studied in the previous section is re-investigated but with connection of the UPFC and the proposed controller discussed in Chapter 3.

5.4.1 Fire-through fault

When a fire-through fault takes place within the RSC S1, the voltage at the PCC drops by 0.5 pu when the connection of UPFC is not connected. On the other hand, this voltage drop is regulated to 0.69 pu by connecting the UPFC to the PCC bus, as shown in Fig. 5.13(a). As discussed in the previous section, without any compensation, the generated active power will drop and the shaft speed will accelerate, as shown in Fig. 5.13(b) and (c). With the connection of the UPFC, the drop in DFIG generated power is reduced, leading to a reduction in the speed overshooting and settling time. There is a slight reduction in the overshooting levels in the voltage across the DC link when the UPFC is connected to the PCC, as shown in Fig. 5.13(d).

Chapter 5

Chapter 5

107

Figure 5.13 Effect of RSC Fire-through on DFIG dynamic performance with and wothout UPFC: (a) Voltage at PCC. (b) Reactive power, (c) Shaft speed. (d) DC link Voltage of DFIG.

When the fire-through takes place within the Grid side converter, the same trend can be observed when the UPFC is connected to the PCC bus. Fig.5.14 (a) shows that the UPFC can rectify the voltage drop at the PCC from 0.47 pu to 0.97 pu. This regulation is critical, since without this compensation, the DFIG must be disconnected according to some grid codes such as, the Spanish grid code, whcih specifies a 0.5 p.u. maximum voltage sag at the PCC to maintain the wind turbine's connection to the grid. The generator's shaft speed is slightly retarded through the fault duration, and it experiences overshooting upon recovery of the fault and settles at a lower steady state level than the pre-set level (1.2 pu), as shown in Fig. 5.14(c). With the connection of the UPFC, the generator's shaft speed profile is improved. Similar to the previous case study, the UPFC introduces a slight improvement to the voltage across the dc link (Fig. 5.14(d)).

Chapter 5
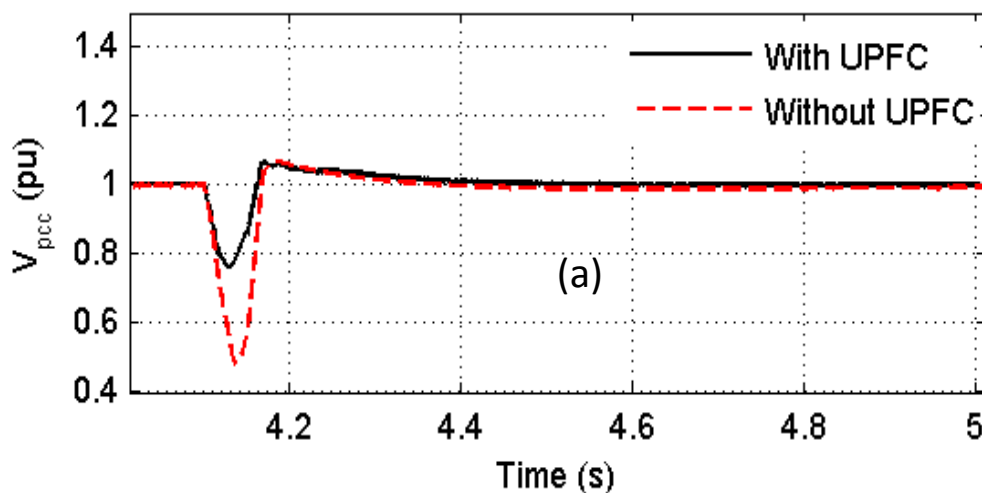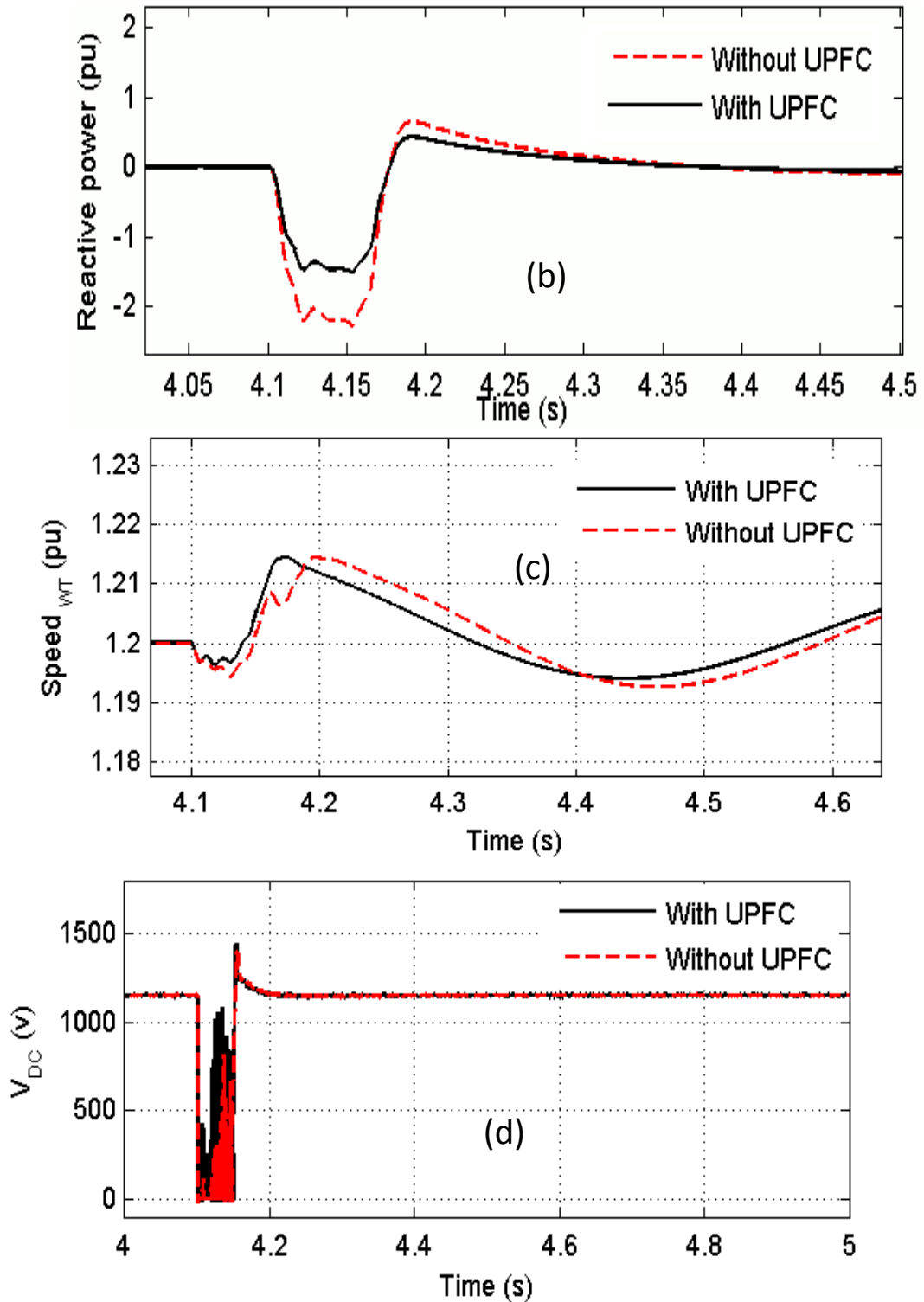
Figure 5.14 Effect of GSC Fire-through on DFIG dynamic performance without and with UPFC: (a) Voltage at PCC. (b) Reactive power, (c) Shaft speed. (d) DC-link Voltage

Chapter 5

5.4.2 Fault Across the DC-Link

In order to assess the robustness of the proposed UPFC controller in improving the overall performance of a DFIG-based WECS under study, two intermittent fault scenarios of a short circuit and an open circuit across the dc link are simulated and analysed with and without the connection of the proposed UPFC controller as elaborated below.

5.4.2.1   Short Circuit Fault

In this case study a short circuit event was applied across the dc-link at t = 4 s and was assumed to last for 5 cycles. As shown in Fig.5.15 (a), when the UPFC is not connected, application of this event causes the voltage at the to decrease to a constant value of 0.37 pu. On the other hand, when the UPFC is connected to the PCC bus, the voltage drop is regulated to 0.7 pu, which satisfies the safety requirement of some wind turbine designers [11, 33, 34, 36, 37]. In the absence of the UPFC, the drop in the generated power causes unwanted acceleration and oscillation of the DFIG shaft. As can be seen in Figure 5.15 (b), connection of the proposed UPFC reduces these adverse effects to acceptable levels.

Similarly, in the base case of no UPFC, the voltage across the DFIG dc link capacitor is affected significantly during the short circuit event as shown in Fig. 5.15 (c). With the UPFC connected to the system, this voltage impact is reduced. The converter terminal voltages drop to zero level as a result of the short circuit across the dc-link as can be seen in Figs. 5.16

Chapter 5
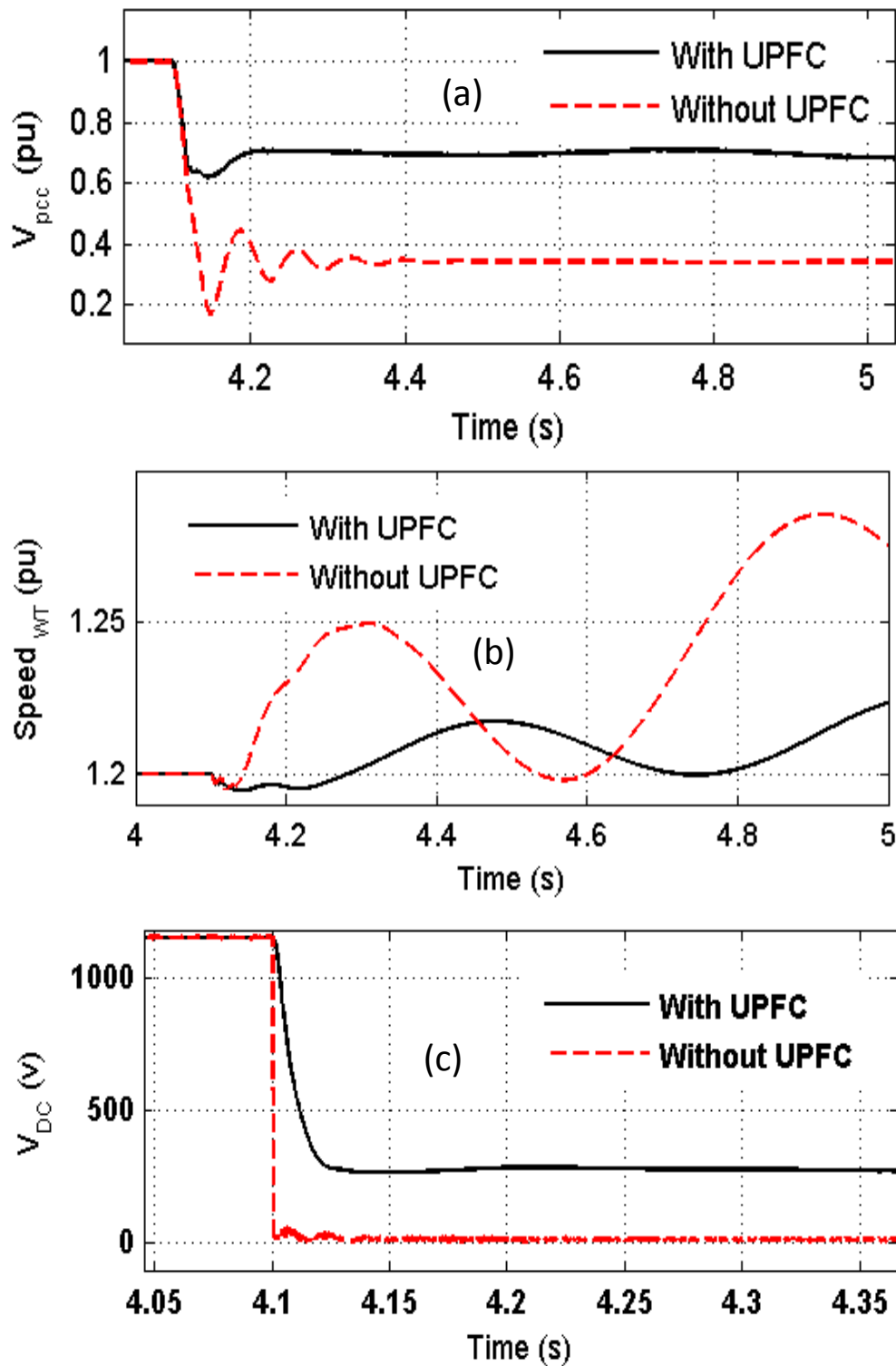
Figure 5.15 Effect of DC link Short Circuit on DFIG dynamic performance with and without UPFC. (a) Voltage at PCC. (b) Shaft speed. (c) DC-link Voltage.

Chapter 5
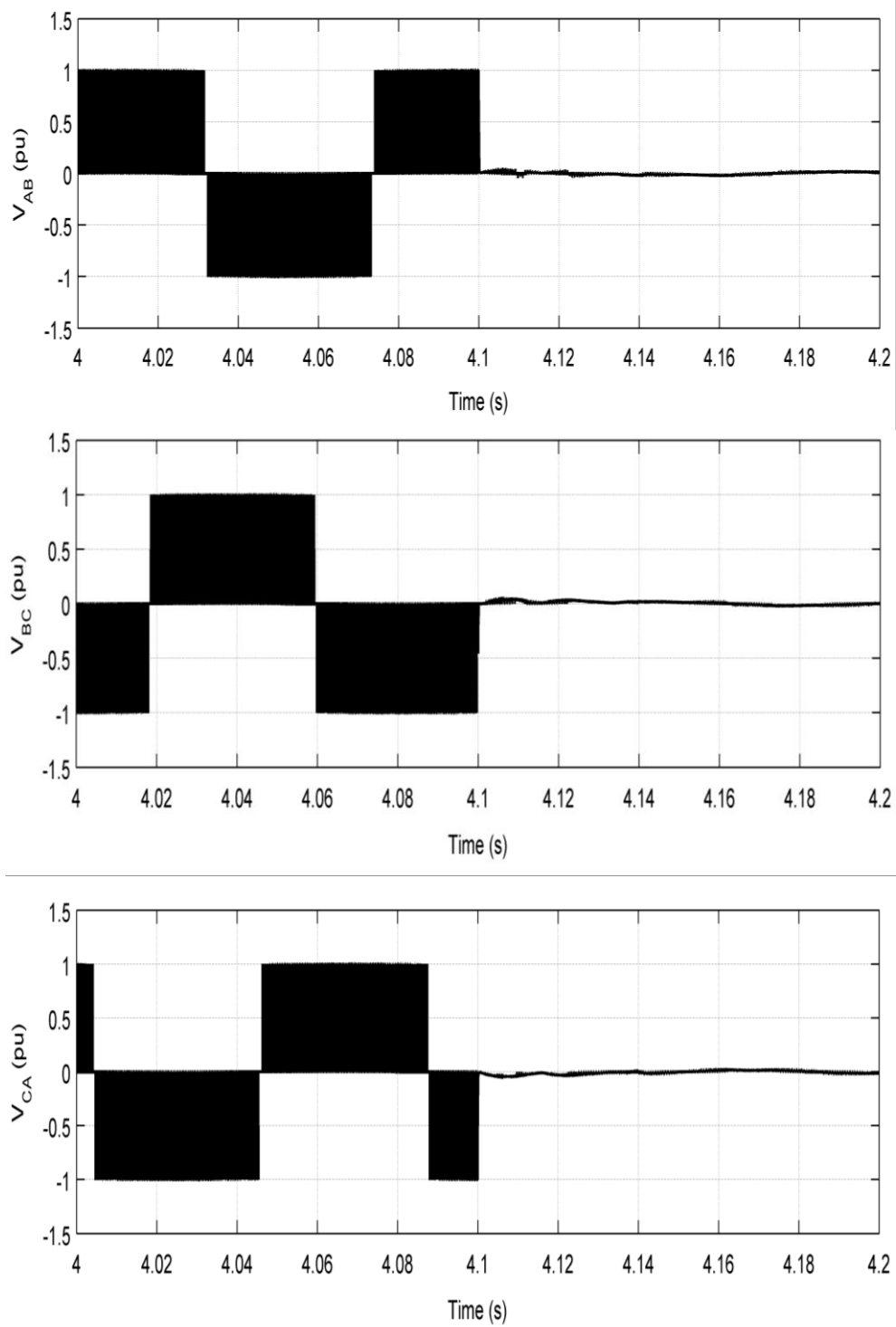
Figure 5.16 Voltage change across GSC terminals during DC link Short Circuit.

Chapter 5

5.4.2.2   Open circuit fault

In this case study, an open circuit fault was simulated within the dc-link and was assumed to last for 5 cycles, starting at t = 4 s. The results presented in Fig. 5.17 (a) reveals that this fault causes the voltage at the PCC to drop slightly and exhibits oscillations in the case when the UPFC was not connected, and these adverse effects were improved when the UPFC the connected to the PCC. By connecting the UPFC to the PCC bus, the voltage oscillations and the settling time of the DFIG shaft speed were reduced slightly, as shown in Fig. 5.17(a) and Fig. 5.17(b). Fig. 5.17(c) shows that the voltage across the capacitor experiences a slight drop. However, the magnitude of the drop is still within the acceptable safety margin of 1.25 pu that will not cause damages to the capacitor of the dc link. The converter terminal voltages increase by more than 5 pu during such fault, as shown in Fig. 5.18.

Chapter 5
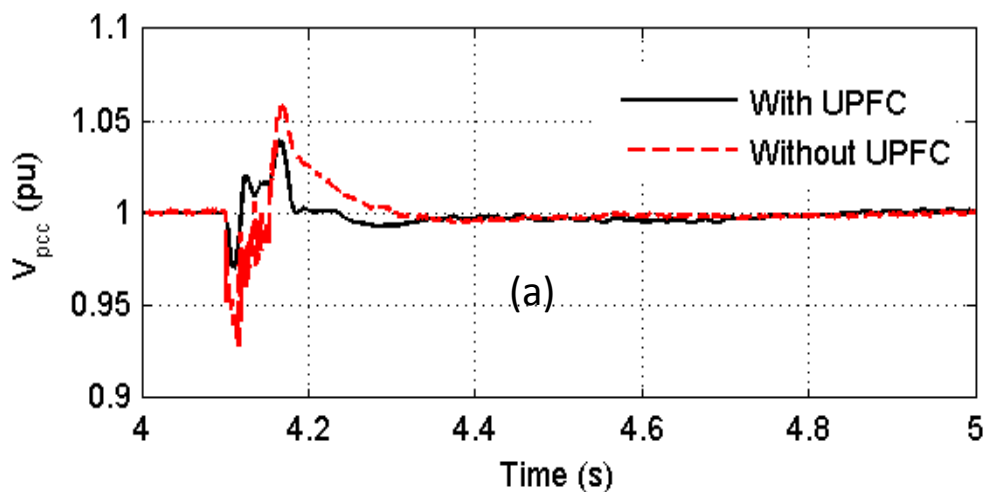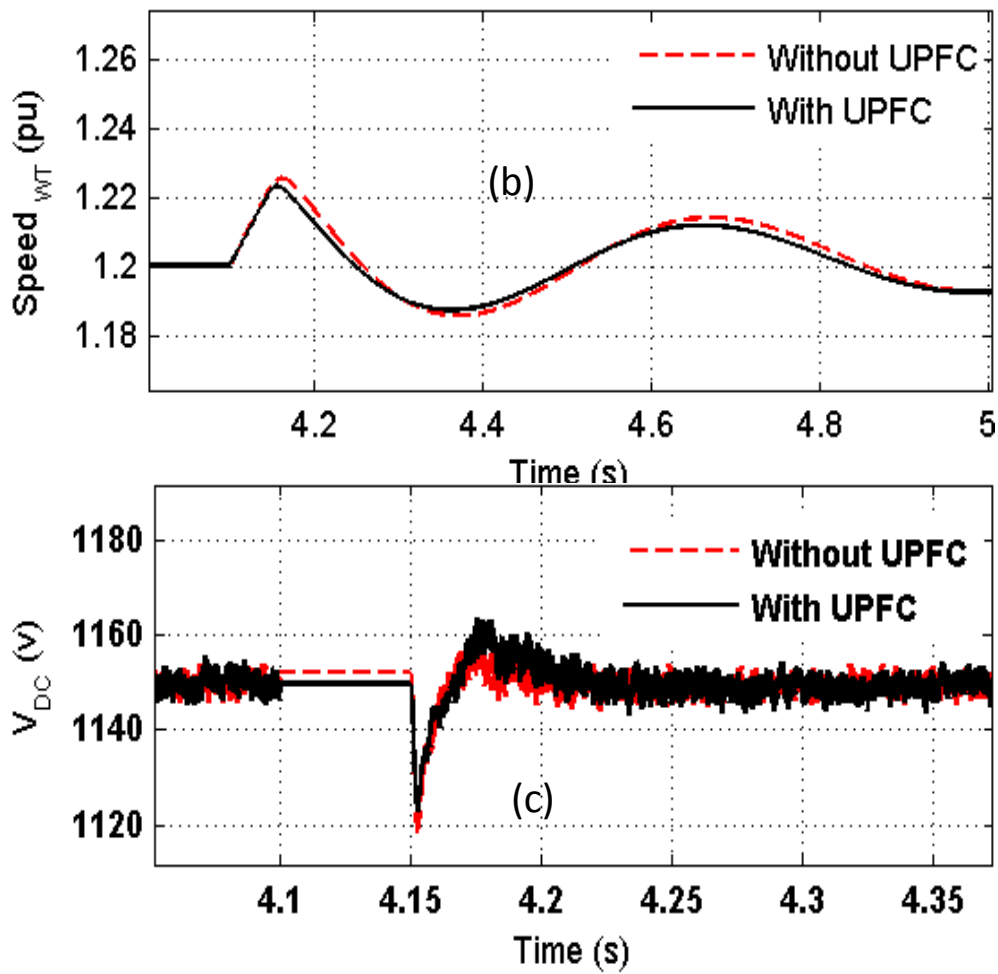
Figure 5.17 Effect of DC link Open Circuit on DFIG dynamic performance with and without UPFC: (a) Voltage at PCC. (b) Shaft speed. (c) DC-link Voltage.

Chapter 5
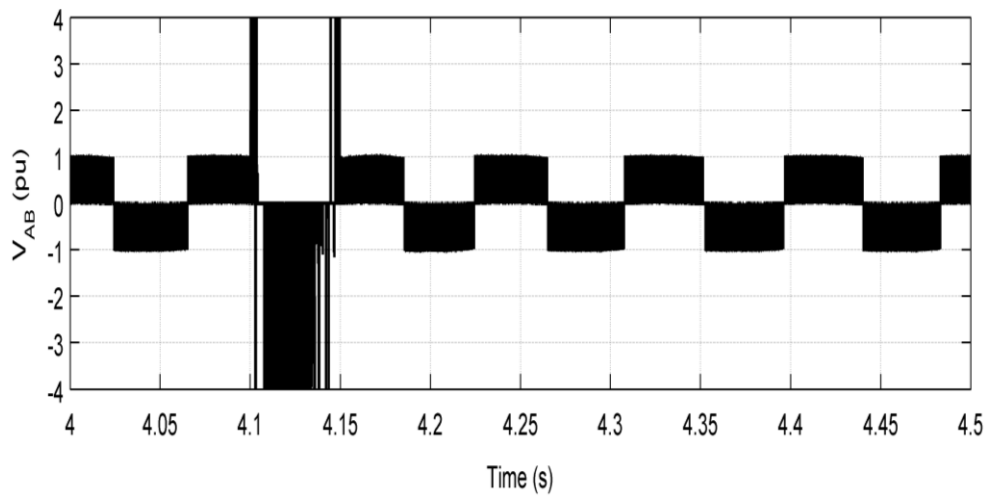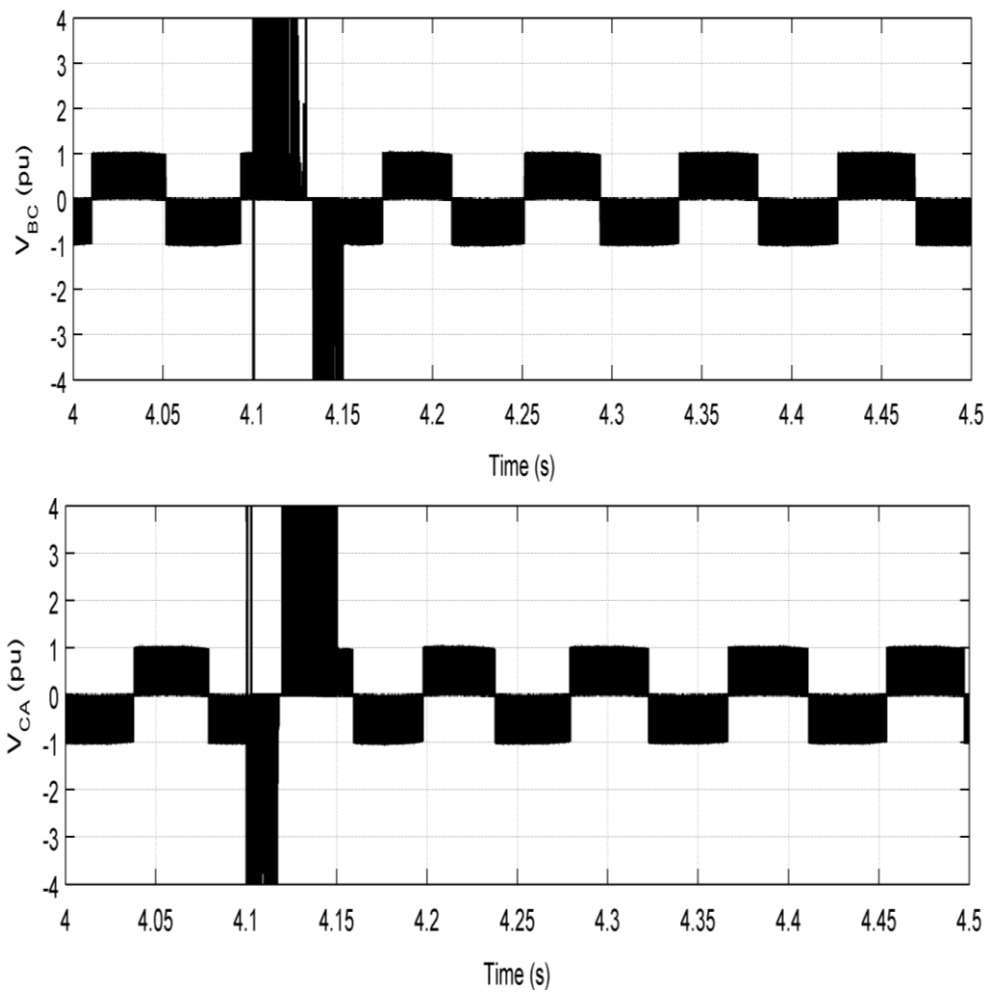
Figure 5.18 Voltage change across GSC terminals during DC link Open Circuit.

5.4.3 UPFC Response

The performance of the UPFC during fire-through and dc-link fault events can be examined through Figs. 5.19 to 5.21. The figures show that when a converter station fault is applied, the UPFC controller acts to instantly exchange the reactive power with the grid to maintain the voltage at the PCC within the safety level required to avoid violation of the limits of transmission line operator codes. As discussed in the

Chapter 5

previous chapter, three UPFC operating conditions can be observed, as follows.

(i) *Standby mode*: this mode takes place during normal operating conditions, where there is no power exchange between the UPFC and the grid. During this mode, the reactive power generation of the wind turbine is maintained at zero level to achieve unity power factor operation and the voltage across the dc link capacitor of the UPFC configuration is maintained at a constant level. This mode of operation is shown in Figs 5.19- 5.21 prior to and after application of the fault event.

(ii) *Capacitive operating mode*, Voltage drop at the PCC activates the UPFC capacitive mode: in this mode the terminal current will lead the bus voltage to support the system by exchanging the required amount of power with the system. The required active and reactive powers are controlled by the phase angle and magnitude of UPFC current and voltage, respectively as shown in Figs. 5.19 to 5.21.

iii) *Inductive operating mode*: During the fault clearance and when the voltage at the PCC increases beyond the pre-set limits, the UPFC controller acts to make the terminal current lagging the terminal voltage and hence the grid's surplus reactive power is absorbed by the UPFC to maintain the voltage at the PCC within the designed safety margins (Figs. 5.19 to 5.21)

Chapter 5
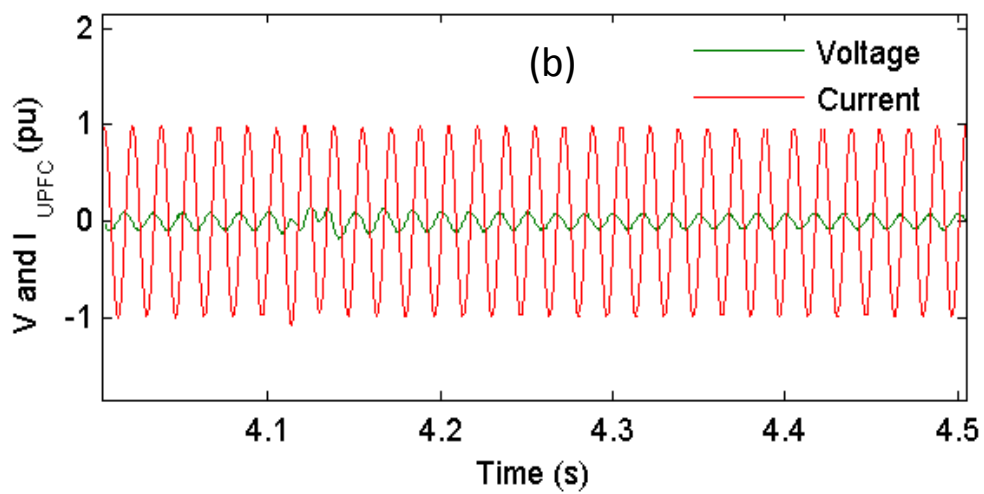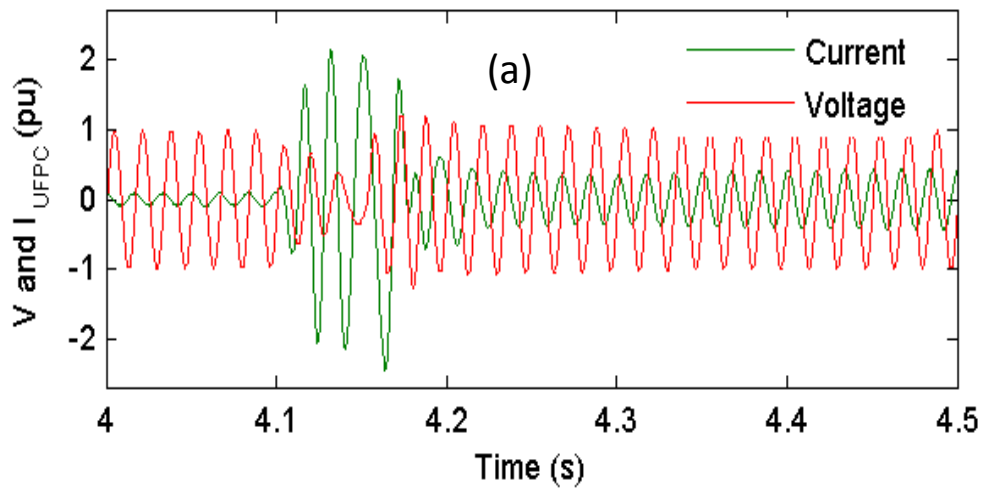
Figure 5.19 UPFC transient responses during RSC (a) Fire-through (b) misfire
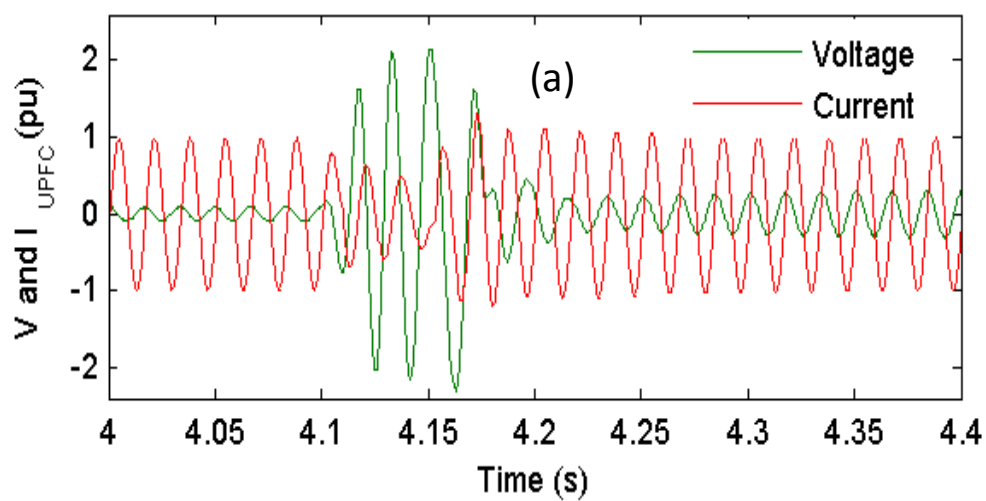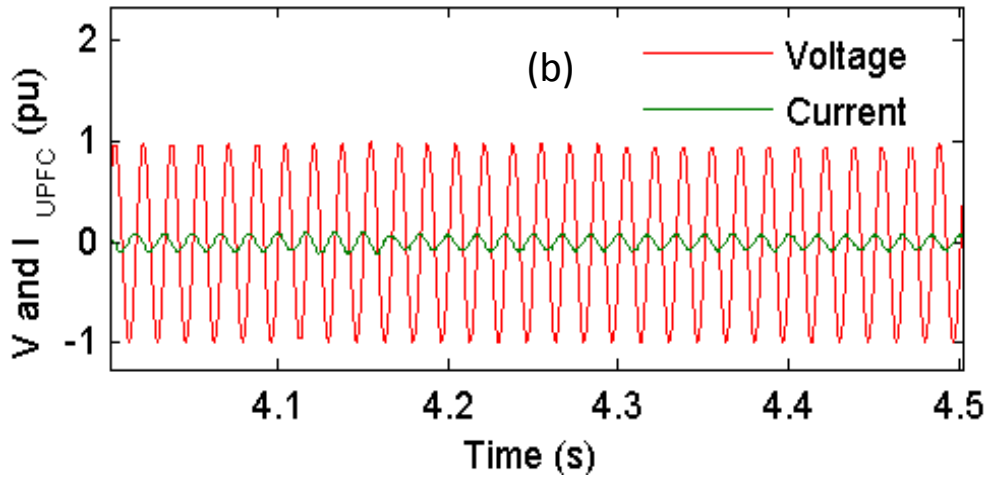
Chapter 5

Figure 5.20 UPFC transient responses during GSC: (a) Fire-through (b) misfire
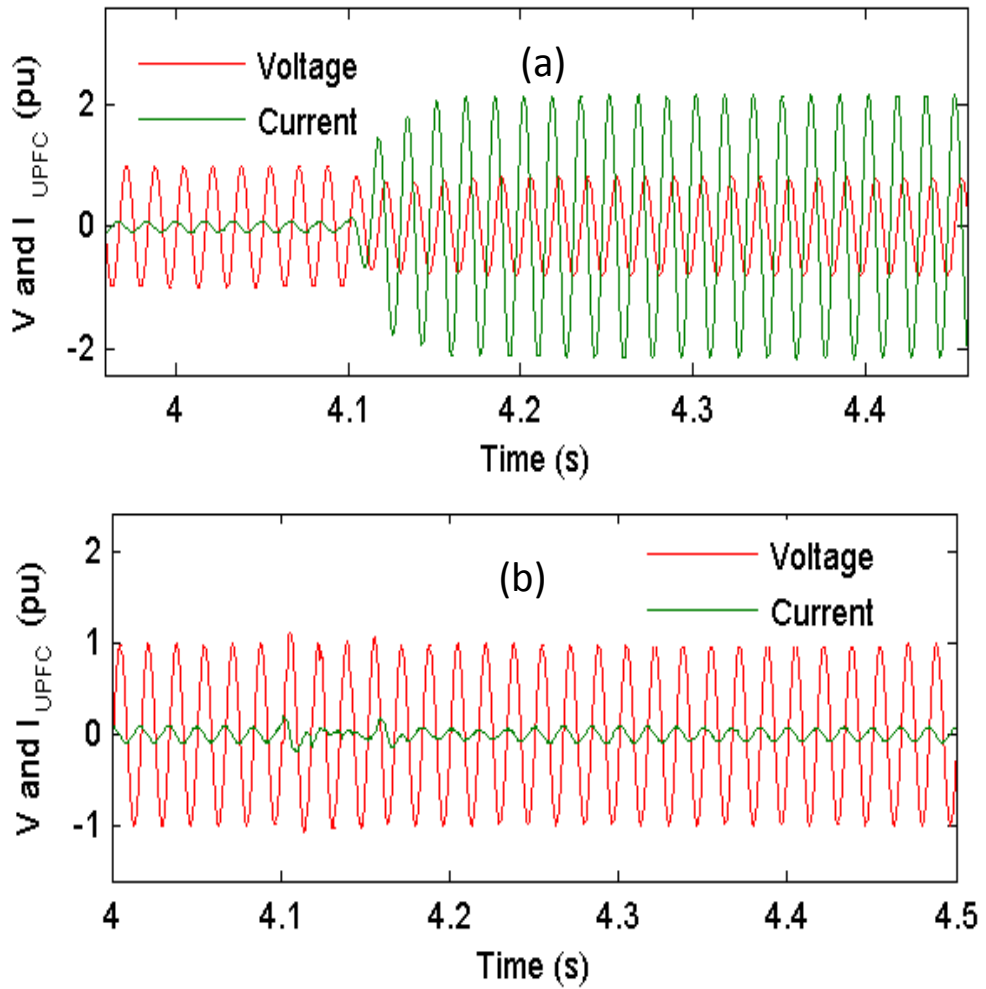
Figure 5.21 UPFC transient responses during fault across the DC link: (a) short circuit (b) open circuit.

Chapter 5

5.5   Summary

This chapter has investigated the impacts of converter station faults and DC link faults on the dynamic performance of DFIG based wind energy conversion system. Fire-through, misfire and DC link faults were simulated and the results were investigated. Simulation results show that the fire-through and DC link faults have severe impact on the DFIG dynamic performance and may result in the disconnection of the wind turbine from the grid to prevent any damage. Misfire fault has a slight and insignificant impact. The UPFC can be successfully introduced to the system to improve the performance of a DFIG-based WECS during fire-through, and dc-link fault. The proposed controller is based on hysteresis current and proportion integral controllers. The simulation results show that the proposed UPFC controller is indeed effective in improving the dynamic performance of the studied DFIG-based WECS during the investigated faults.

Chapter 5

6

CONCLUSIONS AND FUTURE WORKS

6.1   Summary

This thesis has introduced a new application of Unified power flow controller (UPFC) to improve the overall performance of a DFIG-based WECS through modulating both active and reactive powers at the point of common coupling during various disturbance events. The proposed control system of the UPFC is based on hysteresis current and

proportion integral controllers. The key conclusions of this research are summarised below:

- The dynamic performance of the DFIG is affected significantly by the voltage sag/swell and the three-phase short circuit at the grid side. Simulation results showed that, in some faults, the voltage at the point of common coupling violates the limits of some of the existing codes, indicating the undesirable calls for disconnecting the WECS from the grid. Introducing the proposed UPFC was shown to improve the dynamic performance of the DFIG during the investigated fault events to the extent with which the connection of the wind turbine to the grid during such faults will be retained.

- Occurrence of sub-synchronous resonance will have a noticeable (significant?) impact on the DFIG performance. This issue was shown to be resolved by adopting the UPFC proposed in this thesis, which was proven to be very effective in damping all SSR modes of the system under study.

- Simulation results of the converter station faults showed that fire-through and short circuit across the dc link can have severe impacts on the dynamic performance of the DFIG, and this in turn can result in severe damages to the WTG. However, with the introduction of UPFC the system performance improves and the impacts of the faults are mitigated. The analysis showed that misfire and open circuit across the dc link have minor effects on the DFIG performance.

Chapter 6

- The proposed control algorithm is simple, easy to implement and is able to improve the performance of the DFIG during fault events at the grid side or within the DFIG's converter station.

- Although the proposed UPFC was shown to be successful in improving the overall performance of the DFIG, it is still a costly piece of equipment at this stage. Wide application of the proposed UPFC is expected in the near future due to the rapid development of power electronics.

6.2 Contributions

This thesis presents new applications for the unified power flow controller to enhance power system quality and stability with high penetration level of wind energy conversion systems (WECS). The key contributions are summarised as below:

- Development of a new control algorithm for UPFC based on PI and HCC to improve the overall performance of DFIG- based WECS.

- Investigating the robustness of the developed control algorithm through investigating the impact of various disturbances at the grid side on the performance of the studied system with and without the proposed controller. Investigated faults included:

  - Voltage sag

  - Voltage swell

  - Three-phase short circuit

Chapter 6

- Investigating the effects of Sub- synchronous resonance on DFIG and improve the system by installing the proposed UPFC controller.

- Introducing a novel application for the UPFC to improve system performance under DFIG converter station faults. Investigated grid side and rotor side converter station faults included:

- Misfire

- Fir-through

- Open circuit across the DC link

- Short circuit across the DC link

6.3   Future Works

A further research might be needed to extend the work presented in this thesis and improve the control system of the DFIG based WECS; this will improve the fault ride through capability during the faults at the grid side, voltage sag, voltage swell and three phase short circuit. Other fault events at the grid side may consider such as flickers and load variations. In a large interconnected system with penetration of wind energy in more than one location, optimization study to identify the number, best location and controller feedback signals is to be undertaken.

Applications of UPFC can be extended to other wind turbine types such as full

Chapter 6

converter variable speed wind turbine generator (FCWTG). It is recommended to study the dynamic performance of the FCWTG during fire-through, misfire and dc-link failure with and without the proposed UPFC.

More research is also suggested to improve the UPFC performance by designing other control systems and comparing their performance with the one proposed in this research. Control approaches based on fuzzy logic [153] and Lyapunov [154] can be investigated. In designing such controllers, complexity and practicality of implementation must be considered.

Integration of storage systems with FACTS devices has been given more concern in recent studies [155]. It would be interesting to investigate the integration of storage system with UPFC to extend its applications in renewable energy systems in particular and in power systems in general.

Chapter 6

References

[1]   S. Mathew, "Wind energy conversion systems," in *Wind Energy*, ed: Springer Berlin Heidelberg, 2006, pp. 89-143.

[2]   S. Mathew, "Wind energy and environment," in *Wind Energy*, ed: Springer Berlin Heidelberg, 2006, pp. 179-207.

[3]   M. Stiebler, "Wind Energy Systems," in *Wind Energy Systems for Electric Power Generation*, ed: Springer Berlin Heidelberg, 2008, pp. 81-113.

[4]   (1March2015). *Global Wind Report 2014*. Available: http://www.gwec.net/wp-content/uploads/2015/03/GWEC_Global_Wind_2014_Report_LR.pdf

[5]   S. M. Muyeen, J. Tamura, and T. Murata, "Introduction," in *Stability Augmentation of a Grid-connected Wind Farm*, ed: Springer London, 2009, pp. 1-22.

[6]   J. G. Slootweg and W. L. Kling, "The impact of large scale wind power generation on power system oscillations," *Electric Power Systems Research,* vol. 67, pp. 9-20, 2003.

[7]   J. M. Carrasco, L. G. Franquelo, J. T. Bialasiewicz, E. Galvan, R. C. P. Guisado, M. A. M. Prats*, et al.*, "Power-Electronic Systems for the Grid Integration of Renewable Energy Sources: A Survey," *Industrial Electronics, IEEE Transactions on,* vol. 53, pp. 1002-1016, 2006.

[8]   J. P. Therattil and P. C. Panda, "Modeling and control of a multi-machine power system with FACTS controller," in *Power and Energy Systems (ICPS), 2011 International Conference on*, 2011, pp. 1-6.

[9]   A. Rajabi-Ghahnavieh, M. Fotuhi-Firuzabad, M. Shahidehpour, and R. Feuillet, "UPFC for Enhancing Power System Reliability," *Power Delivery, IEEE Transactions on,* vol. 25, pp. 2881-2890, 2010.

[10]   H. Akagi, E. H. Watanabe, and M. Aredes, "Instantaneous Power Theory and Applications to Power Conditioning," ed: Wiley-IEEE Press.

[11]   H. Polinder, D.-J. Bang, H. Li, and Z. Cheng, "Concept Report on Generator Topologies, Mechanical and Electromagnetic Optimization," Project UpWind2007.

[12]   L. M. Hunter, Labor, S. Population Program, and S. Population Matters Project, *Environmental Implications of Population Dynamics*. Santa Monica, CA, USA: RAND Corporation, 2001.

[13]   I. P. C. Change, *Climate Change 2014: Mitigation of Climate Change*: Cambridge University Press, 2015.

[14]   M. Kaltschmitt, N. J. Themelis, L. Y. Bronicki, L. Söder, and L. A. Vega, *Renewable Energy Systems*: Springer New York, 2012.

[15]   B. Sorensen, *Renewable Energy: Physics, Engineering, Environmental Impacts, Economics & Planning*: Elsevier Science, 2010.

[16]   G. Boyle, *Renewable Energy: Power for a Sustainable Future*: OUP Oxford, 2012.

[17]   A. E. F. P. E. R. Resources, N. R. Council, and N. A. Engineering, *Electricity from Renewable Resources:: Status, Prospects, and Impediments*: National Academies Press, 2010.

[18]   H. J. Boenig and J. F. Hauer, "Commissioning Tests Of The Bonneville Power Administration 30 MJ Superconducting Magnetic Energy Storage Unit," *IEEE Transactions on Power Apparatus and Systems,* vol. PAS-104, pp. 302-312, 1985.

[19]   R. DiPippo, "Geothermal Power Plants - Principles, Applications, Case Studies and Environmental Impact (2nd Edition)," ed: Elsevier.

[20]   R. Bertani, " Geothermal Power Generation in the World 2010–2014 Update Report," Proceedings World Geothermal Congress 2015, Melbourne, Australia19–25 April 2015.

[21]   P. Musgrove, *Wind Power*. New York: Cambridge University Press, 2010.

[22]   B. Wu, Y. Lang, N. Zargari, and S. Kouro, "Introduction," in *Power Conversion and Control of Wind Energy Systems*, ed: John Wiley & Sons, Inc., 2011, pp. 1-23.

[23]   T. Ackermann, *Wind Power in Power Systems*: Wiley, 2012.

[24]   V. Akhmatov, *Induction Generators for Wind Power*: Multi-Science Pub., 2005.

[25]   B. Fox, *Wind Power Integration: Connection and System Operational Aspects*: Institution of Engineering and Technology, 2007.

[26]   H. Polinder, J. A. Ferreira, B. B. Jensen, A. B. Abrahamsen, K. Atallah, and R. A. McMahon, "Trends in Wind Turbine Generator Systems," *Emerging and Selected Topics in Power Electronics, IEEE Journal of,* vol. 1, pp. 174-185, 2013.

[27]   B. Wu, Y. Lang, N. Zargari, and S. Kouro, *Power Conversion and Control of Wind Energy Systems*: Wiley, 2011.

[28]   B. Wu, Y. Lang, N. Zargari, and S. Kouro, "Doubly Fed Induction Generator Based WECS," in *Power Conversion and Control of Wind Energy Systems*, ed: John Wiley & Sons, Inc., 2011, pp. 237-274.

[29]   O. Anaya-Lara, N. Jenkins, and J. Ekanayake, *Wind Energy Generation Systems : Modelling and Control*. Hoboken, NJ, USA: Wiley, 2009.

[30]   M. Stiebler, "Grid Integration and Power Quality," in *Wind Energy Systems for Electric Power Generation*, ed: Springer Berlin Heidelberg, 2008, pp. 147-170.

[31]   M. Stiebler, *Wind Energy Systems for Electric Power Generation*. Berlin: Springer, 2008.

[32]   E. F. Fuchs and M. A. S. Masoum, "Power Quality in Power Systems and Electrical Machines," ed: Elsevier, 2008.

[33]   Alt, x, M. n, Go, O. ksu, R. Teodorescu, *et al.*, "Overview of recent grid codes for wind power integration," in *Optimization of Electrical and Electronic Equipment (OPTIM), 2010 12th International Conference on*, 2010, pp. 1152-1160.

[34]   C. E. P. R. Institute, "Technical Rule for Connecting Wind Farm into Power Network," ed, 2009

[35]   M. Mohseni and S. M. Islam, "Review of international grid codes for wind power integration: Diversity, technology and a case for global standard," *Renewable and Sustainable Energy Reviews,* vol. 16, pp. 3876-3890, 2012.

[36]   M. Tsili and S. Papathanassiou, "A review of grid code technical requirements for wind farms," *Renewable Power Generation, IET,* vol. 3, pp. 308-332, 2009.

[37]   A. Western Power, "Technical Rules
 ", ed,
 2011. .

[38] L. G. c. E.-H. Narain G. Hingorani, consulting editor., *Understanding FACTS : concepts and technology of flexible AC transmission systems* New York : IEEE Press 2000.

[39] P. Therond, P. Cholley, D. Daniel, E. Joncquel, L. Lafon, and C. Poumarede, "FACTS research and development program at EDF," in *Flexible AC Transmission Systems (FACTS) - The Key to Increased Utilisation of Power Systems, IEE Colloquium on (Digest No.1994/005)*, 1994, pp. 6/1-615.

[40] X.-P. Zhang, C. Rehtanz, and B. Pal, "FACTS-Devices and Applications," in *Flexible AC Transmission Systems: Modelling and Control*, ed: Springer, 2012, pp. 1-30.

[41] R. Mathur and R. Varma, "SVC Applications," in *Thyristor-Based FACTS Controllers for Electrical Transmission Systems*, ed: Wiley-IEEE Press, 2002, pp. 221-276.

[42] N. Hingorani and L. Gyugyi, "Static Series Compensators: GCSC, TSSC, TCSC and SSSC," in *Understanding FACTS:Concepts and Technology of Flexible AC Transmission Systems*, ed: Wiley-IEEE Press, 2000, pp. 209-265.

[43] N. Hingorani and L. Gyugyi, "Static Shunt Compensators: SVC and STATCOM," in *Understanding FACTS:Concepts and Technology of Flexible AC Transmission Systems*, ed: Wiley-IEEE Press, 2000, pp. 135-207.

[44] N. Hingorani and L. Gyugyi, "Combined Compensators: Unified Power Flow Controller (UPFC) and Interline Power Flow Controller (IPFC)," in *Understanding FACTS:Concepts and Technology of Flexible AC Transmission Systems*, ed: Wiley-IEEE Press, 2000, pp. 297-352.

[45] N. G. Hingorani and L. Gyugyi, *Understanding FACTS: Concepts and Technology of Flexible AC Transmission Systems*: Wiley, 2000.

[46] D. J. Gotham and G. T. Heydt, "Power flow control and power flow studies for systems with FACTS devices," *Power Systems, IEEE Transactions on,* vol. 13, pp. 60-65, 1998.

[47] B. K. Perkins and M. R. Iravani, "Dynamic modeling of a TCSC with application to SSR analysis," *Power Systems, IEEE Transactions on,* vol. 12, pp. 1619-1625, 1997.

[48]   E. V. Larsen, J. J. Sanchez-Gasca, and J. H. Chow, "Concepts for design of FACTS controllers to damp power swings," *Power Systems, IEEE Transactions on,* vol. 10, pp. 948-956, 1995.

[49]   M. Noroozian, L. Angquist, M. Ghandhari, and G. Andersson, "Improving power system dynamics by series-connected FACTS devices," *Power Delivery, IEEE Transactions on,* vol. 12, pp. 1635-1641, 1997.

[50]   K. Duangkamol, Y. Mitani, K. Tsuji, and M. Hojo, "Fault current limiting and power system stabilization by static synchronous series compensator," in *Power System Technology, 2000. Proceedings. PowerCon 2000. International Conference on*, 2000, pp. 1581-1586 vol.3.

[51]   M. I. Marei, E. F. El-Saadany, and M. M. A. Salama, "A Flexible DG Interface Based on a New RLS Algorithm for Power Quality Improvement," *Systems Journal, IEEE,* vol. 6, pp. 68-75, 2012.

[52]   A. Berizzi, M. Delfanti, P. Marannino, M. S. Pasquadibisceglie, and A. Silvestri, "Enhanced Security-Constrained OPF With FACTS Devices," *IEEE Transactions on Power Systems,* vol. 20, pp. 1597-1605, 2005.

[53]   R. M. Mathur and R. K. Varma, "Thyristor-Based FACTS Controllers and Electrical Transmission Systems," ed: Wiley-IEEE Press, pp. 413-461.

[54]   M. Ebadian and M. Alizadeh, "Effect of Static VAR Compensator to improve an induction motor's performance," in *IPEC, 2010 Conference Proceedings*, 2010, pp. 209-214.

[55]   S. M. H. Hosseini, J. Olamaee, and H. Samadzadeh, "Power oscillations damping by Static Var Compensator using an Adaptive Neuro-Fuzzy controller," in *Electrical and Electronics Engineering (ELECO), 2011 7th International Conference on*, 2011, pp. I-80-I-84.

[56]   W. Li and T. Dinh-Nhon, "Stability improvement of an integration of an offshore wind farm and a marine-current farm using a static VAR compensator," in *PES General Meeting | Conference & Exposition, 2014 IEEE*, 2014, pp. 1-5.

[57]   H. Chong, A. Q. Huang, M. E. Baran, S. Bhattacharya, W. Litzenberger, L. Anderson*, et al.*, "STATCOM Impact Study on the Integration of a Large Wind Farm

into a Weak Loop Power System," *Energy Conversion, IEEE Transactions on,* vol. 23, pp. 226-233, 2008.

[58]   B. Singh and K. V. Srinivas, "Three-Level 12-Pulse STATCOM with Constant DC Link Voltage," in *India Conference (INDICON), 2009 Annual IEEE*, 2009, pp. 1-4.

[59]   J. A. Suul, M. Molinas, and T. Undeland, "STATCOM-Based Indirect Torque Control of Induction Machines During Voltage Recovery After Grid Faults," *Power Electronics, IEEE Transactions on,* vol. 25, pp. 1240-1250, 2010.

[60]   H. Chong, A. Q. Huang, M. E. Baran, S. Bhattacharya, W. Litzenberger, L. Anderson*, et al.*, "STATCOM Impact Study on the Integration of a Large Wind Farm into a Weak Loop Power System," *Energy Conversion, IEEE Transactions on,* vol. 23, pp. 226-233, 2008.

[61]   C. Wessels, N. Hoffmann, M. Molinas, and F. W. Fuchs, "StatCom control at wind farms with fixed-speed induction generators under asymmetrical grid faults," *Industrial Electronics, IEEE Transactions on,* vol. 60, pp. 2864-2873, 2013.

[62]   W. Li and T. Dinh-Nhon, "Stability Enhancement of DFIG-Based Offshore Wind Farm Fed to a Multi-Machine System Using a STATCOM," *Power Systems, IEEE Transactions on,* vol. 28, pp. 2882-2889, 2013.

[63]   A. Moharana, R. K. Varma, and R. Seethapathy, "SSR Alleviation by STATCOM in Induction-Generator-Based Wind Farm Connected to Series Compensated Line," *Sustainable Energy, IEEE Transactions on,* vol. 5, pp. 947-957, 2014.

[64]   Q. Wei, G. K. Venayagamoorthy, and R. G. Harley, "Real-Time Implementation of a STATCOM on a Wind Farm Equipped With Doubly Fed Induction Generators," *Industry Applications, IEEE Transactions on,* vol. 45, pp. 98-107, 2009.

[65]   H. Chong, Z. Yang, C. Bin, A. Q. Huang, Z. Bin, M. R. Ingram*, et al.*, "Evaluation of Cascade-Multilevel-Converter-Based STATCOM for Arc Furnace Flicker Mitigation," *Industry Applications, IEEE Transactions on,* vol. 43, pp. 378-385, 2007.

[66]   W. Li and T. Dinh-Nhon, "Dynamic Stability Improvement of Four Parallel-Operated PMSG-Based Offshore Wind Turbine Generators Fed to a Power System

Using a STATCOM," *Power Delivery, IEEE Transactions on,* vol. 28, pp. 111-119, 2013.

[67] K. Kabiri, S. Henschel, J. R. Marti, and H. W. Dommel, "A discrete state-space model for SSR stabilizing controller design for TCSC compensated systems," *Power Delivery, IEEE Transactions on,* vol. 20, pp. 466-474, 2005.

[68] L. Kejun, S. Ying, L. Wei-Jen, and C. Jintao, "Impedance Control of Thyristor Controlled Series Capacitor to Improve the Transfer Capability of Remote Wind Farms," in *Industry Applications Society Annual Meeting (IAS), 2010 IEEE*, 2010, pp. 1-6.

[69] H. Hosseini and B. Tousi, "Mitigating SSR in hybrid system with steam and wind turbine by TCSC," in *Electrical Power Distribution Networks (EPDC), 2012 Proceedings of 17th Conference on*, 2012, pp. 1-6.

[70] R. K. Varma, S. Auddy, and Y. Semsedini, "Mitigation of Subsynchronous Resonance in a Series-Compensated Wind Farm Using FACTS Controllers," *Power Delivery, IEEE Transactions on,* vol. 23, pp. 1645-1654, 2008.

[71] M. Khederzadeh, "Power quality enhancement by TCSC application to mitigate the impact of transformer inrush current," in *Transmission and Distribution Conference and Exposition, 2008. T&D. IEEE/PES*, 2008, pp. 1-5.

[72] N. Kakimoto and A. Phongphanphanee, "Subsynchronous resonance damping control of thyristor-controlled series capacitor," *Power Delivery, IEEE Transactions on,* vol. 18, pp. 1051-1059, 2003.

[73] T. Dinh-Nhon and W. Li, "Application of a static synchronous series compensator to improve stability of a SG-based power system with an offshore wind farm," in *Power and Energy Society General Meeting, 2012 IEEE*, 2012, pp. 1-7.

[74] H. Barati, A. L. Ara, M. Ehsan, M. Fotuhi-Firuzabad, and S. M. T. Bathaee, "Application of Static Synchronous Series Compensator to Damp Sub-Synchronous Resonance," in *Power Electronics, Drives and Energy Systems, 2006. PEDES '06. International Conference on*, 2006, pp. 1-6.

[75]   M. Farahani, "Damping of subsynchronous oscillations in power system using static synchronous series compensator," *Generation, Transmission & Distribution, IET,* vol. 6, pp. 539-544, 2012.

[76]   S. Golshannavaz, M. Farsadi, and D. Nazarpour, "Low frequency oscillations damping by static synchronous series compensator equipped with an auxiliary fuzzy logic controller," in *Electrical Engineering (ICEE), 2011 19th Iranian Conference on*, 2011, pp. 1-1.

[77]   W. Li and V. Quang-Son, "Power Flow Control and Stability Improvement of Connecting an Offshore Wind Farm to a One-Machine Infinite-Bus System Using a Static Synchronous Series Compensator," *Sustainable Energy, IEEE Transactions on,* vol. 4, pp. 358-369, 2013.

[78]   E. Fuchs and M. A. S. Masoum, *Power Quality in Power Systems and Electrical Machines*: Elsevier Science, 2011.

[79]   H. Abu-Rub, A. Iqbal, and J. Guzinski, *High Performance Control of AC Drives with Matlab / Simulink Models*: Wiley, 2012.

[80]   R. Dávalos M, J. M. Ramírez, and R. Tapia O, "Three-phase multi-pulse converter StatCom analysis," *International Journal of Electrical Power & Energy Systems,* vol. 27, pp. 39-51, 2005.

[81]   N. Talebi and A. Akbarzadeh, "Damping of Low Frequency Oscillations in power systems with neuro-fuzzy UPFC controller," in *Environment and Electrical Engineering (EEEIC), 2011 10th International Conference on*, 2011, pp. 1-4.

[82]   C. Chia-Chi and T. Hung-Chi, "Application of Lyapunov-based adaptive neural network upfc damping controllers for transient stability enhancement," in *Power and Energy Society General Meeting - Conversion and Delivery of Electrical Energy in the 21st Century, 2008 IEEE*, 2008, pp. 1-6.

[83]   J. Guo, M. L. Crow, and J. Sarangapani, "An Improved UPFC Control for Oscillation Damping," *Power Systems, IEEE Transactions on,* vol. 24, pp. 288-296, 2009.

[84]   P. K. Dash, S. Morris, and S. Mishra, "Design of a nonlinear variable-gain fuzzy controller for FACTS devices," *Control Systems Technology, IEEE Transactions on,* vol. 12, pp. 428-438, 2004.

[85]   Y. L. Kang, G. B. Shresta, and T. T. Lie, "Application of an NLPID controller on a UPFC to improve transient stability of a power system," *Generation, Transmission and Distribution, IEE Proceedings-,* vol. 148, pp. 523-529, 2001.

[86]   R. K. Khadanga and S. Panda, "Gravitational search algorithm for Unified Power Flow Controller based damping controller design," in *Energy, Automation, and Signal (ICEAS), 2011 International Conference on*, 2011, pp. 1-6.

[87]   S. Ray and G. K. Venayagamoorthy, "Wide-Area Signal-Based OptimalNeurocontroller for a UPFC," *Power Delivery, IEEE Transactions on,* vol. 23, pp. 1597-1605, 2008.

[88]   L. Liming, Z. Pengcheng, K. Yong, and C. Jian, "Power-Flow Control Performance Analysis of a Unified Power-Flow Controller in a Novel Control Scheme," *Power Delivery, IEEE Transactions on,* vol. 22, pp. 1613-1619, 2007.

[89]   S. Kannan, S. Jayaram, and M. M. A. Salama, "Real and reactive power coordination for a unified power flow controller," *Power Systems, IEEE Transactions on,* vol. 19, pp. 1454-1461, 2004.

[90]   P. K. Dash, S. Mishra, and G. Panda, "A radial basis function neural network controller for UPFC," *Power Systems, IEEE Transactions on,* vol. 15, pp. 1293-1299, 2000.

[91]   M. J. Kumar, S. S. Dash, A. S. P. Immanuvel, and R. Prasanna, "Comparison of FBLC (Feed-Back Linearisation) and PI-Controller for UPFC to enhance transient stability," in *Computer, Communication and Electrical Technology (ICCCET), 2011 International Conference on*, 2011, pp. 376-381.

[92]   H. I. Shaheen, G. I. Rashed, and S. J. Cheng, "Design of new nonlinear optimal predictive controller for Unified Power Flow Controller," in *Power and Energy Society General Meeting - Conversion and Delivery of Electrical Energy in the 21st Century, 2008 IEEE*, 2008, pp. 1-10.

[93]   F. Shalchi, H. Shayeghi, and H. A. Shayanfar, "Robust control design for UPFC to improve damping of oscillation in distribution system by H_2 method," in *Electrical Power Distribution Networks (EPDC), 2011 16th Conference on*, 2011, pp. 1-10.

[94]   T. Ackermann, *Wind Power in Power System*. West Sussex: John Wiley and Sons Ltd, 2005.

[95]   R. H. Park, "Two-reaction theory of synchronous machines generalized method of analysis-part I," *American Institute of Electrical Engineers, Transactions of the,* vol. 48, pp. 716-727, 1929.

[96]   M. Milosevic. (19 February). *Hysteresis Current Control in Three-Phase Voltage Source Inverter.* Available: http://www.eeh.ee.ethz.ch/uploads/tx_ethpublications/milosevic_hysteresis.pdf

[97]   L. Malesani and P. Tenti, "A novel hysteresis control method for current-controlled voltage-source PWM inverters with constant modulation frequency," *IEEE Transactions on Industry Applications,* vol. 26, pp. 88-92, 1990.

[98]   J. M. Carrasco, L. G. Franquelo, J. T. Bialasiewicz, E. Galvan, R. C. P. Guisado, M. A. M. Prats*, et al.*, "Power-Electronic Systems for the Grid Integration of Renewable Energy Sources: A Survey," *IEEE Transactions on Industrial Electronics,* vol. 53, pp. 1002-1016, 2006.

[99]   T. Ackerman, *Wind Power in Power System*. West Sussex: John Wiley and Sons Ltd, 2005.

[100] S. Seman, J. Niiranen, and A. Arkkio, "Ride-Through Analysis of Doubly Fed Induction Wind-Power Generator Under Unsymmetrical Network Disturbance," *IEEE Transactions on Power Systems* vol. 21, pp. 1782-1789, 2006.

[101] J. Lopez, E. Gubia, E. Olea, J. Ruiz, and L. Marroyo, "Ride Through of Wind Turbines With Doubly Fed Induction Generator Under Symmetrical Voltage Dips," *IEEE Transactions on Industrial Electronics,* vol. 56, pp. 4246-4254, 2009.

[102] M. Mohseni, S. M. Islam, and M. A. S. Masoum, "Impacts of Symmetrical and Asymmetrical Voltage Sags on DFIG-Based Wind Turbines Considering Phase-Angle Jump, Voltage Recovery, and Sag Parameters," *IEEE Transactions on Power Electronics,* vol. 26, pp. 1587-1598, 2011.

[103] Y. Xiangwu, G. Venkataramanan, P. S. Flannery, W. Yang, D. Qing, and Z. Bo, "Voltage-Sag Tolerance of DFIG Wind Turbine With a Series Grid Side Passive-

Impedance Network," *IEEE Transactions on Energy Conversion* vol. 25, pp. 1048-1056, 2010.

[104] S. Hu, X. Lin, Y. Kang, and X. Zou, "An Improved Low-Voltage Ride-Through Control Strategy of Doubly Fed Induction Generator During Grid Faults," *IEEE Transactions on Power Electronics,* vol. 26, pp. 3653-3665, 2011.

[105] S. M. Muyeen, R. Takahashi, T. Murata, and J. Tamura, "A Variable Speed Wind Turbine Control Strategy to Meet Wind Farm Grid Code Requirements," *Power Systems, IEEE Transactions on,* vol. 25, pp. 331-340, 2010.

[106] V. Ahkmatov. (2003, 25 February). *Analysis of dynamic behaviour of power systems with large amount of wind power.* Available: http://www.dtu.dk/upload/centre/cet/projekter/99-05/05-va-thesis.pdf

[107] A. M. S. Yunus, M. A. S. Masoum, and A. Abu-Siada, "Application of SMES to Enhance the Dynamic Performance of DFIG During Voltage Sag and Swell," *Applied Superconductivity, IEEE Transactions on,* vol. 22, pp. 5702009-5702009, 2012.

[108] A. M. S. Yunus, A. A. Siada, and M. A. S. Masoum, "Application of SMES Unit to Improve the High Voltage Ride Through Capabillty of DFIG-Grid Connected during Voltage Swell," in *IEEE Power and Energy Society Innovative Smart Grid Technologies Conference (ISGT 2011)*, Perth, Australia, 2011.

[109] Alt, x, M. n, Go, O. ksu, R. Teodorescu, *et al.*, "Overview of recent grid codes for wind power integration," in *12th International Conference on Optimization of Electrical and Electronic Equipment (OPTIM), 2010* 2010, pp. 1152-1160.

[110] W. Li, L. Hao-Wen, and W. Cheng-Tai, "Stability Analysis of an Integrated Offshore Wind and Seashore Wave Farm Fed to a Power Grid Using a Unified Power Flow Controller," *Power Systems, IEEE Transactions on,* vol. 28, pp. 2211-2221, 2013.

[111] L. Gyugyi, "A unified flow control concept for flexible AC transmission systems," in *AC and DC Power Transmission, 1991., International Conference on*, 1991, pp. 19-26.

[112] E. Gholipour and S. Saadate, "Improving of transient stability of power systems using UPFC," *Power Delivery, IEEE Transactions on,* vol. 20, pp. 1677-1682, 2005.

[113] S. Shojaeian, J. Soltani, and G. A. Markadeh, "Damping of Low Frequency Oscillations of Multi-Machine Multi-UPFC Power Systems, Based on Adaptive Input-Output Feedback Linearization Control," *Power Systems, IEEE Transactions on,* vol. 27, pp. 1831-1840, 2012.

[114] N. Tambey and M. L. Kothari, "Damping of power system oscillations with unified power flow controller (UPFC)," *Generation, Transmission and Distribution, IEE Proceedings-,* vol. 150, pp. 129-140, 2003.

[115] D. Thukaram, L. Jenkins, and K. Visakha, "Improvement of system security with unified-power-flow controller at suitable locations under network contingencies of interconnected systems," *Generation, Transmission and Distribution, IEE Proceedings-,* vol. 152, pp. 682-690, 2005.

[116] R. L. Vasquez-Arnez and L. C. Zanetta, "Compensation strategy of autotransformers and parallel lines performance, assisted by the UPFC," *Power Delivery, IEEE Transactions on,* vol. 20, pp. 1550-1557, 2005.

[117] H. Chen, Y. Wang, and R. Zhou, "Transient and voltage stability enhancement via coordinated excitation and UPFC control," *Generation, Transmission and Distribution, IEE Proceedings-,* vol. 148, pp. 201-208, 2001.

[118] M. Januszewski, J. Machowski, and J. W. Bialek, "Application of the direct Lyapunov method to improve damping of power swings by control of UPFC," *Generation, Transmission and Distribution, IEE Proceedings-,* vol. 151, pp. 252-260, 2004.

[119] G. Andersson, P. Donalek, R. Farmer, N. Hatziargyriou, I. Kamwa, P. Kundur*, et al.*, "Causes of the 2003 major grid blackouts in North America and Europe, and recommended means to improve system dynamic performance," *Power Systems, IEEE Transactions on,* vol. 20, pp. 1922-1928, 2005.

[120] M. D. Ilic, H. Allen, W. Chapman, C. A. King, J. H. Lang, and E. Litvinov, "Preventing Future Blackouts by Means of Enhanced Electric Power Systems Control: From Complexity to Order," *Proceedings of the IEEE,* vol. 93, pp. 1920-1941, 2005.

[121] J. Machowski, J. W. Bialek, and J. R. Bumby, "Power System Dynamics and Stability," ed: John Wiley & Sons.

[122] J. D. Glover, M. Sarma, and T. Overbye, *Power Systems Analysis and Design*: Cengage Learning, 2007.

[123] K. R. Padiyar, *Power System Dynamics* New Delhi : BS Publiations 2008.

[124] A. F. Abdou, A. Abu-Siada, and H. R. Pota, "Damping of subsynchronous oscillations and improve transient stability for wind farms," in *Innovative Smart Grid Technologies Asia (ISGT), 2011 IEEE PES*, 2011, pp. 1-6.

[125] R. G. Farmer, A. L. Schwalb, and E. Katz, "Navajo project report on subsynchronous resonance analysis and solutions," *Power Apparatus and Systems, IEEE Transactions on,* vol. 96, pp. 1226-1232, 1977.

[126] W. Li and L. Ching-Huei, "Application of dynamic resistance braking on stabilizing torsional oscillations," in *TENCON '93. Proceedings. Computer, Communication, Control and Power Engineering.1993 IEEE Region 10 Conference on*, 1993, pp. 145-148 vol.5.

[127] "First benchmark model for computer simulation of subsynchronous resonance," *Power Apparatus and Systems, IEEE Transactions on,* vol. 96, pp. 1565-1572, 1977.

[128] L. Ha Thu and S. Santoso, "Increasing wind farm transient stability by dynamic reactive compensation: Synchronous-machine-based ESS versus SVC," in *Power and Energy Society General Meeting, 2010 IEEE*, 2010, pp. 1-8.

[129] H. Zhou, H. Wei, X. Qiu, J. Xu, X. Wei, and S. Wang, "Improvement of Transient Voltage Stability of the Wind Farm Using SVC and TCSC," in *Power and Energy Engineering Conference (APPEEC), 2011 Asia-Pacific*, 2011, pp. 1-4.

[130] A. F. Abdou, A. Abu-Siada, and H. R. Pota, "Application of SVC on stabilizing torsional oscillations and improving transient stability," in *Power and Energy Society General Meeting, 2012 IEEE*, 2012, pp. 1-5.

[131] A. Abu-Siada, "Damping of large turbo-generator subsyncronous resonance using superconducting magnetic energy storage unit," in *Universities Power Engineering Conference (AUPEC), 2010 20th Australasian*, 2010, pp. 1-4.

[132] J. B. X. Devotta, M. G. Rabbani, and S. Elangovan, "Application of superconducting magnetic energy storage unit for damping of subsynchronous oscillations in power systems," *Energy Conversion and Management,* vol. 40, pp. 23-37, 1999.

[133] W. Li, L. Shin-Muh, and H. Ching-Lien, "Damping subsynchronous resonance using superconducting magnetic energy storage unit," *Energy Conversion, IEEE Transactions on,* vol. 9, pp. 770-777, 1994.

[134] O. Wasynczuk, "Damping Subsynchronous Resonance Using Energy Storage," *Power Engineering Review, IEEE,* vol. PER-2, pp. 36-37, 1982.

[135] A. F. Abdou, A. Abu-Siada, and H. R. Pota, "Application of a STATCOM for damping subsynchronous oscillations and transient stability improvement," in *Universities Power Engineering Conference (AUPEC), 2011 21st Australasian*, 2011, pp. 1-5.

[136] E. Eitelberg, J. C. Balda, E. S. Boje, and R. G. Harley, "Stabilizing SSR oscillations with a shunt reactor controller for uncertain levels of series compensation," *Power Systems, IEEE Transactions on,* vol. 3, pp. 936-943, 1988.

[137] L. Wang and C.-H. Lee, "Stabilizing torsional oscillations using a shunt reactor controller," *Energy Conversion, IEEE Transactions on,* vol. 6, pp. 373-380, 1991.

[138] R. M. Hamouda, Z. R. AlZaid, and M. A. Mostafa, "Damping torsional oscillations in large turbo-generators using Thyristor Controlled Braking Resistors," in *Power Engineering Conference, 2008. AUPEC '08. Australasian Universities*, 2008, pp. 1-6.

[139] A. Ghorbani and S. Pourmohammad, "A novel excitation controller to damp subsynchronous oscillations," *International Journal of Electrical Power & Energy Systems,* vol. 33, pp. 411-419, 2011.

[140] W. Li, "Damping of torsional oscillations using excitation control of synchronous generator: the IEEE Second Benchmark Model investigation," *Energy Conversion, IEEE Transactions on,* vol. 6, pp. 47-54, 1991.

[141] F. D. Jesus, E. H. Watanabe, L. F. W. Souza, and J. E. R. Alves, "Analysis of SSR Mitigation Using Gate Controlled Series Capacitors," in *Power Electronics Specialists Conference, 2005. PESC '05. IEEE 36th*, 2005, pp. 1402-1407.

[142] R. Rajaraman, I. Dobson, R. H. Lasseter, and S. Yihchih, "Computing the damping of subsynchronous oscillations due to a thyristor controlled series capacitor," *Power Delivery, IEEE Transactions on,* vol. 11, pp. 1120-1127, 1996.

[143] A. Abu-Siada and S. Islam, "Application of SMES Unit in Improving the Performance of an AC/DC Power System," *IEEE Transactions on Sustainable Energy,* vol. 2, pp. 109-121, 2011.

[144] G. Abad, J. López, M. A. Rodríguez, L. Marroyo, and G. Iwanski, "Introduction to A Wind Energy Generation System," in *Doubly Fed Induction Machine*, ed: John Wiley & Sons, Inc., 2011, pp. 1-85.

[145] A. F. Abdou, H. R. Pota, A. Abu-Siada, and Y. M. Alharbi, "Application of STATCOM-HTS to improve DFIG performance and FRT during IGBT short circuit," in *Power Engineering Conference (AUPEC), 2014 Australasian Universities*, 2014, pp. 1-5.

[146] A. M. Shiddiq-Yunus, A. A. Siada, and M. A. S. Masoum, "Impact of SMES on DFIG Power Dispatch during Intermittent Misfire and Fire-through Faults," *IEEE Transactions on Applied Superconductivity,* 2012.

[147] J. Arrillaga, *High Voltage Direct Current Transmission*. London: Peter Peregrinus Ltd, 1983.

[148] J. Arrillaga, *High Voltage Direct Current Transmission*: Institution of Electrical Engineers, 1998.

[149] G. Abad, J. López, M. A. Rodríguez, L. Marroyo, and G. Iwanski, "Back-to-Back Power Electronic Converter," in *Doubly Fed Induction Machine*, ed: John Wiley & Sons, Inc., 2011, pp. 87-154.

[150] H. B. A. Sethom and M. A. Ghedamsi, "Intermittent Misfiring Default Detection and Localisation on a PWM Inverter Using Wavelet Decomposition," *Journal of Electrical System,* vol. 4, pp. 222-234, 2008.

[151] K. R. Padiyar, *HVDC Power Transmission Systems*. New Delhi: John Wiley & Sons, 1990.

[152] L. Bin and S. Sharma, "A survey of IGBT fault diagnostic methods for three-phase power inverters," in *International Conference on Condition Monitoring and Diagnosis, 2008. CMD 2008.* , 2008, pp. 756-763.

[153] H. Li and M. M. Gupta, Eds., *Fuzzy Logic and Inteligent System*. Massachusetts: Kluwer Academic Publisher, 1995, p.^pp. Pages.

[154] H. K. Khalil and J. Grizzle, *Nonlinear systems* vol. 3: Prentice hall New Jersey, 1996.

[155] P. F. Ribeiro, B. K. Johnson, M. L. Crow, A. Arsoy, and Y. Liu, "Energy storage systems for advanced power applications," *Proceedings of the IEEE,* vol. 89, pp. 1744-1756, 2001.

Appendix

Appendix A-1

		Parameters	Value
DFIG based WECS	Generator	Number of pair poles, p	3
		Mutual Inductance, L_m (p.u.)	2.9
		Stator Leakage Inductance, $L_{\sigma s}$ (p.u.)	0.18
		Rotor Leakage Inductance, $L_{\sigma r}$ (p.u.)	0.16
		Stator Resistance, R_s (p.u.)	0.23
		Rotor Resistance, R_r (p.u.)	0.016
		Moment of Inertia (s)	0.685
		Rated Power MW	1.5
		Stator Voltage (V)	575
		Frequency(Hz)	60
	Drive Train	Wind Turbine Inertia Constant, H (s)	4.32
		Shaft Spring Constant (p.u. of Mechanical Torque/Rad)	80.27
		Shaft Mutual Damping(p.u. of Mechanical Torque/pu dw)	1.5
		Turbine Initial Speed (p.u.)	1.2
		Initial Output Torque (p.u.)	0.8
	Converters	Grid Side Coupling Inductor, L (p.u.)	0.3
		Grid Side Coupling Inductor R (p.u.)	0.003
		Nominal DC bus Voltage (V)	1150
		DC Bus Capacitor (F)	10000e-6
	Wind	Wind speed at nominal speed and at Cp max (m/s)	11
		Initial wind speed (m/s)	11

Appendix A-2

Parameters	Value
Positive sequence resistances R_1 (Ohms/km)	0.1153
Zero sequence resistances R_0 (Ohms/km)	0.413
Positive sequence inductances L_1 (H/km)	1.05×10^{-3}
Zero sequence inductances L_0 (H/km)	3.32×10^{-3}
Positive sequence capacitances C_1 (F/km)	11.33×10^{-9}
Zero sequence capacitances C_0 (F/km)	5.01×10^{-9}

The leftmost column of the table, spanning all six parameter rows, is labeled "Transmission Line".

Appendix A-3

	Parameters	Value
UPFC	Transformer rating MVA	5
	Transformer Primary (KV)	25
	Transformer secondary (KV)	1.25

Appendix B-1

Parameters		Value
Synchronous generator	VLL (Kv)	22
	IL (Kv)	15.746
	ω_b (rad/s)	376.99
	R_a (pu)	0.0045
	X_L (pu)	1.65
	X_d (pu)	1.59
	X_q (pu)	0.25
	X'_d (pu)	0.20
	X''_d (pu)	0.46
	X''_q (pu)	0.20
	T'_{do} (s)	4.5
	T''_{do} (s)	0.040
	T'_{qo} (s)	0.55
	T''_{qo} (s)	0.09

Appendix B-2

		Parameters	Value
Torsional System Data	Spring Constant	Exc-Gen (Ibf-ft /rad)	4.39 x 106
		Gen-LP (Ibf-ft /rad)	97.97 x 106
		LP-HP (Ibf-ft /rad)	50.12 x 106
	inertia	Exc (Ibm-ft2)	1383
		Gen (Ibm-ft2)	176204
		LP (Ibm-ft2)	310729
		HP (Ibm-ft2)	49912
	Damping	Exc (Ibf-ft-sec/rad)	4.3
		Gen (Ibf-ft-sec/rad)	547.9
		LP (Ibf-ft-sec/rad)	966.2
		HP (Ibf-ft-sec/rad)	155.2

Appendix B-3

Parameters		Value
Transmission Line	R_1 (Ohms)	18.5
	R_2 (Ohms)	16.75
	L_1 (H)	0.49006
	L_1 (H)	0.5305
	C (μF)	24.11

Appendix B-4

		Parameters	Value
DFIG based WECS	Generator	Number of pair poles, p	3
		Mutual Inductance, L_m (p.u.)	2.9
		Stator Leakage Inductance, $L_{\sigma s}$ (p.u.)	0.18
		Rotor Leakage Inductance, $L_{\sigma r}$ (p.u.)	0.16
		Stator Resistance, R_s (p.u.)	0.23
		Rotor Resistance, R_r (p.u.)	0.016
		Moment of Inertia (s)	0.685
		Rated Power MW	1.5
		Stator Voltage (V)	575
		Frequency(Hz)	60
	Drive Train	Wind Turbine Inertia Constant, H (s)	4.32
		Shaft Spring Constant (p.u. of Mechanical Torque/Rad)	80.27
		Shaft Mutual Damping(p.u. of Mechanical Torque/pu dw)	1.5
		Turbine Initial Speed (p.u.)	1.2
		Initial Output Torque (p.u.)	0.8
	Converters	Grid Side Coupling Inductor, L (p.u.)	0.3
		Grid Side Coupling Inductor R (p.u.)	0.003
		Nominal DC bus Voltage (V)	1150
		DC Bus Capacitor (F)	10000e-6
	Wind	Wind speed at nominal speed and at Cp max (m/s)	11
		Initial wind speed (m/s)	11

Appendix B-5

Parameters		Value
UPFC	Transformer rating MVA	100
	Transformer Primary (KV)	500
	Transformer secondary (KV)	15

Appendix C-1

Parameters			Value
DFIG based WECS	Generator	Number of pair poles, p	3
		Mutual Inductance, L_m (p.u.)	2.9
		Stator Leakage Inductance, $L_{\sigma s}$ (p.u.)	0.18
		Rotor Leakage Inductance, $L_{\sigma r}$ (p.u.)	0.16
		Stator Resistance, R_s (p.u.)	0.23
		Rotor Resistance, R_r (p.u.)	0.016
		Moment of Inertia (s)	0.685
		Rated Power MW	3
		Stator Voltage (V)	575
		Frequency(Hz)	60
	Drive Train	Wind Turbine Inertia Constant, H (s)	4.32
		Shaft Spring Constant (p.u. of Mechanical Torque/Rad)	80.27
		Shaft Mutual Damping(p.u. of Mechanical Torque/pu dw)	1.5
		Turbine Initial Speed (p.u.)	1.2
		Initial Output Torque (p.u.)	0.8
	Converters	Grid Side Coupling Inductor, L (p.u.)	0.3
		Grid Side Coupling Inductor R (p.u.)	0.003
		Nominal DC bus Voltage (V)	1150
		DC Bus Capacitor (F)	10000e-6
	Wind	Wind speed at nominal speed and at Cp max (m/s)	11
		Initial wind speed (m/s)	11

Appendix C-2

Parameters	Value
Positive sequence resistances R_1 (Ohms/km)	0.1153
Zero sequence resistances R_0 (Ohms/km)	0.413
Positive sequence inductances L_1 (H/km)	1.05×10^{-3}
Zero sequence inductances L_0 (H/km)	3.32×10^{-3}
Positive sequence capacitances C_1 (F/km)	11.33×10^{-9}
Zero sequence capacitances C_0 (F/km)	5.01×10^{-9}

(Row group label: Transmission Line)

Appendix C-3

	Parameters	Value
UPFC	Transformer rating MVA	5
	Transformer Primary (KV)	25
	Transformer secondary (KV)	1.25